# Study of the proton-rich nucleus $^8$B in the resonance scattering of radioactive $^7$Be by hydrogen

V. Z. Gol'dberg,[a] G. V. Rogachev, M. S. Golovkov, V. I. Dukhanov, I. N. Serikov, and V. A. Timofeev
*Kurchatov Institute, Russian Science Center, 123182 Moscow, Russia*

(Submitted 8 May 1998)
Pis'ma Zh. Éksp. Teor. Fiz. **67**, No. 12, 959–963 (25 June 1998)

The excitation function is measured for $^7$Be$+p$ elastic resonance scattering at an angle of 180° in the center-of-mass frame. The measurements are made by a new method which combines the advantages of inverse kinematics and thick targets. New information is obtained about the structure of the levels in the $^8$B nucleus. © *1998 American Institute of Physics.* [S0021-3640(98)00112-1]

PACS numbers: 25.40.Ny, 27.20.+n

The study of exotic nuclei is one of the most interesting topics in nuclear physics today. The production of radioactive beams is the most fundamental means of advancing along the difficult path of attaining the limits of nuclear stability.

In the prominent research centers of the world, radioactive beams are produced by fragmentation of ''ordinary'' nuclei accelerated up to high energies (from 35 MeV/A up to 1 GeV/A). Complicated magnetic systems are used to separate the products of fragmentation. The selected products of nuclear reactions (radioactive beams) have an energy close to that of the primary beams and are characterized by a large energy spread (as compared with ''ordinary'' beams) and an intensity at least seven orders of magnitude lower than that of the primary beams. It should be noted that the high energy of radioactive beams can also be viewed as a disadvantage for effecting standard nuclear reactions, since this energy is much higher than the Fermi energy in nuclei. Decreasing the energy leads to a sharp loss of intensity.

In Ref. 1 a method of using ordinary cyclotrons to obtain radioactive beams is described. In this method heavy ions with energy 5–10 MeV/A bombard a target consisting of a light material. The cost in terms of primary-beam intensity and thickness of the primary target (on account of the comparatively low energy) is largely compensated by favorable kinematics and large cross sections of the process, which can be of a resonance character because of the low relative energy in the center-of-mass frame. Finally, the radioactive-beam energy obtained lies in a range that is convenient for studying (secondary) resonance scattering by a method employing the advantages of inverse kinematics and very thick gas targets (the Gol'dberg method[2–4]). The present letter reports the first physical results obtained on the cyclotron at the Kurchatov Institute Russian Science Center. Using the above-indicated methods of obtaining radioactive beams, we obtained new experimental data on the levels of the $^8$B nucleus. This nucleus is of

 

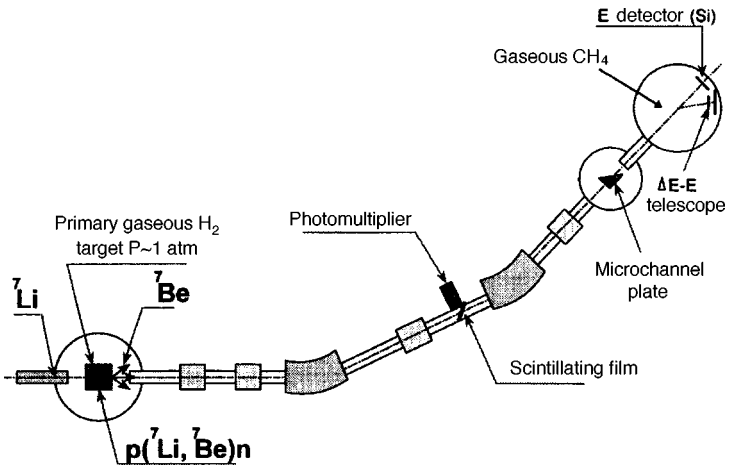


FIG. 1. Diagram of the experimental MASÉ apparatus used to obtain a radioactive $^7$Be beam in the cyclotron at the Kurchatov Institute Russian Science Center. A scattering chamber filled with methane ($CH_4$) is located at the end of the MASÉ.

well-known astrophysical interest as a source of solar neutrinos and is interesting as a boundary nucleus — a likely candidate for having a proton halo. Information about the level scheme in the $^8$B nucleus (which is the mirror nucleus of $^8$Li) is also important for explaining the $\beta$ decay of $^8$He and as a test for three-body approaches to solving problems in nuclear physics. In addition, because of the experimental difficulties of studying the $^8$B nucleus, the quantum characteristics of only one excited state with isotopic spin $T=3^+$ (2.32 MeV) are known reliably.

In the present work the levels of $^8$B were studied in resonance elastic scattering of $^7$Be by hydrogen. The $^7$Be nucleus was obtained in the reaction $^8$Li($p$, $n$) by bombarding a gaseous hydrogen target with $^7$Li ions accelerated to 53 MeV in the cyclotron at the Kurchatov Institute Russian Science Center. The $^7$Be nuclei (and other products of the interaction of $^7$Li with the primary target) were analyzed with an MASÉ magnetic separator. The experimental arrangement is shown in Fig. 1. A thin (20 $\mu$m) organic scintillator, which was viewed by a photomultiplier, was placed at the center of the separator. The scintillating film served as a degrader (making it possible to achieve better separation of $^7$Be by adjusting the magnetic stiffness in the second arm of the MASÉ in accordance with the $^7$Be losses in the film) and as a source of the time signal for time-of-flight analysis of the particles. Moreover, the pulse-height spectrum of the photomultiplier was analyzed, making it possible to separate $^7$Be from lighter impurities $^4$He, $^3$He, and $p$. At the end of the separator (in front of the secondary target) the ions passed through a thin film — a source of electrons for a microchannel plate (MCP). The photomultiplier and MCP signals were used for analysis of the time of flight through a 2-m-long section of the MASÉ. The temporal resolution was equal to approximately 1 ns. Such an analysis made it possible to separate $^7$Be without appreciable admixtures of other particles. The intensity of a 32 MeV $^7$Be beam (in front of the secondary target) was equal to $10^4$ particles/s. The separated beam of radioactive $^7$Be nuclei was directed onto an entrance foil partitioning the scattering chamber volume from the MASÉ. The scattering chamber was

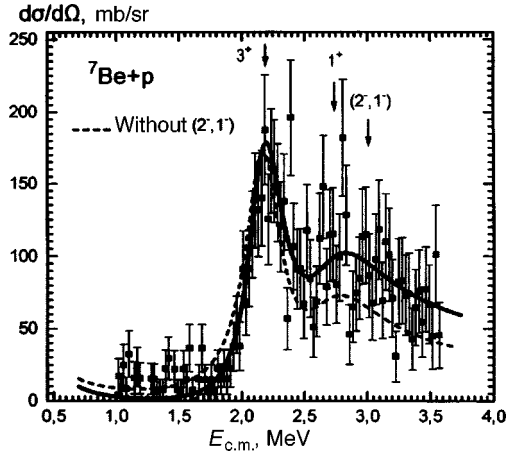


FIG. 2. $^7$Be+$p$ elastic scattering excitation function measured at an angle of 180° in the center-of-mass frame. The solid curve is a best fit according to the potential model using three resonances ($3^+$ fixed). The dashed line shows the fit without the $2S(2^-,1^-)$ level.

filled with methane ($CH_4$) at a pressure chosen so that the $^7$Be nuclei would stop in front of the detector, arranged at an angle of 0° in the laboratory frame. Besides the single detector, a $\Delta$E–E telescope, placed next to the single detector at an angle close to 0°, was used. The detector detected recoil protons produced as a result of the scattering of $^7$Be by the protons in the methane molecules. The analysis was performed according to the specific and total energy losses in the telescope and according to the time of flight (relative to the MCP signal) and energy in the single detector. Control measurements were performed with a $^7$Li primary beam obtained under the same conditions as the $^7$Be beam. The overall accuracy of the energy calibration (better than 20 keV) and the energy resolution (better than 30 keV) were estimated according to the known levels of $^8$Be. More information about the methods used can be found in Refs. 2–4.

Figure 2 shows the measured excitation function, converted to the center-of-mass frame, for the elastic scattering of $^7$Be by hydrogen at an angle of 180°. The absolute accuracy of the measurements is determined mainly by the admixtures of other particles in the $^7$Be beam, other gases in the $CH_4$, uncertainties in the determination of the pressure in the target, and uncertainties in the calculation of the specific losses of $^7$Be in the gas. Estimation of all factors shows that this accuracy is better than 25%.

We chose a potential approach in the spirit of Ref. 5 for analysis of the excitation function. The conventional $R$-matrix analysis was rejected because the expected density of states is low, and the potential approach makes it possible to compare easily the spectra of the $^8$Li and $^8$B mirror nuclei. The standard Woods–Saxon potential with ''reasonable'' parameters was used to describe the spectrum of the states of the $^8$Li and $^8$B nuclei. It is easy to match the positions of the levels by varying the depth of the potential, but the computed widths of the states are always found to be appreciably greater than the experimental values (specifically, this fact clearly indicates the complicated, non-single-particle character of the states studied). To permit matching of the width, an additional Gaussian barrier (repulsive potential) at the surface of the nucleus

TABLE I. Levels in $^8$B.

| Level, $I^\pi$ | Energy, MeV ± keV | $\Gamma_{\text{c.m.}}$, keV |
|---|---|---|
| $3^+$ | 2.32±20 | 350±30 |
| $1^+$ | 2.83±150 | 780±200 |
| $(1^-, 2^-)$ | 3.0 | wide |

was introduced in the Woods–Saxon potential. This purely mathematical trick enabled us to describe both the position and the widths of the states. The position and width of the $3^+$ level (2.32 MeV) in $^8$B were fixed in accordance with existing data.[6] The position and width of the $1^+$ level (the 3.21 MeV mirror level in $^8$Li) were varied so as to obtain the best description of the excitation function (Fig. 2). It was found that in all cases of the hypothetical arrangement of the $1^+$ level, in the region studied, the computed cross section was appreciably less than the measured cross section. An example of the calculation is shown in Fig. 2 (dashed line). Since the calculation is based on the single-channel approximation, it predicts the maximum cross section attainable in the absence of decay channels other than decay from $^8$B states back into the $^7$Be ground state. Therefore the result obtained is a direct indication of the existence of another unknown state in the $^8$B nucleus in the region studied. The states closest to this region are states with $l=2$ $(1d)$ and $l=0$ $(2S)$. However, the state with $l=2$ is always too narrow (because of the high centrifugal barrier) compared with the wide measured structure. The assumption that there exists a $2S$ state makes it possible to obtain a very good description of the experiment, as one can see in Fig. 2 (solid curve; the calculation was normalized to experiment with a normalization factor of 1.2). The results obtained are summarized in Table I.

Comparing the data on the $1^+$ level in $^8$B (2.83 MeV), found in the present work, with data on the $1^+$ level in $^8$Li (3.2 MeV)[6] shows that the widths and position of the levels differ from the calculations which take the Coulomb corrections into account on the basis of the potential model. Although data on the $1^+$ level in $^8$Li are sparse (Ref. 7) and investigation of the $\beta$ decay of $^8$He (Ref. 8) shows that this level must be ''shifted'' to lower excitation energies (just as in the present work), the observed discrepancies between the results of the present work and the published data for the $1^+$ level should not be regarded as conclusively established. To obtain a conclusive solution of this problem the statistical reliability of the present results must be improved. Apparently, the most important concrete result of the present work is the observation of a wide, low-lying, $2S$ state in the $A=8$ nucleus. Indeed, the unexpected depression of the $2S$ states plays the main role in the production of a halo of light nuclei lying at the limit of stability, for example, in $^{11}$Be, $^{11}$Li, and so on. The reason for the appearance of the low-lying (or ground) $2S$ states in light nuclei is unclear and is being actively discussed.[9] One of the main ideas for explaining this phenomenon reduces to the assumption of a large deformation of nuclei which have a low binding energy and apparently originates from a conjecture about the structure of the $^{11}$Be nucleus which was published in the monograph by Bohr and Mottleson.[10] In cases of large deformations the single-particle widths of the $S$ levels should decrease sharply.[10] Our earlier observations of wide $2S$ states in $^{11}$N (Ref. 5) and now in $^8$B argue against this hypothesis. It remains to be seen how the new data on the wide $2S$ level will affect the calculations of the cross section for the radiative capture of protons by $^7$Be at energies corresponding to the temperature of the sun.

We thank the Russian Fund for Fundamental Research for financial support under Grant 97-02-17113 and the Soros International Science Foundation for supporting these investigations at an earlier stage.

[a)]e-mail: GOLD@nucint.kiae.su

[1] V. Z. Gol'dberg, Yad. Fiz. **56**(9), 31 (1993) [Phys. At. Nucl. **56**, 1167 (1993)].
[2] K. P. Artemov, O. P. Belyanin, A. L. Vetoshkin *et al.*, Yad. Fiz. **52**, 634 (1990) [Sov. J. Nucl. Phys. **52**, 408 (1990)].
[3] V. Z. Goldberg, *International Conference on Clustering Phenomena in Atoms and Nuclei 1991*, edited by M. Brenner *et al.*, Springer Series in Nuclear and Particle Physics, 1992, p. 366.
[4] K. P. Artemov, M. S. Golovka, V. Z. Gol'dberg *et al.*, Yad. Fiz. **55**, 2615 (1992) [Sov. J. Nucl. Phys. **55**, 1460 (1992)].
[5] L. Axelsson, M. J. G. Borge, S. Fayans *et al.*, Phys. Rev. C **54**, R1511 (1996).
[6] F. Ajzenberg-Selove, Nucl. Phys. A **490**, 1 (1988).
[7] H. D. Knox and R. O. Lane, Nucl. Phys. A **359**, 131 (1981).
[8] L. V. Grigorenko, N. B. Shul'gina, and M. V. Zhukov, Nucl. Phys. A **607**, 277 (1996).
[9] P. G. Hansen, A. S. Jensen, and B. Jonson, Annu. Rev. Nucl. Part. Sci. **45**, 591 (1995).
[10] A. Bohr and B. Mottelson, *Nuclear Structure*, Vols. 1 and 2, Benjamin, New York, 1969, 1975 [Russian translation, Mir, Moscow, 1977].

Translated by M. E. Alferieff

# Sub-Doppler absorption resonances induced by strong radiation

A. S. Baev and A. K. Popov[a)]

*Institute of Physics, Siberian Branch of the Russian Academy of Sciences, Krasnoyarsk State University; Krasnoyarsk State Technical University, 660036 Krasnoyarsk, Russia*

(Submitted 6 April 1998; resubmitted 21 May 1998)
Pis'ma Zh. Éksp. Teor. Fiz. **67**, No. 12, 964–968 (25 June 1998)

New possibilities are demonstrated for eliminating uncompensated Doppler broadening in different types of nonlinear optical processes by means of atomic coherence effects in strong electromagnetic fields are demonstrated. © *1998 American Institute of Physics.* [S0021-3640(98)00212-6]

PACS numbers: 52.50.Gy, 42.50.Hz, 42.65.−k

**1**. Doppler broadening of resonances imposes a number of fundamental limitations on the selectivity of the interaction of electromagnetic radiation with atomic and molecular systems.[1] Methods of two-photon excitation in counterpropagating waves are widely used to eliminate the inhomogeneous broadening of two-photon transitions. However, these methods are applicable only in the case of stepped configurations of the transitions and equal frequencies of the interacting waves. Appreciable departures from the intermediate resonances will substantially reduce the two-photon interaction cross sections. For overcoming these limitations, methods based on the use of strong fields and the change in the frequency-correlation properties of multiphoton processes in strong resonance fields were proposed in Ref. 2 and in subsequent publications.[3–9] It was shown that inhomogeneous broadening can be eliminated and sub-Doppler resonances can be realized even for transition configurations of the Raman-scattering type. In this case, resonance interaction with all atoms simultaneously, irrespective of their velocities, is possible. Methods of inducing sub-Doppler spectral structures in strong laser fields have been attracting increasing attention in recent years in the context of using quantum coherence effects to manipulate the optical properties of atoms and molecules in order to form large cross sections for nonlinear optical processes, spectral windows of transmission and amplification without population inversion, large dispersion of materials and effective population of high-lying levels (Refs. 10–12 and references cited therein). In the present letter we propose new ways of compensating the Doppler broadening and of capturing atoms into resonance over a wide interval of velocities on account of coherence and strong-field effects. The results are illustrated by numerical examples for one of the transition schemes.

**2**. The main idea consists of the following. Let an atom interact with one strong field $E_2$ at a frequency $\omega_2$ close to the transition frequency $\omega_{21}$ (Fig. 1, where $E_3=0$). On account of induced transitions between the resonance states, their probability amplitudes

 

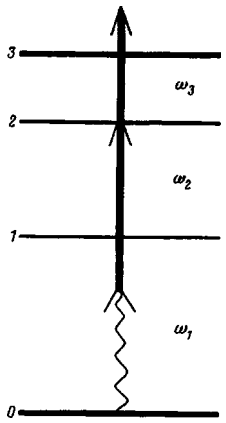


FIG. 1. Transition scheme for eliminating Doppler broadening and capture of atoms into resonance over a wide interval of velocities.

are modulated; for a high frequency of the induced transitions this modulation is manifested, for probe radiation at an adjacent transition, as a splitting of the common level into two quasilevels. Resonance detunings for weak probe radiation $\Omega_1=\omega_1-\omega_{10}$ correspond to the values[2,3,6,9]

$$\Omega_1^{(1,2)}=-\alpha_{1,2}=-\frac{1}{2}\{\Omega_2\pm\sqrt{4|G_{12}|^2+\Omega_2^2}\}, \tag{1}$$

where $\Omega_2=\omega_2-\omega_{21}$, and $G_{12}=E_2d_{12}/2\hbar$ is the Rabi frequency. Hence it follows that the correlation factors of the frequencies $\omega_1$ and $\omega_2$ at the corresponding resonances are determined by the expression

$$M_{1,2}=\frac{d\alpha_{1,2}}{d\Omega_2}=\frac{1}{2}\left[1\pm\frac{\Omega_2}{\sqrt{4|G_{12}|^2+\Omega_2^2}}\right], \tag{2}$$

so that $M_1+M_2=1$ always. In weak fields ($|G_{12}|^2\ll\Omega_2^2$) one has $\Omega_1^{(1)}=-\Omega_2$ and $\Omega_1^{(2)}=0$, while the correlation factors assume the values $M_2=1$ and $M_1=0$, corresponding to two-photon and step processes. In strong fields ($|G_{12}|^2\gg\Omega_2^2$) the correlation factors $M_1$ and $M_2$ become equal, with a value of 1/2, i.e., they do not correspond to either single- or two-photon processes.

For atoms moving with velocity $\mathbf{v}$ all the detunings, on account of the Doppler shift, must be replaced by $\Omega'_{1,2}=\Omega_{1,2}-\mathbf{k}_{1,2}\cdot\mathbf{v}$, where $\mathbf{k}_{1,2}$ are the wave vectors of the corresponding radiation. With the aid of Eq. (1), from the condition $\Omega_1^{1,2}-\mathbf{k}_1\cdot\mathbf{v}=-\alpha_{1,2}(\Omega'_2)$ for $|\Omega_2|\gg|\mathbf{k}_2\cdot\mathbf{v}|$ we obtain, to first order in $\mathbf{k}_2\cdot\mathbf{v}/\Omega_2$,

$$\Omega_1^{(1,2)}-\mathbf{k}_1\cdot\mathbf{v}=-(\alpha_{1,2}-M_{1,2}\mathbf{k}_2\cdot\mathbf{v}). \tag{3}$$

In weak fields ($|G_{12}|^2\ll\Omega_2^2$) we obtain from Eq. (3) the well-known condition for two-photon resonance to occur for all atoms simultaneously: $\mathbf{k}_1=-\mathbf{k}_2$ ($\omega_1=\omega_2$). For transition configurations of the Raman-scattering type the condition (3) becomes

$$\Omega_1^{(1,2)}-\mathbf{k}_1\cdot\mathbf{v}=\alpha_{1,2}-M_{1,2}\mathbf{k}_2\cdot\mathbf{v} \tag{4}$$

In strong fields, since $M_{1,2}$ differ substantially from 1, the conditions (3) and (4) can also be satisfied for $k_1 \neq k_2$. Therefore, with the correct choice of the intensity of the strong radiation the field-induced level shifts, which in turn depend on the velocities, can compensate the Doppler shifts and result in capture of the atoms into resonance over the entire velocity interval, even for $\omega_1 \neq \omega_2$, i.e., even at Raman-scattering type transitions.[2,3,9]

**3**. We shall now present the results of an investigation of new possibilities for manipulating sub-Doppler resonances with the aid of additional strong fields for different types of nonlinear optical resonance processes. For definiteness, we shall consider the nonlinear optical process shown in Fig. 1. For greater clarity, we shall consider the case where the radiation field at the 01 transition is so weak that the change in the populations of the levels can be neglected. Then the formula for the probability of absorption of $\hbar\omega_1$ photons per unit time can be represented in the form (see Ref. 13, Eqs. (24) and (26))

$$w(\Omega_1) = 2\,\mathrm{Re}\left\{ \frac{|G_{01}|^2}{P_{01}} \frac{1}{1+|G_{12}|^2/P_{01}P_{02}[1+|G_{23}|^2/P_{02}P_{03}]} \right\}, \tag{5}$$

where

$$G_{01} = E_1 d_{01}/2\hbar, \quad G_{23} = E_3 d_{23}/2\hbar,$$

$$P_{01} = \Gamma_{01} + i(\Omega_1 - \mathbf{k}_1 \cdot \mathbf{v}), \quad P_{02} = \Gamma_{02} + i[\Omega_1 + \Omega_2 - (\mathbf{k}_1 + \mathbf{k}_2) \cdot \mathbf{v}],$$

$$P_{03} = \Gamma_{03} + i(\Omega_1 + \Omega_2 + \Omega_3 - \mathbf{k_s} \cdot \mathbf{v}), \quad \mathbf{k_s} = \mathbf{k}_1 + \mathbf{k}_2 + \mathbf{k}_3,$$

and $\Gamma_{ij}$ are the homogeneous half-widths of the corresponding transitions.

Reducing this expression to a common denominator, we obtain

$$w(\Omega_1) = 2\,\mathrm{Re}\left\{ |G_{01}|^2 \frac{P_{02}P_{03} + |G_{23}|^2}{P_{01}\tilde{P}_{02}P_{03}} \right\}, \tag{6}$$

where $\tilde{P}_{02}$ describes a two-photon resonance modified by strong fields:

$$\tilde{P}_{02} = P_{02} + \frac{|G_{12}|^2}{P_{01}} + \frac{|G_{23}|^2}{P_{03}}. \tag{7}$$

Assuming that the detuning of the fields from single-photon resonances is much greater than not only the homogeneous but also the Doppler widths of the transitions, and taking the Doppler shifts into account in Eq. (7) in the first nonvanishing approximation, we obtain

$$\tilde{P}_{02} = \tilde{\Gamma}_{02} + i\tilde{\Omega}_{02} - i\left\{ \left( 1 + \frac{|G_{12}|^2}{\Omega_1^2} \right) \mathbf{k}_1 + \mathbf{k}_2 + \frac{|G_{23}|^2}{(\Omega_1 + \Omega_2 + \Omega_3)^2} \mathbf{k_s} \right\} \cdot \mathbf{v}, \tag{8}$$

where $\tilde{\Omega}_{02}$ and $\tilde{\Gamma}_{02}$ have the form

$$\tilde{\Omega}_{02} = \Omega_1 + \Omega_2 - \frac{|G_{12}|^2}{\Omega_1} - \frac{|G_{23}|^2}{\Omega_1 + \Omega_2 + \Omega_3}, \tag{9}$$

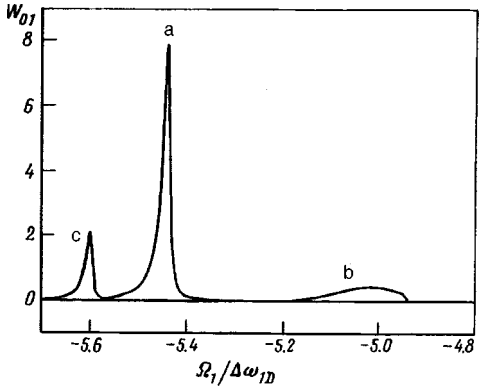


FIG. 2. Probe-field absorption resonances: Curve a — sub-Doppler resonance in a strong field $E_2$ ($E_3=0$), b — the same, if the conditions for eliminating Doppler broadening are not satisfied, c — compensation of the residual Doppler broadening by means of a strong field $E_3$. All curves are normalized to the value of the linear absorption at the center of the Doppler-broadened single-photon resonance.

$$\tilde{\Gamma}_{02}=\Gamma_{02}+\frac{|G_{12}|^2}{\Omega_1^2}\Gamma_{01}+\frac{|G_{23}|^2}{(\Omega_1+\Omega_2+\Omega_3)^2}\Gamma_{03}.$$

Formula (8) demonstrates the possibility of obtaining a narrowed two-photon resonance in absorption of the probe field in the presence of two strong fields with different ratios of the wave vectors of the interacting radiations, even if the conditions for compensation of the Doppler broadening at the transition 02 in the absence of the field $E_3$ are not satisfied. The effects under discussion are a consequence of atomic coherence excited by the strong fields at the interacting transitions.

We shall illustrate the main results in a numerical model of the transitions of the Li atom with the following parameters: $\lambda_{01}=670.784$ nm, $\lambda_{12}=610.364$ nm, $\lambda_{23}=1091.91$ nm, $\Gamma_{01}=2.85$ MHz, $\Gamma_{12}=8.35$ MHz, $\Gamma_{23}=6.30$ MHz, and the Doppler half-widths are, respectively, $\Delta\omega_{1D}=1.362$ GHz, $\Delta\omega_{2D}=1.497$ GHz, and $\Delta\omega_{3D}=0.837$ GHz. The homogeneous half-width of the two-photon transition is $\Gamma_{02}=5.5$ MHz.

**4**. Let us consider first the case where the field $E_3$ is switched off. Let the detuning of the field $E_2$ from resonance be much greater than the Doppler width of the transition 12, and let the intensity correspond to the condition $k_1=M_1k_2$, where $M_1$ is the correlation factor (2). For the present numerical model with detuning $\Omega_2=6.68$ GHz the Rabi frequency required to eliminate its broadening is $G_{12}=2.32$ GHz. The half-width of the narrowed ''quasi-two-photon'' resonance in the field of the counterpropagating waves of different frequency is equal to approximately 10 MHz, while the position of the resonance is shifted relative to that of the resonance in weak fields (Fig. 2, curve a). The resonance detuning of the probe field in this case is determined by Eq. (1) for $\Omega_1^{(1)}$.

For transitions with frequencies differing by almost a factor of 2 ($\omega_{10}/\omega_{21}\geqslant 0.5$), the quantity $G_{12}$ required to obtain a narrow resonance increases to 10–100 GHz, which corresponds to a light field with intensity of the order of 10 MW/cm$^2$.

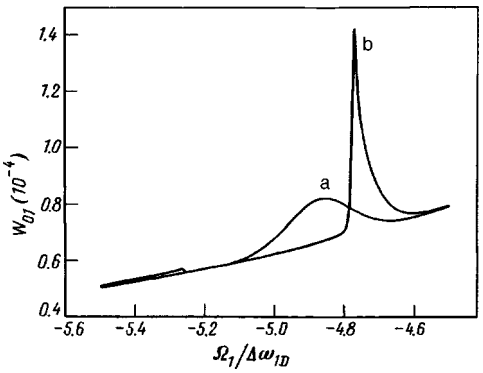


FIG. 3. Probe-field absorption resonances in the presence of another weak counterpropagating wave with different frequency $\omega_2$: Curve a — Doppler-broadened two-photon resonance in the absence of the field $E_3$, b — compensation of Doppler broadening by means of a strong field $E_3$. The curves are normalized to the value of the linear absorption at the center of the Doppler-broadened single-photon resonance.

If the intensity of the strong field $E_2$ is less than optimal ($G_{12}=1.16$ GHz), then the condition for obtaining a Doppler-free resonance is not satisfied, and the height of the peak decreases while the width increases (Fig. 2, curve b). Switching on an additional strong field $E_3$ propagating in a direction opposite to the shortest-wavelength radiation $E_2$ makes it possible to reduce once again the width of the resonance to a minimum (Eq. (9)) and to increase the absorption cross section for $\omega_1$ photons (Fig. 2, curve c). The required values are $G_{23}=2.15$ GHz and $\Omega_3=-5.04$ GHz.

**5**. Let us examine one more variant of sub-Doppler spectroscopy, where the intensity of the counterpropagating waves $E_1$ and $E_2$ is low, while their frequencies are chosen to be different so as to approach an intermediate resonance with level 1. In this case, the absorption cross section grows approximately by 6 orders of magnitude, but the condition for compensation of Doppler broadening at the transition 02 is not satisfied, and the two-photon absorption linewidth cannot be narrower than $|k_1-k_2|\bar{v}$ ($\bar{v}$ is the thermal velocity). When an additional strong field of frequency $\omega_3$, propagating in the opposite direction to the wave $E_2$, is switched on, it becomes possible (Eq. (8)) to obtain a narrowed line having a linewidth comparable to the minimum possible two-photon absorption linewidth in weak fields (i.e., when $\mathbf{k}_1=-\mathbf{k}_2$) (Fig. 3). The illustrations correspond to the same transitions in Li with $G_{12}=8.35$ MHz and $\Omega_2=6.68$ GHz ($(k_2-k_1)/k_1\approx 0.1$). Curve a corresponds to $E_3=0$; curve b corresponds to the same conditions but in the presence of a strong field $E_3$ with $G_{23}=0.45$ GHz and $\Omega_3=0.94$ GHz, propagating in the same direction as the wave $E_1$.

**6**. In conclusion, we note that the possibilities examined above can be easily extended to transition schemes of the Raman-scattering type as well as to schemes where all three fields interact with a common intermediate level.

When the difference of the frequencies of the fields interacting with adjacent transitions is large, compensation of the Doppler broadening requires high intensities of the additional radiation. As the intensity of the radiation increases, the Doppler-free resonance undergoes field-induced broadening. However, this conflict can be overcome, since the magnitude of the field-induced broadening is proportional to the product of the in-

tensities of the interacting radiation, while elimination of Doppler broadening can be accomplished by increasing the intensity of only one of the fields.

This work was performed under the financial support of the Russian Fund for Fundamental Research (Grants 96-02-00010C, 97-02-00016G, and 97-02-16092).

[a)]e-mail: popov@cc.krascience.rssi.ru

---

[1] V. S. Letokhov and V. P. Chebotaev, *Nonlinear Laser Spectroscopy*, Springer-Verlag, Berlin, 1977 [Russian original, Nauka, Moscow, 1975].
[2] T. Ya. Popova, A. K. Popov, S. G. Rautian, and A. A. Feoktistov, Zh. Éksp. Teor. Fiz. **57**, 444 (1969) [Sov. Phys. JETP **30**, 243 (1970)].
[3] A. K. Popov and L. N. Talashkevich, in *Proceedings of the International Conference on the Physics and Chemistry of Laser-Induced Processes in Molecules*, Edinburgh, U. K., 1978 (in *Laser-Induced Processes in Molecules*, edited by K. L. Kompa and S. F. Smith, Springer-Verlag, 1979, p. 161); Opt. Commun. **28**, 315 (1979).
[4] C. Cohen-Tannoudji, F. Hoffbeck, and S. Reynaud, Opt. Commun. **27**, 71 (1978).
[5] S. Reynaud, M. Himbert, J. Dupont-Roc *et al.*, Phys. Rev. Lett. **42**, 756 (1979).
[6] A. K. Popov, in *Proceedings of the International Conference LASERS '79*, STS Press, McLean, Virginia, 1980, p. 295.
[7] A. K. Popov and V. M. Shalaev, Opt. Commun. **35**, 189 (1980); in *Proceedings of the International Conference LASERS'81*, USA, STS Press, McLean, Virginia, 1981, p. 148; Appl. Phys. (N.Y.) **27**, 63 (1981); Opt. Spektrosk. **49**, 617 (1980) [Opt. Spectrosc. **49**, 336 (1980)]; Kvantovaya Élektron. (Moscow) **7**, 1362 (1980) [Sov. J. Quantum Electron. **10**, 785 (1980)];Kvantovaya Élektron. (Moscow) **9**, 488 (1982) [Sov. J. Quantum Electron. **12**, 289 (1982)].
[8] S. Reynaud, M. Himbert, J. Dalibard *et al.*, Opt. Commun. **42**, 39 (1982).
[9] A. K. Popov, *Introduction to Nonlinear Optics* [in Russian], Nauka, Novosibirsk, 1983.
[10] G. S. Agarwal and W. Harshawardhan, Phys. Rev. Lett. **77**, 1039 (1996).
[11] G. Vemuri, G. S. Agarwal, and D. Nageswara Rao, Phys. Rev. A **53**, 2842 (1996).
[12] Yifu Zhu and T. N. Wasserlauf, Phys. Rev. A **54**, 3653 (1996).
[13] A. K. Popov, Izv. Ross. Akad. Nauk, Ser. Fiz. **60**, 99 (1996).

Translated by M. E. Alferieff

# Growth of crystallites consisting of $C_{60}$ molecules on heated (100)Mo

Z. Vakar, N. R. Gall', I. V. Makarenko, E. V. Rut'kov, A. N. Titkov, A. Ya. Tontegode, and M. M. Usufov

*A. F. Ioffe Physicotechnical Institute, Russian Academy of Sciences, 194021 St. Petersburg, Russia*

(Submitted 27 February 1998; resubmitted 5 May 1998)
Pis'ma Zh. Éksp. Teor. Fiz. **67**, No. 12, 969–972 (25 June 1998)

The initial stages of growth of films of $C_{60}$ molecules on a (100)Mo surface are studied by high-resolution Auger spectroscopy and atomic force microscopy under ultrahigh vacuum conditions. It is shown that at $T<750$ K, after a specific coating with molecular density $1.5\times10^{14}$ cm$^{-2}$, which the authors term a high-temperature (HT) monolayer, has formed on the surface, crystallites in the form of ''towers'' with flat tops grow on the surface. The fraction of the area occupied by towers depends strongly on the substrate temperature and the flux density of the molecules on the surface but is virtually independent of the exposure time. At temperatures $T>760$ K the $C_{60}$ molecules making up the crystallites desorb, while the molecules making up the HT monolayer decompose, and the carbon released is dissolved in the interior of the substrate. 
[S0021-3640(98)00312-0]

PACS numbers: 81.05.Tp, 81.15.Ef, 61.16.Ch

The adsorption of fullerene molecules on solid surfaces and the growth of films consisting such molecules are attracting great scientific and practical interest.[1–6] Unfortunately, at the present time there is no reliable information about the character of the growth of thin films consisting of fullerene molecules at high temperatures (500–800 K). Earlier, we studied the adsorption of $C_{60}$ molecules and the contact and thermal stability of these molecules on (111)Ir (Ref. 1) and (1010)Re (Ref. 2) surfaces, and we showed that up to temperatures $\sim$700–750 K the $C_{60}$ molecules do not decompose on the surface of these metals. In the present work our intention is to study the growth mechanisms of thin films of $C_{60}$ molecules on the (100) face of a textured Mo ribbon.

The experiments were conducted in an ultrahigh vacuum (UHV) high-resolution ($\Delta E/E<0.1\%$) Auger spectrometer.[7] Thin $50\times1.0\times0.02$ mm molybdenum ribbons were used as substrates. The ribbons were textured by heat treatment with an ac current at $T=2200$ K, and the (100) face, with a work function $e\varphi=4.45$ eV, emerged at the surface. The surface was uniform with respect to the work function. According to x-ray diffraction data, the degree of orientation of the (100) face to the surface was $\sim$99%. The ribbons were cleaned by annealing first in an oxygen atmosphere ($p_{O_2}=1\times10^{-5}$ torr,

 

$T=1600$ K) and then in UHV ($p=10^{-10}$ torr) at $T=2200$ K. After cleaning, no Auger peaks other than those of molybdenum were observed on the surface of a ribbon.

The $C_{60}$ molecules were deposited *in situ* from a Knudsen cell, loaded with a 99.5% pure powder of $C_{60}$ molecules. The source made it possible to obtain a stable flux of molecules in the range $\nu_{C_{60}}=10^{11}-10^{14}$ molecules/cm$^2$s. Special mass-spectrometric investigations showed that the flux from the evaporator consisted only of $C_{60}$ molecules.

In our Auger electron spectroscopy (AES) investigations we employed the KVV Auger signal of carbon with $E\simeq 270$ eV and the NOO Auger signal of molybdenum with $E=221$ eV. To characterize adsorbed layers greater than one monolayer thick we used predominantly the degree of attenuation of the Auger signal of the substrate — this method is very informative because of the high intensity of the Mo Auger signal. Auger signals were recorded directly from the heated sample and during deposition of the $C_{60}$ molecules.

The topography of the fullerene films formed was investigated by atomic force microscopy (AFM) under room conditions. For this, the samples were removed from the UHV chamber and placed in the atomic force microscope, which gives close to atomic spatial resolution in investigations of dielectric films.

The AES investigations showed that the adsorption of $C_{60}$ molecules on (100)Mo at room temperature results in layerwise filling of the surface with the adsorbate. At first a monolayer of $C_{60}$ molecules with approximate density $N_{C_{60}}=2\times 10^{14}$ molecules/cm$^2$ is formed. This monolayer decreases the intensity of the Auger signal of the substrate by a factor of four.[3] Two layers screen the substrate by a factor of 16, three layers by a factor of 64, and so on.

Adsorption of molecules on heated metal gives completely different results. It was found that $C_{60}$ molecules on heated Mo decompose at temperatures $T>760$ K, whereupon the energy of the negative spike of the carbon Auger peak increases from $E=269$ eV, corresponding to fullerenes,[1,2] to $E=272$ eV, characteristic for chemisorbed carbon.[7] At lower temperatures, 300–750 K, $C_{60}$ molecules are evidently adsorbed on (100)Mo without decomposing.

Figure 1a shows the change in the carbon and molybdenum Auger signals as a result of the adsorption of $C_{60}$ molecules, deposited with constant flux $\nu_{C_{60}}=5.6\times 10^{11}$ molecules/cm$^2$s (plots *1* and *3*), on a substrate heated to different temperatures. Both Auger signals from the surface rapidly (within 3–4 min) reach quasisteady values characteristic for each temperature and remain practically unchanged with further deposition. These quasisteady values are presented in Fig. 1a.

As one can see, a shelf is present in the plot in the region 700–760 K. We believe that it corresponds to filling of the first layer with fullerene molecules (Fig. 1b). If the distribution of $C_{60}$ molecules on the surface is assumed to be uniform, the concentration of the molecules is somewhat lower than in a monolayer — $N_{C_{60}}=1.5\times 10^{14}$ molecules/cm$^2$. This layer screens the Mo Auger signal by a factor of 2.5, and the density of $C_{60}$ molecules in it does not depend on the density of the deposition flux. We termed such a coating a high-temperature (HT) monolayer. All $C_{60}$ molecules which are deposited on top of the HT monolayer at temperatures $T>700$ K desorb, and further accumulation of material on the surface does not occur. The $C_{60}$ molecules are impossible to

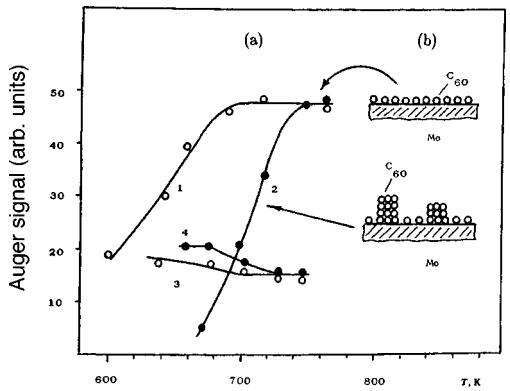


FIG. 1. a — Changes in the quasisteady values of the Auger signals of carbon (curves *3* and *4*) and Mo (curves *1* and *2*) accompanying the deposition of $C_{60}$ molecules on a heated substrate by a constant flux, $\nu_{C_{60}}=5.6\times10^{11}$ molecules/cm$^2$s (curves *1* and *3*) and $\nu_{C_{60}}=6.7\times10^{12}$ molecules/cm$^2$s (curves *2* and *4*). b — Diagram of the structure of an adlayer. Top — high-temperature monolayer of $C_{60}$ molecules, bottom — growth of crystallites in the form of towers.

remove from the HT monolayer by thermal desorption — below 760 K they do not come off; at higher temperatures they decompose, and the carbon released is dissolved in the bulk of the substrate.

In the case of deposition at a low temperature ($T<700$ K), the carbon Auger signal starts to grow, while the molybdenum Auger signal starts to fall off; this attests to accumulation of molecules on the surface. The transition to each successively lower temperature results in a rapid change in both Auger signals to their new quasisteady values, after which further changes occur extremely slowly.

If deposition is stopped at any temperature in the interval 500–700 K, while the temperature of the ribbon is maintained constant, then the Auger signal intensities do not change with time. To remove the deposited molecules the temperature must be raised up to 750 K. In the process the $C_{60}$ molecules desorb and only a HT monolayer remains on the surface. However, the desorption time is directly proportional to the initial exposure in the flux of $C_{60}$ molecules! This means that despite the very weak changes in both Auger signals after the signals reach their quasisteady values, the $C_{60}$ molecules continue to accumulate on the surface, even though Auger spectroscopy is insensitive to the increase in their concentration.

Increasing the flux density of the $C_{60}$ molecules undergoing adsorption (curves *2* and *4* in Fig. 1a) increased the temperature at which fullerene molecules start to accumulate on the surface and shifted the entire curve to higher temperatures.

To explain the observed effects we assumed that they are due to the growth of three-dimensional crystallites consisting of $C_{60}$ molecules. The crystallites consist of towers, whose height and cross section increase as the deposition time increases, but much more rapidly in height than in perimeter (Fig. 1b). An increase in the height of the towers has virtually no effect on either the increase in the carbon Auger signal (the contribution of the third layer of $C_{60}$ molecules to the total carbon Auger signal is 6%, the contribution of the fourth layer is $<2\%$) or on the screening of the substrate, and the Mo

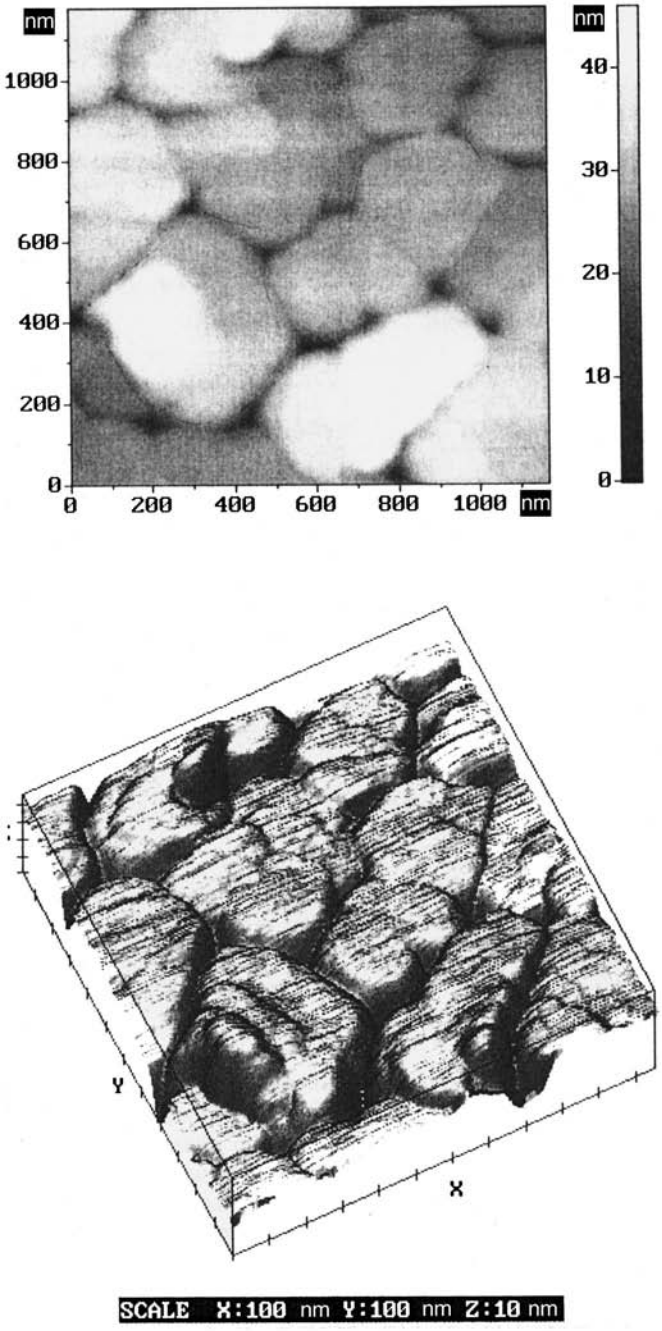


FIG. 2. AFM image of the surface of a molybdenum sample with a film of $C_{60}$ molecules grown on it. The film was grown for 20 min at $T=620$ K with a flux density $\nu_{C_{60}}=1\times10^{13}$ molecules/cm$^2$s.

Auger signal is determined only by the parts of the surface which are free of towers.

At each temperature and $C_{60}$ flux density the fraction of the surface which is occupied by the growing towers takes on a unique quasiconstant value (which changes very slowly). Actually, if the crystallites had tended to merge, then the Auger signal of the substrate would have decreased to zero as a result of the substrate being screened by the fullerene film. However, in all the experiments the Mo Auger signal is nonzero and has an appreciable finite value. Only at the final stages of growth at low temperatures ($\sim$500 K) or for very long deposition times do the crystallites merge to form a continuous fullerite film.

It is logical to suppose that homogeneous nucleation of crystallites of $C_{60}$ molecules occurs in the film. Their concentration should be proportional to the density of the incident flux and should depend strongly on the temperature of the sample. This explains well the rapid decrease in the Auger signal of the substrate on switching from one temperature to another, lower temperature — the concentration of fullerene crystallites increases, and as a result of this the fraction of the surface free of crystallites decreases.

The assumptions examined above concerning the growth of crystallites have found good confirmation in the investigations with an atomic force microscope. Figure 2 shows AFM micrographs of a molybdenum sample on which $C_{60}$ molecules were adsorbed at $T=620$ K over a time of 20 min with a flux density $\nu_{C_{60}}=1\times10^{13}$ molecules/cm$^2$s. Tower-like crystallites with flat tops and separated by deep valleys can be clearly seen . The crystallites are close in area and height; their average transverse size is $\sim$3000 Å, and their density on the surface is $\sim10^9$ cm$^{-2}$.

In summary, an unusual mechanism of film growth was observed at high temperatures under conditions of high-temperature adsorption of $C_{60}$ molecules on a (100)Mo surface— formation of crystallites in the form of towers whose vertical growth rate is appreciably higher than the cross-sectional growth rate. For long deposition times the crystallites merge and a continuous fullerite film forms. This character of the growth of a film of $C_{60}$ molecules can be expected to obtain on other substrates as well.

This work was supported in part by the State Program of the Russian Federation ''Fullerenes and Atomic Clusters,'' Project 98060.

[1] E. V. Rut'kov, A. Ya. Tontegode, and Y. S. Grushko, JETP Lett. **57**, 724 (1993).
[2] N. R. Gall, E. V. Rut'kov, A. Ya. Tontegode, and M. M. Usufov, Mol. Mater. **7**, 187 (1996).
[3] N. R. Gall, E. V. Rut'kov, A. Ya. Tontegode, and M. M. Usufov, *International Workshop on Fullerenes and Atomic Clusters – 1997*, St. Petersburg, Russia, 1997.
[4] Y. Yoshida, N. Tanigaki, and K. Yase, Thin Solid Films **281-282**, 80 (1996).
[5] S. Suto, A. Kasuya, C.-W. Hu *et al.*, Thin Solid Films **281-282**, 602 (1996).
[6] M. C. Abramo and C. Caccomo, J. Chem. Phys. **106**, 6475 (1997).
[7] N. A. Gall, S. N. Mikhailov, E. V. Rut'kov, and A. Ya. Tontegode, Surf. Sci. **191**, 185 (1987).

Translated by M. E. Alferieff

# Quantum corrections to the conductance of AlGaAs/GaAs-based quasiballistic quantum wires

Z. D. Kvon and M. M. Voronin
*Institute of Semiconductor Physics, Siberian Branch Russian Academy of Sciences, 630090 Novosibirsk, Russia*

Kijoon Kim and Hu Jong Lee
*Department of Physics, Pohang University of Science and Technology, 790-784 Pohang, Korea*

(Submitted 20 October 1997; resubmitted 7 May 1998)
Pis'ma Zh. Éksp. Teor. Fiz. **67**, No. 12, 973–976 (25 June 1998)

Quantum conductance corrections (QCCs) due to weak localization and interaction effects of quantum quasiballistic wires are investigated for the first time. At temperatures in the range $2\ \mathrm{K}<T<12\ \mathrm{K}$ a crossover of these corrections from one-dimensional behavior to zero-dimensional behavior is observed. It is shown that the phase coherence length in the wires studied is less than the length $L_T=(\hbar D/kT)^{1/2}$ at all temperatures. It is found that the conventional theory of QCCs describes correctly the experimental temperature dependence of the QCCs but gives a much lower value than the experimental one.
 [S0021-3640(98)00412-5]

PACS numbers: 73.61.Ey, 73.20.Fz

Quantum interference effects such as the Aharonov–Bohm effect, universal conductance fluctuations, and the weak localization effect in AlGaAs/GaAs heterostructure wires have been the most interesting topics of study in the physics of low-dimensional systems for a decade or so.[1,2] Investigations of the quantum corrections to the conductance of wires has a significant place in this field of research. It has been shown[3–6] that the temperature dependence of the conductance $G$ and the behavior of the magnetoconductance of such wires are in good consistency with the theoretical predictions of weak localization and interaction effects in the one dimension (1D) with the boundary scattering effects taken into account.[6] However, all the previous works have concentrated on the investigation of the quantum conductance corrections (QCCs) of wires in quasiclassical diffusive regime, in which the mean free path $l$ is much less than the length $L$ of the wire and the width $W$ of the wire is much larger than the electron wave length $\lambda$. It is also well known that in the other limit, $l\gg L$ and $W\sim\lambda$ (i.e., the quantum ballistic regime), in the absence of diffusive scattering from the wire boundaries the weak-localization and interaction effects do not occur, but instead a quantized conductance is manifested.[1] However, very often one also encounters a situation where $l$ is comparable to or slightly larger than $L$, and some diffusive boundary scattering occurs at the same time (i.e., a quasiballistic regime). All the quasiballistic and ballistic interferometers operate under such a

 

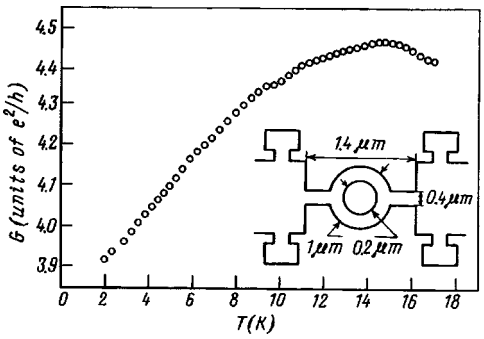


FIG. 1. The typical temperature dependence of the conductance $G$ of a sample. Inset: the sample geometry.

condition.[7–9] To our knowledge, no experimental studies of the QCCs of wires in this regime have been reported. Thus it will be interesting to examine whether the characteristics of the QCCs in the quasiballistic regime are similar to those in the diffusive or ballistic regime. In this study we report, for the first time, the temperature dependence of the conductance of quasiballistic quantum wires for $l \geqslant L \gg W \sim \lambda$ and under conditions of boundary scattering. We have observed clean quantum correction effects to the conductance of the wires as well as the one-dimension-to-zero-dimension (0D) crossover of the corrections. We also show that the phase coherence length $L_\phi$ in the structures studied is less than $L_T = (\hbar D/kT)^{1/2}$.

In this study measurements were taken for 4 samples. The samples had the geometry of a Aharonov–Bohm-type interferometer with a lithographic width of the wire of 0.4 $\mu$m, as shown in the inset of Fig. 1. The samples were fabricated by means of electron lithography and plasma etching on the basis of the high-mobility two-dimensional electron gas formed in AlGaAs/GaAs heterostructures with an electron mobility of $\mu = 4 \times 10^5 \text{cm}^2/\text{V} \cdot \text{s}$, a carrier concentration $N_S = 2 \times 10^{11}\ \text{cm}^{-2}$, and $l = 2.8$ $\mu$m. The ring was located at the center of a Hall bridge with a wire width of 50 $\mu$m and a spacing of 100 $\mu$m between the potentiometric contacts. The total wire length, taking into account the size of the depletion region, was approximately $L \approx 2$ $\mu$m, and the effective wire width was about $W \approx 50-100$ nm. The wire width $W$ was determined from the value of magnetic field corresponding to suppression of the Aharonov–Bohm oscillations when the magnetic length $L_H$ becomes less than $W/2$. Data were taken in the temperature range 0.2 K$< T <$20 K in magnetic fields up to 9 T applied perpendicular to the plane of the substrate. The wire resistance was taken using the conventional phase-sensitive detection technique with a low bias current of 1–10 nA to avoid heating.

Figure 1 shows the typical temperature dependence of the conductance of a wire in the temperature range 2–17 K. In the figure we can identify two temperature regions. In the first one, for $T > 15$ K, the conductance increases as the temperature decreases, which is due to the conventional phonon scattering. In the lower-temperature region below $T < 15$ K, however, the conductance $G$ decreases as $T$ decreases. In this study we concentrate on the behavior in the latter temperature region. We believe that the decrease of the conductance in this temperature region was caused by corrections to $G$ due to the weak localization effect. According to the theoretical predictions, the quantum correction

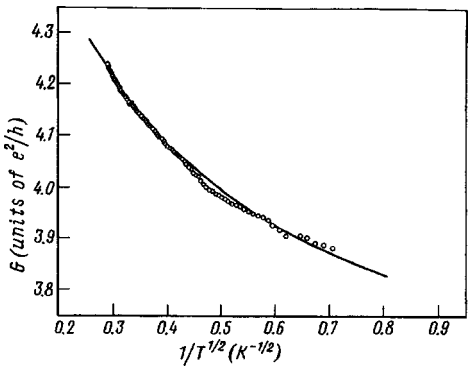


FIG. 2. A replot of the conductance $G$ in Fig. 1 as a function of $T^{-1/2}$. The solid line is a fit to Eq. (1) with $D=4\times10^3$ cm$^2$/V·s, $g_{1D}=7.8$, and $G_0=5.34\cdot$ e$^2$/h.

to $G$ due to the localization in 1D has a temperature dependence $\Delta G\propto T^{-1/2}$ for $\min\{L_\phi, L_T\}\gg W$ and $\max\{L_\phi, L_T\}\ll L$. Figure 2 demonstrates the typical temperature dependence of $\Delta G$ as function of $T^{-1/2}$ in the temperature range of $2\text{ K}<T<13$ K. It is seen that for $T>6$ K the correction $\Delta G$ well follows the $T^{-1/2}$ temperature dependence, but for $T<6$ K the data begin to deviate slightly from this dependence, showing less sensitivity to the temperature change. This implies that under these conditions $\max\{L_\phi, L_T\}$ becomes comparable with the wire length $L$, and 1D-to-2D crossover takes place at around 6 K. At present there is no theory available for giving a quantitative description of the temperature dependence of $\Delta G$ in the quasiballistic regime ($l\geqslant L$), as in our samples. In our samples we have one more complicating factor. It stems from the fact that our samples have a doubly connected geometry. However, still we can analyze the data of our samples in terms of a 1D singly connected wire, since the data in Figs. 1 and 2 were taken in zero magnetic field. Also the behavior of $\Delta G$ in Fig. 2 is very similar to that for quasiclassical disordered wires, so that one can try to fit the data to a theory which is valid for the case of $\lambda\ll l\ll W\ll L$ in a singly connected wire. Including the interaction effect, the theory gives the following expression[4,10] for $\Delta G$ for all temperatures including $T=0$:

$$\Delta G=-g_{1D}\frac{e^2}{\sqrt{2}\pi^2\hbar}\left[\frac{2}{\pi L_T}+\frac{1.79}{L}\right]^{-1}-\frac{e^2}{\pi\hbar}\left[\coth\left(\frac{L}{L_\phi}\right)-\frac{L_\phi}{L}\right], \tag{1}$$

where $g_{1D}$ is a constant depending on the electron–electron interaction in 1D wires. As can be seen in Eq. (1), the value of $\Delta G$ is determined by $L_\phi$ (the weak localization term), $L_T$ (the interaction term), and the length of the wire $L$. Thus information on the phase coherence length $L_\phi$ is essential for examining the behavior of the observed $\Delta G$ in terms of Eq. (1). However, determination of $L_\phi$ by the usual negative magnetoresistance (MR) was impossible for our samples since no negative MR was observed in our quasiballistic samples for $T>1.6$ K. Moreover, the theory of the MR was developed only for 1D wire systems in the quasiclassical diffusion regime, where the conditions $\lambda\ll W$ and $l\ll L$ are satisfied.[1] We determined $L_\phi$ in a piece of wire comprising an interferometer in a sample. In Fig. 3 the typical MR of the wire whose $G$ values are shown in Figs. 1 and 2 is presented at different temperatures. At temperatures above 1.6 K, we distinctly observe a

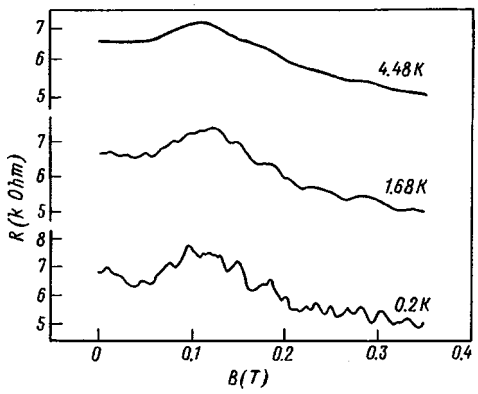


FIG. 3. The magnetoresistance of the same wire sample whose conductance $G$ is shown in Figs. 1 and 2, at various temperatures.

positive MR up to $B=0.1$ T, which remains essentially constant regardless of the temperature change above 1.6 K. This implies that in our samples the MR is governed by the slight diffusive scattering from the boundaries.[1] Also the Aharonov–Bohm oscillations (ABOs) are seen in the data, becoming more prominent as soon the temperature decreases below 2 K. This indicates that the phase-coherence length $L_\phi$ becomes comparable to the wire length at $T<2$ K. At the same time, as we have said, $\max\{L_\phi, L_T\}$ should be comparable to $L$ at $T<6$ K, since in this temperature range the temperature dependence of $\Delta G$ begins to deviate from the $T^{-1/2}$ dependence, indicating that in the temperature range of 2 K$<T<$6 K the condition $L_T>L_\phi$ held in our wires. The phase-coherence length $L_\phi$ can be found from the temperature dependence of the ABOs. The amplitude of the ABOs is proportional to $\exp(-L_P/L_\phi)$ for the case of $L_P>L_\phi$, where $L_P$ is one half of the ring circumference, which can be determined from the period of the ABOs if one assumes that $L_\phi=\alpha T^{-1/2}$. The fit in Fig. 2 was done with the value of $L_\phi[\mu m]=0.4\,T^{-1/2}\,[\mathrm{K}]^{-1/2}$ determined in this way and with three fitting parameters: the diffusion coefficient $D=4\times10^3$ cm$^2$/V·s, the constant $g_{1\mathrm{D}}=7.8$, and the value of the conductance at $T\to\infty$ without the phonon scattering being not taken into account, $G_0=5.34\cdot e^2/h$. The value $D=4\times10^3$ cm$^2$/V·s means that the mean free path $l_w$ in the wire is 2.2 $\mu$m. It is significantly larger than the estimation of $l_w$ from the conductance value ($l_w\sim0.5$ $\mu$m). The value of $g_{1\mathrm{D}}=7.8$ turns out to be quite a bit larger than the value of approximately unity[1] observed previously in AlGaAs/GaAs systems. We believe that the discrepancies occurred mainly because we adopted in the fit ordinary theory of the QCCs developed for dirty quasiclassical wires in the diffusive scattering regime, which thus supposedly had no justification for application to the wires in the quantum quasiballistic regime. More theoretical study is necessary to describe the behavior of the QCCs in this regime.

In summary, we have studied the quantum corrections to the conductance of a AlGaAs/GaAs-based quantum quasiballistic wires. A 1D-to-0D crossover of the corrections has been observed. We have found that the conventional theory of quantum conductance corrections, which is supposedly valid for the diffusive regime only, also gives a good description of the observed temperature dependence of the conductance correc-

tions in the quantum quasiballistic regime, but it gives values of the QCCs much lower than those measured in experiment.

This work was supported in part by BSRI of the Ministry of Education, Korea, under Contract 96-2437 and the Ministry of Defense, Korea, through MARC; by Grant 5-4 of the program ''Physics of Quantum and Wave Processes'' and by Grant 1-038 of the program ''Physics of Solid State Nanostructures'' of the Ministry of Science and Technology, Russia.

[1] C. W. J. Beenaker and H. van Houten, Solid State Phys. **44**, 1 (1991).
[2] S. Washburn and R. A. Webb, Rep. Prog. Phys. **55**, 1131 (1992).
[3] T. J. Tornton, M. Pepper, H. Ahmed *et al.*, Phys. Rev. Lett. **56**, 1198 (1986).
[4] K. K. Choi, D. C. Tsui, and S. C. Palmater, Phys. Rev. B **33**, 8216 (1986).
[5] K. K. Choi, D. C. Tsui, and K. Alavi, Phys. Rev. B **36**, 7751 (1987).
[6] H. van Houten, C. W. J. Beenaker, B. J. Wan Wees, and J. E. Mooji, Surf. Sci. **196**, 144 (1988).
[7] G. Timp, A. M. Chang, J. E. Cunningham *et al.*, Phys. Rev. Lett. **58**, 2814 (1987).
[8] J. Liu, W. X. Gao, K. Ismail *et al.*, Phys. Rev. B **48**, 15148 (1993).
[9] A. A. Bykov, Z. D. Kvon, E. B. Olshanetsky *et al.*, JETP Lett. **58**, 543 (1993).
[10] B. L. Altshuler, A. G. Aronov, and A. Yu. Zyuzin, Zh. Éksp. Teor. Fiz. **86**, 709 (1984) [Sov. Phys. JETP **59**, 415 (1984)].

Published in English in the original Russian journal. Edited by Steve Torstveit.

# Anharmonicity and superconductivity in $Ba_{0.6}K_{0.4}BiO_3$

A. P. Menushenkov,[a] K. V. Klement'ev, P. V. Konarev, and A. A. Meshkov
*Moscow State Engineering Physics Institute, 115409 Moscow, Russia*

(Submitted 12 May 1998)
Pis'ma Zh. Éksp. Teor. Fiz. **67**, No. 12, 977–982 (25 June 1998)

The temperature dependence of the x-ray absorption spectra above the $L_3$ absorption edge of bismuth in the superconducting oxide $Ba_{0.6}K_{0.4}BiO_3$ are investigated. It is found that the local structure is different from the simple cubic structure indicated by x-ray and neutron-diffraction data. It is shown that the oxygen atoms move in an anharmonic double-well potential arising as a result of the existence of two nonequivalent types of octahedral environments of bismuth. Vibrations in such potential modulate the Bi–O bond lengths at the low frequency of the rotational (''tilting'' type) mode of the oxygen octahedra and thus give rise to a strong electron–phonon interaction, which explains the quite high superconducting transition temperatures $T_c \sim 30$ K. © *1998 American Institute of Physics.*
[S0021-3640(98)00512-X]

PACS numbers: 74.72.Yg, 78.70..Dm, 61.66.Fn, 63.20.Ry

The question of the possible equivalence of superconductivity mechanisms in the $BaBiO_3$-based cubic perovskite systems $BaPb_{1-x}Bi_xO_3$ (BPB) and $Ba_{1-x}K_xBiO_3$ (BKB) and in copper-based high-$T_c$ superconductors (HTSCs), which have a layered two-dimensional perovskite structure, remains the key to understanding the nature of high-temperature superconductivity. Important features of the structure of perovskite, such as lattice instability with respect to a soft rotational mode (tilting type) of $CuO_n$ or $BiO_6$ complexes[1,2] and strongly anisotropic thermal vibrational factors for the oxygen ions,[3,4] attesting to a large vibrational amplitude of these ions in the rotational mode,[5] are characteristic for both classes of superconducting oxides — bismuthates and cuprates. The characteristic features indicated make the vibrations of oxygen ions in perovskite-like structures strongly anharmonic. This anharmonic character of the vibrations can be described by motion in a double-well potential and is the basis of the anharmonic model of HTSCs.[6] In this model it has been shown that the anharmonic coupling constant $\lambda_s$ is greater than the constant $\lambda_{ph}$ in the harmonic approximation:

$$\lambda_s/\lambda_{ph} \approx d^2\tilde{\omega}/\langle u^2\rangle\omega_s \gg 1, \tag{1}$$

which explains the high critical temperatures of both cuprate HTSCs and BPB-BKB systems (here $d$ is the amplitude of vibrations in a potential with two minima, $\omega_s$ is the frequency of the soft rotational mode, and $\langle u^2\rangle$ is the mean-square displacement of the ions in the harmonic approximation with average frequency $\tilde{\omega}$).

 

In the anharmonic model a correlation has been established between $T_c$ and structural transitions in La(M)$CuO_4$ (M=Sr, Ba).[7] In experiments on inelastic neutron scattering in $YBa_2Cu_3O_7$ a lattice instability has been observed near $T_c$ relative to displacements of oxygen ions in a local mode of the type where the entire $CuO_5$ pyramid rotates, just as in $LaCuO_4$ (Ref. 8); this has been confirmed by investigations of the local structure by the method of polarization-dependent extended x-ray absorption fine structure (EXAFS) spectroscopy.[9]

These data all indicate a possible connection between the structural instability of perovskitelike lattices and the transition to the superconducting state. However, the layered structure of copper-oxide compounds, the presence of nonequivalent copper sites, and the large number of different Cu–O bond lengths complicate the analysis of the EXAFS spectra. At the same time, the simplicity of the three-dimensional cubic structure of BPB–BKB systems greatly facilitates the interpretation of the experimental data while some similarity is maintained with the features characteristic for perovskitelike lattices.

EXAFS investigations[10,11] of the superconducting composition of BKB with $x=0.4$ have shown that the local structure differs from the ideal cubic structure indicated by the integral methods of structural analysis which are based on neutron or x-ray diffraction.[12] Thus, analysis of the four closest coordination spheres around bismuth[11] has established the presence of local disorder in the form of a rotation of the oxygen octahedra by an angle $\sim 4-5°$ around pseudocubic axes of the type [110] and [111]. The question of the dynamic or static character of the indicated rotation of octahedra cannot be unequivocally resolved solely on the basis of an EXAFS experiment, but the following experimental data support a dynamic character:

— the absence of any indications of static disorder in measurements of the strongly anisotropic thermal factors of oxygen vibrations extended in the direction perpendicular to the Bi–O bond;[3]

— analysis of the radial pair distribution function in neutron-diffraction experiments, indicating a dynamic distortion of the lattice;[13]

— the character of the Raman scattering spectra;[14,15]

— the results of an investigation of diffuse scattering of electrons,[16] and

— data from investigations of NMR and NQR spectra on $^{137}$Ba ions in BPB.[17]

In addition to this, it should be noted that the photoemission spectra indicate a nonequivalence of the environment around bismuth in BKB[18,19] and the impossibility of describing the features of the Bi $4f$ doublet on the basis of an undistorted cubic lattice,[20] while these spectra can be interpreted in favor of a dynamical distortion of the lattice.[21]

In the present letter we report the results of an analysis of low-temperature investigations of EXAFS spectra of the nearest-neighbor oxygen environment of bismuth in $Ba_{0.6}K_{0.4}BiO_3$, performed in the approximation of a dynamical character of the local distortions of the lattice. Analysis shows that the oxygen atoms move in a strongly anharmonic double-well potential which arises as a result of the existence of two different types of octahedral environment of bismuth, remaining nonequivalent in the simple cubic lattice also. The parameters of the potential depend strongly on the potassium content and the temperature. Vibrations in such a potential lead to modulation of the Bi–O bond lengths with a low frequency of the rotational mode of the oxygen octahedra

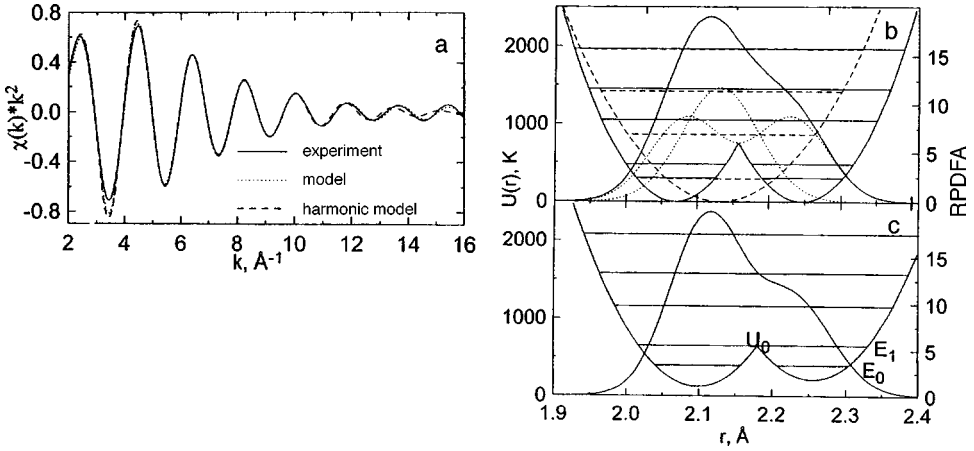


FIG. 1. Analysis of the first coordination sphere of the absorption spectrum at Bi $L_3$ in $Ba_{0.6}K_{0.4}BiO_3$: a — Experimental EXAFS function (solid line), model function (dotted line), and model function in the one-sphere harmonic approximation (dashed line); model potentials for the case of independent (b) and coupled (c) motions of oxygen atoms with the corresponding energy levels and the RPDFA. The model EXAFS function (see dotted line) was constructed for the potential (c).

and thus give rise to a strong electron–phonon interaction; this explains the relatively high superconducting transition temperatures observed in these compounds.

Using a Si(311) double-crystal monochromator, the x-ray absorption spectra were recorded in the D13 line of the DCI storage ring at the LURE synchrotron center (Orsay, France) at an energy of 1.85 GeV with a maximum positron beam current in the ring of 300 mA. The energy resolution of the spectra was $\sim 2$ eV at 13 keV. The low-temperature measurements were performed using a continuous-flow helium cryostat. In an earlier work[22] we described the method for analyzing the EXAFS spectra.

After the frequency dependence of the absorption coefficient above the Bi $L_3$ edge was isolated, the EXAFS function $\chi(k)$ was filtered by means of a Fourier transform in order to obtain the contribution from the nearest oxygen sphere. Figure 1a shows the form of the experimental function $\chi(k)k^2$ (solid line) for the BKB sample with $x=0.4$ at a temperature of 7 K. The phase disruption and necking in the region 12–14 $Å^{-1}$ show that the complicated form of the function cannot be described by a one-sphere harmonic approximation (see dashed curve), so that the vibrational potential of the oxygen atoms is different from a harmonic potential and has a quite complicated form. (It should be noted that the phase disruption and necking noted above were also observed in previously published EXAFS spectra,[10,23] but were not taken into account in the analysis because the spectra were processed in a region artificially limited to values of the wave vector less than 14 $Å^{-1}$.)

To reconstruct the form of the potential we employed the method of constructing a model EXAFS function $\chi(k)$, which has been used previously for describing strongly anharmonic vibrations of the apical oxygen in $YBa_2Cu_3O_{7-\delta}$ (Ref. 9). The potential was constructed on the basis of a model scheme (proposed in Ref. 24) for the dynamic distortion of the BKB lattice which takes into account the asymmetry of the rotational mode (see Fig. 2).

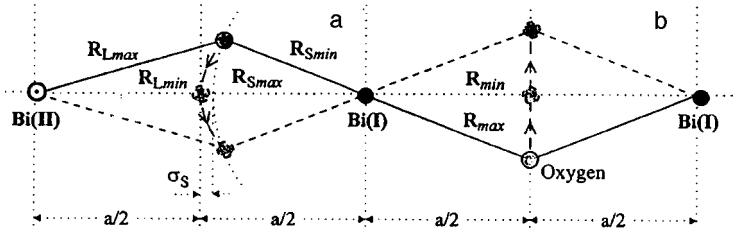


FIG. 2. Scheme of the dynamic local distortion of the $Ba_{0.6}K_{0.4}BiO_3$ lattice. For simplicity, the motion of two of the six oxygen atoms of each octahedron is shown.

EXAFS investigations[10,22] of $BaBiO_3$ have shown that bismuth occupies two nonequivalent positions characterized not only by different lengths (static distortion of the ''breathing'' mode) but also by different Bi–O bond stiffnesses. The $Bi(I)O_6$ octahedral complexes, with a shorter radius, $R_s = 2.12$ Å, have a stiffer bond, characterized by an Einstein temperature $\Theta_E = 490$ K, than do the $Bi(II)O_6$ complexes, with a longer radius ($R_l = 2.28$ Å, $\Theta = 290$ K).[10] The different bond stiffnesses in $BiO_6$ complexes are due to the different electronic structure of the complexes: $Bi(I)L^2O_6$ and $Bi(II)O_6$, where $L^2$ signifies the presence of a pair of holes in the O $2p$ orbitals of the octahedral oxygen environment of bismuth in accordance with the model of Bi valence disproportionation, proposed in Ref. 25. (More precisely, $L^2$ should be understood to be a pair of holes in a strongly hybridized antibonding $6s(\mathrm{Bi})\mathrm{O}2p_\sigma^*$ orbital of the octahedral complex.) A consequence of the differences in the Bi–O bond stiffnesses is the asymmetry, which we observed, of the static rotation of the oxygen octahedra (distortions of the rotational mode) in $BaBiO_3$ at low temperatures.[22]

When $BaBiO_3$ is doped with potassium, the substitution of $K^+$ for every two $Ba^{2+}$ ions produces an additional pair of holes in the $6s(\mathrm{Bi})\mathrm{O}2p_\sigma^*$ orbitals. The number of small, stiff octahedra (carrying a pair of holes) increases in accordance with the ratio of the number of small and large octahedra in $Ba_{1-x}K_xBiO_3$, equal to $(1+x)/(1-x)$. As a result, the static distortions of the ''breathing'' and rotational modes vanish and the average Bi–O bond lengths equalize, but because the Bi–O bond stiffnesses remain different the bismuth positions remain nonequivalent.[24] Therefore the dynamics of the rotational oscillations of oxygen is asymmetric relative to the bismuth atoms in the case when different types of $Bi(I)O_6$–$Bi(II)O_6$ octahedra are adjacent (region in Fig. 2) and symmetric in the case when identical $Bi(I)O_6$ octahedra are adjacent (region b in Fig. 2).

To describe the EXAFS function in the single-scattering approximation it is sufficient to examine a system of two absorber–scatterer atoms, representing their relative vibrations by the vibration of a particle with the reduced mass in the field of a potential that depends on the distance between the particles. For the O atom in region b this potential is harmonic because of the equivalence of the neighboring octahedral complexes: $U_b(r) = A(r-x_1)^2/2$. For region a in Fig. 2, if the absorber atom is Bi(I), then the Bi–O distance to the nearest oxygen atoms is less than half the lattice parameter. However, if the absorber atom is Bi(II), then the Bi–O distance to the nearest oxygen atoms is greater than half the lattice parameter. As a result, two maxima for the first coordination sphere arise in the distribution function of the oxygen atoms relative to bismuth, while the vibrational potential has two minima which are symmetric relative to the center

of the Bi(I)–Bi(II) bond and can be described as a double parabolic potential: $U_a(r) = B(r-x_2)^2/2$ for $r<r_0$ and $B(r-x_3)^2/2$ for $r>r_0$, where $r_0$ is determined from the continuity condition. Next, finding for this potential the eigenenergies $E_n$ and the corresponding wave functions $\Psi_n$, we obtain the radial pair distribution function of the atoms (RPDFA) for Bi–O:

$$g(r)=N\sum |\psi_n(r)|^2\exp(-E_n/kT)/\sum \exp(-E_n/kT),$$

where $N$ is the coordination number, whence we find the EXAFS function:

$$\chi(k)=\frac{1}{k}\sum_{``a'',``b''} |F(k,\pi)| \int_{r_{\min}}^{r_{\max}} [g(r)\sin(2kr+\phi_j(k))/r^2]dr \qquad (2)$$

(here $\varphi(k)$ is the phase shift and $F(k)$ is the scattering amplitude).

Model potentials with the energy levels and the RPDFA for BKB with $x=0.4$ at $T=7$ K are presented in Fig. 1b for the case when the atoms in the regions a and b in Fig. 2 move independently of one another. However, the rotational oscillation of neighboring oxygen atoms in the model of coupled ''stiff'' octahedra is coherent[24] and for this reason the coupled system undergoes oscillations in the total potential obtained by summing the potentials of the regions a and b (Fig. 2), taken with the corresponding weights $(1-x)$ and $x$ (see Fig. 1c). The model EXAFS function constructed on the basis of the potential obtained for the coupled vibrations is presented in Fig. 1a (dotted curve) and shows practically complete agreement with experiment. Figure 1c also shows the RPDFA and the lower energy levels $E_0$ and $E_1$ of the total double-well potential. It should be noted that the large amplitude of the RPDFA in the region of the potential barrier and the fact that $E_1$ is greater than $U_0$ indicate a high probability of tunneling of an oxygen atom between octahedra, i.e., a *dynamic* interchange of positions $Bi(I)O_6 \leftrightarrow Bi(II)O_6$ (the regions a and b likewise change places and a pair of holes is transferred (tunnels) from one octahedron to another). At low temperatures tunneling of the states $Bi(I)O_6 \leftrightarrow Bi(II)O_6$ is most likely involves an oxygen ion traversing the Bi(I)–Bi(II) line (such motion is due to the rotational mode, since the distance between the potential minima is shortest in that case). For this reason, the tunneling frequency should be determined by the frequency $\omega_s$ of the rotational mode. An estimate of the tunneling frequency gives the value $\omega_t = E_1 - E_0 = 251$ K (174 $cm^{-1}$), which agrees well with the frequency $\omega_s = 170-180$ $cm^{-1}$ obtained from the Raman scattering spectra.[15]

It should be noted that formula (1) was obtained in Ref. 6 in the approximation of equal deformation potentials for the anharmonic mode ($s$) and in the harmonic approximation ($ph$), which were averaged over the Fermi surface: $J_s^2 = J_{ph}^2$. However, calculations[26,27] show that the deformation potential of the ''breathing'' (harmonic) mode is almost an order of magnitude greater than the deformation potential of the ''rotational'' (anharmonic) mode, which casts doubt on the correctness of the estimate (1). Our results remove this conflict, indicating that as a result of the nonequivalence of the $BiO_6$ complexes, the asymmetric rotational oscillation in region a of Fig. 2 gives rise to a dynamic interchange $Bi(I)O_6 \leftrightarrow Bi(II)O_6$, which causes an additional modulation of the Bi–O bond lengths that is equivalent to the excitation of the ''breathing'' mode at the low frequency $\omega_t = \omega_s$. Apparently, this is the main reason for the strong electron–phonon interaction in the BKB system and should lead to a large effective electronic

attraction constant $\lambda_s$ ($\lambda_s \sim 1/\omega_s^2$ (Ref. 6)). Our estimates give $\lambda_s \approx 2.6$ for $\omega_s \approx 170$ cm$^{-1}$, which, in accordance with the expression $T_c \approx 0.05\omega_s(\lambda_s - 0.25)$ obtained for an intermediate coupling strength,[28] leads to a critical temperature $T_c \approx 30$ K in $Ba_{0.6}K_{0.4}BiO_3$, in good agreement with experiment.

We thank the program committee at LURE (France) for the opportunity to perform experiments in the synchrotron beam, S. Benazeth and J. Purans for assisting in the experiment, and A. P. Rusakov for providing the BKB samples. This work was supported in part by the Russian Fund for Fundamental Research (Grant 96-02-19099a) and by the program ''Universities of Russia.''

[a)]e-mail: menushen@htsc.mephi.ru

[1] W. E. Pickett, R. E. Cohen, and H. Krakauer, Physica B **169**, 45 (1991); Phys. Rev. Lett. **67**, 228 (1991).
[2] S. Ushida, K. Kitazawa, and S. Tanaka, Phase Transit. **8**, 95 (1987).
[3] J. P. Wignacourt, J. S. Swinnea, H. Steinfink, and J. B. Goodenough, Appl. Phys. Lett. **53**, 1753 (1988).
[4] G. H. Kwei, J. A. Goldstone, A. C. Lawson *et al.*, Phys. Rev. B **39**, 7378 (1989).
[5] R. M. Hazen, in *Physical Properties of High-Temperature Superconductors*, Vol. 2, edited by D. M. Ginsberg, World Scientific, Singapore, 1990, p. 221.
[6] N. M. Plakida, V. L. Aksenov, and S. L. Drechsler, in *Proceedings of the Adriatico Research Conference on HTSC*, Trieste, July 5–8, 1987, World Scientific, Singapore, 1987, p. 1071; Europhys. Lett. **4**, 1309 (1987).
[7] M. K. Grawford, W. E. Farneth, R. L. Harlow *et al.*, Physica C **235-240**, 170 (1994).
[8] M. Arai, R. Yamada, Y. Hidaka *et al.*, Phys. Rev. Lett. **69**, 359 (1992).
[9] J. Mustre de Leon, S. D. Conradson, I. Batistić *et al.*, Phys. Rev. B **45**, 2447 (1992).
[10] S. M. Heald, D. DiMarzio, M. Croft *et al.*, Phys. Rev. B **40**, 8828 (1989).
[11] Y. Yacoby, S. M. Heald, and E. A. Stern, Solid State Commun. **101**, 801 (1997).
[12] S. Pei, J. D. Jorgensen, B. Dabrowski *et al.*, Phys. Rev. B **41**, 4126 (1990).
[13] H. D. Rosenfeld and T. Egami, in *Lattice Effects in High-$T_c$ Superconductors*, edited by Y. BarYam and T. Egami, World Scientific, Singapore, 1992, p. 105.
[14] S. Sugai, S. Ushida, K. Kitazawa *et al.*, Phys. Rev. Lett. **55**, 426 (1985); S. Sugai, Y. Emomoto, and T. Murakami, Solid State Commun. **72**, 1193 (1989).
[15] K. F. McCarty, H. B. Radousky, D. G. Hinks *et al.*, Phys. Rev. B **40**, 2662 (1989); H. Minami, T. Uzumaki, and H. Uwe, in *Proceedings of the Eighth International Symposium on Superconductivity*, Hamamatsu, 1995, *Advances in Superconductivity VIII*, Springer-Verlag, Tokyo, 1996, p. 429.
[16] Y. Koyama and M. Ishimaru, Phys. Rev. B **45**, 9966 (1992); Y. Koyama, S.-I. Nakamura, and Y. Ynoue, Phys. Rev. **46**, 9186 (1992).
[17] K. Kumagai, Yu. V. Piskunov, A. Yu. Yakubovskii *et al.*, Physica C **274**, 209 (1997).
[18] T. J. Wagener, H. M. Meyer III, D. M. Hill *et al.*, Phys. Rev. B **40**, 4532 (1989).
[19] M. W. Ruckman, D. Di Marizio, Y. Jeon *et al.*, Phys. Rev. B **39**, 7359 (1989).
[20] M. Qvarford, V. G. Nazin, A. A. Zakharov *et al.*, Phys. Rev. B **54**, 6700 (1989).
[21] H. Namatame, A. Fujimori, H. Torii *et al.*, Phys. Rev. B **50**, 13674 (1994).
[22] A. P. Menushenkov, S. Benazeth, J. Purans *et al.*, Physica C **277**, 257 (1997).
[23] S. Salem-Sugui Jr., E. E. Alp, S. M. Mini *et al.*, Phys. Rev. B **43**, 5511 (1991).
[24] A. P. Menushenkov, in *Proceedings of the International Workshop on High Temperature Superconductivity — Ten Years After Its Discovery*, Jaipur, India, 1996, edited by K. B. Karg and S. M. Bose, Narosa Publishing House, 1998, p. 155; Nucl. Instrum. Methods Phys. Res. A **405**, 365 (1998).
[25] A. Yu. Ignatov, A. P. Menushenkov, and V. A. Chernov, Physica C **271**, 32 (1996).
[26] L. F. Mattheiss and D. R. Hannan, Phys. Rev. B **28**, 4227 (1983); Phys. Rev. Lett. **60**, 2681 (1988).
[27] M. Shirai, N. Szuki, and K. Motizuki, J. Phys.: Condens. Matter **2**, 3553 (1990).
[28] J. M. Rowell, Solid State Commun. **19**, 1131 (1976).

Translated by M. E. Alferieff

# Observation of coupled $4f$-electron–phonon excitations in the Van Vleck paramagnet TmES in high magnetic fields

D. A. Tayurskiĭ
*Kazan State University, 420008 Kazan, Russia; University of Kanazawa, 920-11, Japan*

M. S. Tagirov
*Kazan State University, 420008 Kazan, Russia*

(Submitted 12 May 1998)
Pis'ma Zh. Éksp. Teor. Fiz. **67**, No. 12, 983–987 (25 June 1998)

A model is proposed for explaining the anomalous behavior of the far-IR absorption spectra of the dielectric Van Vleck paramagnet thulium ethyl sulfate TmES. The good agreement obtained between the calculations and experiment on the basis of the idea of a resonance interaction between $Tm^{3+}$ ions in one of the excited doublet states and optical phonons gives grounds for asserting that coupled $4f$-electron–phonon excitations exist in TmES single crystals in high magnetic fields at liquid-helium temperatures. © *1998 American Institute of Physics.* [S0021-3640(98)00612-4]

PACS numbers: 63.20.Kr, 78.30.Jw, 75.20.Ck

Electron–phonon interaction effects in rare-earth compounds have been under investigation for a long time now. Among different manifestations of the interaction between optical or acoustic phonons and localized $4f$ electrons, the cooperative Jahn–Teller effect — a phase transition observed in some rare-earth zircons, pnictides, and spinels – should be mentioned first and foremost.[1] This phase transition consists of the ''freezing in'' of a static deformation of the crystal lattice and simultaneous orientation of the electric and magnetic multipole moments of the rare-earth (RE) ions and can be attributed to the interaction of rare-earth ions via the phonon field.

Another effect of the interaction between optical phonons and the multipole moments of RE ions in the ground state is observed in a number of RE trifluorides and trichlorides in an external magnetic field at low temperatures (for example, in the paramagnets $CeF_3$ (Ref. 2) and $CeCl_3$ (Ref. 3) and the Ising ferromagnet $LiTbF_4$ (Ref. 4)). If the magnetic field and temperature are such that ordering of the RE magnetic moments in an external field is possible, then on account of the strong spin–orbit interaction this will also lead to ordering of the multiple moments, which in turn changes the phonon spectrum even in the absence of the cooperative Jahn–Teller effect. Specifically, splitting of twofold degenerate phonon states in a magnetic field,[3,4] described by the expression

$$\Delta\omega = \Delta\omega_s \cdot \tanh(g\mu_B B/kt),$$

where $g$ is the $g$ factor of the electronic ground state and $\Delta\omega_s$ is the maximum value of

 

the splitting, has been observed by the method of Raman and infrared spectroscopy. Moreover, ''anticrossing'' between optical phonons and excitations in the $4f$-electron system has been observed in the compounds mentioned. The $4f$-electron–phonon interaction also appears in RE compounds where magnetism of the electronic ground state is absent. For example, splitting of twofold degenerate phonon states in a magnetic field and collective $4f$-electron excitations of the Frenkel type have been observed[5–7] in the Van Vleck paramagnet $PrF_3$.

In the present work the resonance interaction between $4f$ electrons and optical phonons in a Van Vleck paramagnet — thulium ethyl sulfate $Tm(C_2H_5SO_4)_3 \cdot 9H_2O$ (TmES) — is studied. The electron–phonon interaction in ethyl sulfate crystals was studied earlier and was manifested, for example, in the effective exchange interaction via the phonon field between RE Kramers ions $Ce^{3+}$ under pressure.[8] In Ref. 9 we reported the first observation of electronic paramagnetic resonance and infrared absorption in TmES as a result of transitions between the singlet ground state and the first excited doublet of the Van Vleck paramagnetic ion $Tm^{3+}$ in magnetic fields up to 10.5 T. In experiments on infrared absorption in magnetic fields above 2 T, an additional absorption line appeared near 49 $cm^{-1}$ (see Fig. 4 in Ref. 9); the position was independent of the magnetic field up to 6 T, and this line was assigned to a phonon level. In fields above 6 T this phonon line and the line corresponding to a transition in the Stark structure of the $Tm^{3+}$ ion from a singlet ground state to one of the states of the nearest doublet (split by the magnetic field), started to split, leading to a surprising ''crossing–anticrossing'' behavior in fields of about 8.5 T. This was also manifested in the very complicated structure of the ESR spectrum. In Ref. 9 it was noted that this behavior cannot be described without taking into account the spin–phonon and spin–spin interactions. In the present letter we propose a simple model which describes the ''crossing–anticrossing'' behavior on the basis of the idea of a resonance interaction between $4f$ electrons and optical phonons and gives good agreement with experimental data.

In Ref. 10 we investigated the effect of high magnetic fields ($B>5$ T) on the Stark structure of the $Tm^{3+}$ ion in a TmES crystal (ground-state term $^3H_6(J=6)$). At liquid-helium temperatures the magnetic properties of the ions are determined by the three lower levels: a nonmagnetic singlet $|g\rangle$ and the first excited doublet $|d_{1,2}\rangle$, split by the magnetic field. Since the splitting between $|g\rangle$ and $|d_1\rangle|d_2\rangle$ in such magnetic fields is greater than 30 $cm^{-1}$, essentially only the ground-state singlet is populated at $T=4.2$ K (see Fig. 1; at 4.2 K the magnetic moment of the $Tm^{3+}$ ion is determined completely by the magnetic moment of the singlet state, while at 30 K, for example, the contribution of excited states of the doublet is substantial), while transitions to the sublevels of the excited doublet can be induced by an oscillating magnetic field, appropriately directed relative to the external magnetic field.[9,10] The dependence of the polarization magnetic moment (the moment due to mixing of the wave functions of the states of the Stark structure as a result of the Zeeman interaction with an external magnetic field) on the magnitude of the magnetic field $\mathbf{B}_0$ for each state of the $Tm^{3+}$ ion — $|g\rangle$, $|d_1\rangle$, and $|d_2\rangle$ — is presented in Fig. 1. One can see clearly that the magnetic moments in the singlet ground state and in the excited doublet states differ from one another. This means that a transition of the $Tm^{3+}$ ion from $|g\rangle$ to $|d_1\rangle$ or $|d_2\rangle$ is accompanied by a change in the magnetic moment, and each of these transitions can be viewed as a transition in a two-level system. Therefore, taking into account also the fact that according to Ref. 11

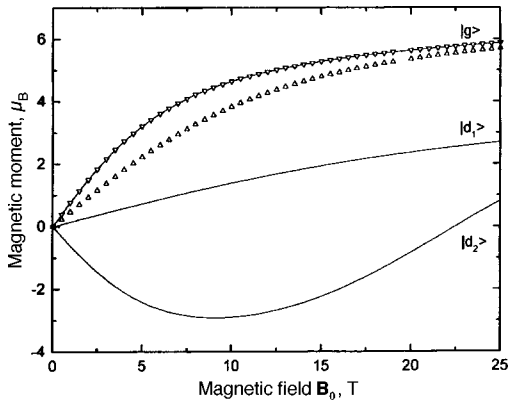


FIG. 1. Field dependence of the magnetic moments of states of the $Tm^{3+}$ ion $|g\rangle$, $|d_1\rangle$, and $|d_2\rangle$ (solid lines) and of the average magnetic moment of the $Tm^{3+}$ ion at temperatures 4.2 K ($\nabla$) and 30 K ($\triangle$).

the lifetime of thulium ions in excited states is quite short, it can be assumed that under our experimental conditions[9] the number of ions in excited states $|d_1\rangle$ and $|d_2\rangle$ is small, so that we can employ the idea of elementary excitations and introduce two types of excitations which do not interact with one another and which correspond to each of the excited states of the doublet. Since in the experiment the ''crossing–anticrossing'' behavior was observed for the phonon line and the transition $|g\rangle \rightarrow |d_2\rangle$, we shall confine ourselves below to elementary excitations of one type corresponding to this transition and described by the Hamiltonian

$$H_{d2} = \sum_q \epsilon_q(B) a_q^+ a_q . \tag{1}$$

Here $a_q^+$ and $a_q$ are Bose creation and annihilation operators for excitations with wave vector $\mathbf{q}$ (Bose statistics was chosen on the basis of the facts that the states of the ''two-level system'' $|g\rangle$ and $|d_2\rangle$ can be described by means of an effective spin $S = 1/2$ and the Holstein–Primakoff transformation can be used because the number of excitations is small) and $\epsilon_q(B)$ is the elementary excitation spectrum as a function of the magnetic field $B$. In experiments on infrared absorption at liquid-helium temperatures single-particle excitations appear only at the zone center ($\mathbf{q} = 0$), so that we shall drop the summation over the wave vectors in Eq. (1) and use the Hamiltonian

$$H_{d2} = \epsilon(B) a^+ a, \tag{1a}$$

where the function $\epsilon(B)$ is found from the experimental points[9] (dotted line in Fig. 2).

The ''excitation'' of the phonon line (49 $cm^{-1}$) in magnetic fields above 2 T is due, in our opinion, to an increase in the polarization moment of the $Tm^{3+}$ ion and is one of the manifestations of the $4f$-electron–phonon interaction. Specifically, either a sufficiently large polarization moment in the singlet ground state can lead to ''freezing in'' of the static deformation and the appearance of localized phonons, or these phonons appear as a result of a reorientation of the magnetic moment of the ion accompanying a transition of the ion from a singlet state into a state of the excited doublet on account of the ac magnetic field (see Fig. 1; the magnetic moments in the states $|g\rangle$ and $|d_2\rangle$ have opposite

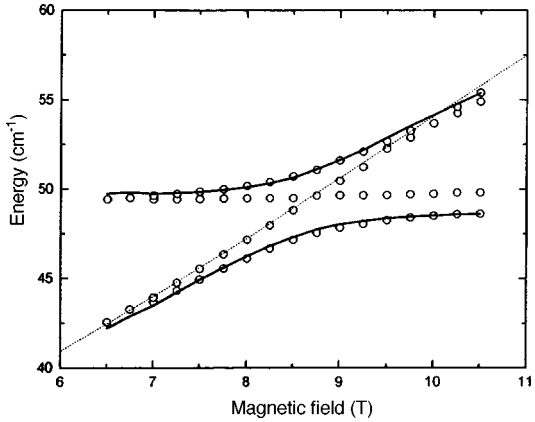


FIG. 2. Energies of elementary excitations in a TmES crystal versus the magnetic field: ○ — experimental points obtained from far-IR Fourier spectroscopy investigations;[9] the dotted line — energy of the transition $|g\rangle \rightarrow |d_2\rangle$ in the system of Stark levels of the $Tm^{3+}$ ion (the function $\epsilon(B)$ in Eq. (1a)); solid lines — computed spectrum of coupled $f$-electron–phonon excitations according to Eq. (4). The values of the adjustable parameters are given in the text.

signs). An answer to the question of which of these two mechanisms is operating can be obtained from experiments investigating the dependence of the intensity of the phonon line on the amplitude of the ac magnetic field (on the intensity of irradiation of the crystal by a laser in the far-IR region). It is obvious that the number of these phonons depends on both the number of thulium ions in the excited state and their polarization moment. For this reason, the following Hamiltonian ($\mathbf{q}=0$) can be used to describe the phonons:

$$H_{\rm ph}=(\omega-\mu(B))b^{+}b, \tag{2}$$

where $b^{+}$ and $b$ are creation (annihilation) operators for phonons with energy $\omega = 49\ \text{cm}^{-1}$ and the function $\mu(B)$ plays the role of a chemical potential and can be approximated by the first term in a series expansion in $B$: $\mu(B)\approx\mu_0+\eta B$. The parameters $\mu_0$ and $\eta$ can be found from the best fit of the theoretical calculations to the experimental data.

The interaction between the $Tm^{3+}$ ions and localized phonons is represented in our formalism by the Hamiltonian

$$H_{\rm int}=u(B)a^{+}b+u^{*}(b)ab^{+}+v(B)a^{+}b^{+}+v^{*}(B)ab, \tag{3}$$

where we employ a linear approximation for the functions $\mu(B)$ and $v(B)$: $u(B)=u_0+u_1B$ and $v(B)=v_0+v_1B$. The interaction parameters $u_0, u_1$, $v_0$, and $v_1$ are also adjustable and are found from the best fit of the calculations to the experimental data.

The problem of finding the excitation spectrum in a system of two types of bosons which interact with one another can be solved by the standard Green's function methods.[12,13] Ultimately, in the region where the frequencies of the phonons and excited states of the thulium ions coincide, the resonance interaction leads to the appearance of two branches of coupled electron–phonon excitations:

$$E^2_{1,2}(B)=1/2((\omega-\mu(B))^2+\epsilon^2(B))+|u(B)|^2+|v(B)|^2\pm\sqrt{D},$$

$$D = 1/2[(\omega - \mu(B))^2 - \epsilon^2(B)]^2 + [(\omega - \mu(B))^2 + \epsilon^2(B)][|u(B)|^2 + |v(B)|^2] + 4|\mu(B)|^2|v(B)|^2 + 2(|u(B)|^2 + |v(B)|^2)(\omega - \mu(B))\epsilon(B).$$

Figure 2 shows the experimental points from Ref. 9 and the computed curves obtained with the following values of the adjustable parameters: $\mu_0 = -0.96\ \mathrm{cm}^{-1}$, $\eta = 0.16\ \mathrm{cm}^{-1}/\mathrm{T}$, $u_0 = v_0 = 0.8\ \mathrm{cm}^{-1}$, and $u_1 = v_1 = 0.15\ \mathrm{cm}^{-1}/\mathrm{T}$. One can see from the experimental points that besides the appearance of two branches of coupled excitations a purely phonon absorption line and an absorption line corresponding to the transition $|g\rangle \rightarrow |d_2\rangle$ in the system of thulium ions are observed. Such ''crossing–anticrossing'' behavior is not surprising for the TmES system. The symmetry group of the crystal contains an inversion operation, so that the phonon branch is twofold degenerate. The unit cell of the crystal contains two $Tm^{3+}$ ions and a sufficiently strong magnetic field can partially destroy the equivalence of these two ions, since the interaction of ions with a magnetic field depends on the orientation of $\mathbf{B}_0$ with respect to the local symmetry axes of the ion, which are different for the two $Tm^{3+}$ ions in a unit cell.

In conclusion, we note that the simple model proposed above for describing coupled $4f$-electron–phonon excitations is, of course, a first approximation to the real situation. The observed complicated structure of the ESR spectra[9] cannot be explained in a model of noninteracting excitations in a system of $Tm^{3+}$ ions. It is very likely that this structure corresponds to Davydov splitting and the appearance of collective magnetic moments as a result of the $4f$-electron–phonon interaction (see, for example, Ref. 14 for a discussion of the possibility of observing Davydov splitting in Van Vleck paramagnets). To answer these and other questions additional experimental investigations must be performed, for example, by the method of infrared Fourier spectroscopy (as a function of the intensity of irradiation of the crystal) and by the method of neutron spectroscopy in order to obtain more information about the magnetic properties of the coupled excitations. However, there is no doubt that coupled $4f$-electron–phonon excitations were observed in the Van Vleck paramagnet TmES. Moreover, it is evident from Fig. 5 of Ref. 9 that in fields above 11 T the absorption line corresponding to the transition $|g\rangle \rightarrow |d_1\rangle$ will ''cross'' both the phonon line ($49\ \mathrm{cm}^{-1}$) and one of the branches of the coupled $4f$-electron–phonon excitations, so that new branches of electron–phonon excitations should be expected to appear in such magnetic fields.

We thank B. Z. Malkin, M. A. Teplov, and H. Suzuki for a discussion of the results obtained in this work and B. I. Kochelaev for his interest in this work.

This work was supported by the Russian Fund for Fundamental Research (97-02-16470).

[1] G. A. Gehring and K. A. Gehring, Rep. Prog. Phys. **38**, 1 (1975).
[2] K. Ahrens and G. Schaack, Phys. Rev. Lett. **42**, 1488 (1979).
[3] G. Schaack, Z. Phys. B **26**, 49 (1977).
[4] W. Dorfler, H. D. Hochheimer, and G. Schaack, Z. Phys. B **51**, 153 (1983).
[5] M. Dahl and G. Schaack, Z. Phys. B **56**, 279 (1984).
[6] M. Dahl, G. Schaack, and B. Schwark, Europhys. Lett. **4**, 929 (1987).
[7] M. Dahl, Z. Phys. B **72**, 87 (1988).
[8] I. M. Krygin and A. D. Prokhorov, Zh. Éksp. Teor. Fiz. **86,** 590 (1984) [Sov. Phys. JETP **59**, 344 (1984)].
[9] H. P. Moll, J. van Toll, P. Wyder *et al.*, Phys. Rev. Lett. **77**, 3459 (1996).
[10] M. S. Tagirov and D. A. Tayurskiĭ, JETP Lett. **61**, 672 (1995).

[11] L. K. Aminov, A. A. Kudryashov, M. S. Tagirov, and M. A. Teplov, Zh. Éksp. Teor. Fiz. **86,** 1791 (1984) [Sov. Phys. JETP **59**, 1042 (1984)].
[12] B. I. Kochelaev, Dokl. Akad. Nauk SSSR **166,** 833 (1966) [Sov. Phys. Dokl. **11**, 130 (1966)].
[13] M. N. Aliev and B. I. Kochelaev, Izv. Vyssh. Uchebn. Zaved. Fiz. **2**, 7 (1968).
[14] L. K. Aminov, Fiz. Tverd. Tela (Leningrad) **23,** 2167 (1981) [Sov. Phys. Solid State **23**, 1266 (1981)].

Translated by M. E. Alferieff

# New phase transition in an easy-axis ''triangular'' antiferromagnet

B. S. Dumesh

*Institute of Spectroscopy, Russian Academy of Sciences, 142092 Troitsk, Moscow Region, Russia*

S. V. Petrov and A. M. Tikhonov

*P. L. Kapitsa Institute of Physics Problems, Russian Academy of Sciences, 117334 Moscow, Russia*

(Submitted 15 May 1998)
Pis'ma Zh. Éksp. Teor. Fiz. **67**, No. 12, 988–993 (25 June 1998)

The NMR of $^{55}$Mn in the quasi-one-dimensional noncollinear antiferromagnet $CsMnI_3$ is investigated at $T=1.3$ K in magnetic fields up to $\sim$80 kOe and angles between the field and $C_6$ axis $\varphi\approx 0.5°$ and $\varphi=7°$. A new reorientational magnetic phase transition is observed in a field $H_{c1}\approx 39.0$ kOe. The magnetic structure for $H>H_{c1}$ is determined. The average $Mn^{2+}$ spins of the magnetic sublattices in the new phase are determined from an analysis of the NMR spectrum to be $\langle S_C\rangle=1.63$ and $\langle S_D\rangle=1.72$. © *1998 American Institute of Physics.* [S0021-3640(98)00712-9]

PACS numbers: 75.30.Kz, 75.50.Ee, 76.60.Es

In recent years a great deal of attention has been devoted to the investigation of easy-axis ''triangular'' antiferromagnets (AFs) $ABX_3$. Among the many unusual properties of these magnets, of greatest interest is the complicated $H-T$ phase diagram ($\mathbf{H}\|C_6$) of the paramagnetic and three antiferromagnetic phases which coexist at the multicritical point $(T_m, H_m)$[1,2] (for $CsMnI_3$ $T_m\approx 10$ K and $H_m\approx 60$ kOe). However, the number of phases is not exhausted by four. Thus, the possible existence of one other low-temperature antiferromagnetic structure ($T<T_{N2}$) in addition to the two structures which are already known, which we shall call 1 and 2, is being actively discussed. According to the simple theory, the boundary between the phases 1 and 2 (Refs. 3 and 4) is a first-order spin-flop transition (model I). However, the jumps characteristic for a first-order phase transition are absent in the longitudinal component of the magnetization, measured in a large series of easy-axis triangular AFs, and in the magnetostriction.[5] According to Refs. 6–8, there could be a new phase which separates phase 1 from phase 2. Instead of the spin-flop transition, there arise two second-order phase transitions (model II). This model describes satisfactorily the observed behavior of the magnetization.[8] However, additional experiments are required in order to obtain a detailed picture. Since the NMR spectrum in a magnetic field is sensitive to the structure of the magnet, the magnetic phase diagram of $CsMnI_3$ can be refined with its help.

$CsMnI_3$ is a hexagonal crystal with a symmetry space group $D_{6h}^4$. All positions of

 

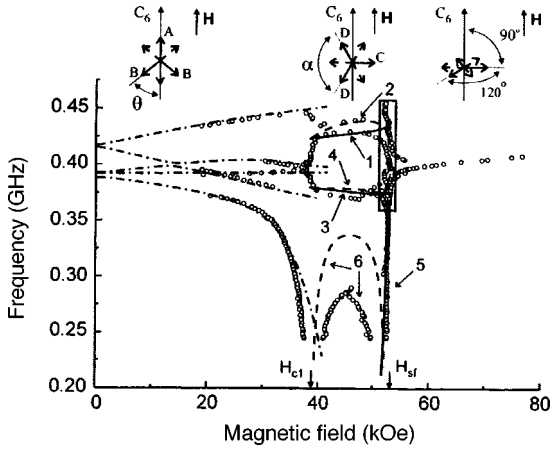


FIG. 1. The NMR spectrum of $^{55}$Mn in $CsMnI_3$ for $\varphi \approx 0.5°$ and $T = 1.3$ K — open circles. Rectangle — expected region of absorption accompanying a spin-flop transition. The rest of the lines were computed (see text). Inset: Magnetic structures of $CsMnI_3$ with $\mathbf{H} \| C_6$.

the $Mn^{2+}$ ions are crystallographically equivalent. The distance between the $Mn^{2+}$ ions along the $C_6$ axis is approximately half that the basal plane. Correspondingly, the exchange constants are $J = 198$ GHz (Ref. 4) and $J' = 1$ GHz (Refs. 9 and 4). Below $T_{N2} = 8.2$ K the magnetic structure consists of antiferromagnetic chains along the $C_6$ axis. In weak magnetic fields the spins of one third of the chains are directed along the axis ($A$ spins), while the rest of the spins make an angle $\theta = 51° \pm 1°$ with it ($B$ spins)[3,4] (see the inset in Fig. 1). All of the $Mn^{2+}$ spins are coplanar to one plane, which we shall call the spin plane. There is no anisotropy in the hexagonal plane, so that in the presence of a magnetic field component perpendicular to the $C_6$ axis the normal to the spin plane is parallel to this component. If a field is applied in the hexagonal plane, then such a structure is stable. For $\mathbf{H} \| C_6$ in the field $H_{sf}$ ($H_{sf} = 53$ kOe with $T = 1.7$ K), according to model I there occurs a spin-flop transition above which all spins turn into a position perpendicular to **H** and form an equilateral triangular structure oriented in the hexagonal plane. For an arbitrary direction of the external field relative to $C_6$ the spin plane rotates smoothly, so that[9]

$$\tan(2\psi) = \frac{H^2 \sin(2\varphi)}{H^2 \cos(2\varphi) - H_{sf}^2}, \tag{1}$$

where $\psi$ is the angle between the normal **n** to the spin plane and the $C_6$ axis, and $\varphi$ is the angle between **H** and $C_6$.

According to model II,[8] for $\mathbf{H} \| C_6$ there are two second-order phase transitions in the fields $H_{c1}$ and $H_{c2}$. An intermediate magnetic phase, in which the spin plane rotates smoothly to the position $\psi = 0$ occurs, lies between them.

If the dynamic frequency shift (DFS) due to the interaction with low-lying AFMR modes is neglected, the spectrum $\omega_{ni}$ of the $i$th $^{55}$Mn NMR branch[a)] is described by the simple formulas

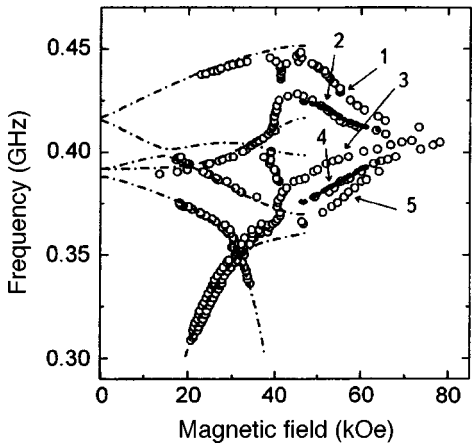


FIG. 2. The NMR spectrum of $^{55}$Mn in $CsMnI_3$ for $\varphi \approx 7°$ and $T = 1.3$ K. Dot-and-dash line — calculation of the spectrum in the low-field phase,[10] filled circles— calculation of the branches *2* and *4* according to Eq. (6).

$$\frac{\omega_{ni}}{\gamma_n} = |\mathbf{H}_{ni} + \mathbf{H}|, \quad \mathbf{H}_{ni} = -\frac{A_0}{\gamma_n \hbar}\langle \mathbf{S}_i \rangle, \tag{2}$$

where $\gamma_n/2\pi = 1.06$ MHz/kOe is the gyromagnetic ratio for $^{55}$Mn nuclei, $H_{ni}$ is the hyperfine field, $\hbar$ is Planck's constant, and $A_0$ is the hyperfine interaction constant. The number of branches in the unshifted NMR spectrum is determined by the number of nonequivalent orientations of the ion spins in the magnetic structure with respect to the field. For $\mathbf{H} \| C_6$ the spectrum should consist of four branches which diverge as the field increases. If model I is correct, then at the spin-flop transition field the splitting of the spectrum should vanish abruptly, so that above it only one NMR branch with frequency $\omega \approx \gamma_n H_n$ should be observed. Conversely, if model II is realized, then the NMR branches will smoothly merge into a single branch in the range $H_{c1} < H < H_{c2}$.

The NMR of $^{55}$Mn in $CsMnI_3$ in fields less than 40 kOe was investigated in Ref. 10, where it was shown that the DFS is strong and the NMR spectrum is described well by the solutions of equations of the form

$$(\omega_{ej}^2 - \omega^2) = \omega^2 \omega_T^2 \sum_i \frac{\rho_i}{\omega_{ni}^2 - \omega^2}, \tag{3}$$

where $\omega_{ej} = \omega_{e2}$, $\omega_{e3}$ are the AFMR modes measured in Ref. 9, the coupling frequency $\omega_T \sim T^{-1/2}$ is determined according to the temperature-dependent gap in the AFMR spectrum, the summation extends over the unshifted NMR branches $\omega_{ni}$ interacting with $\omega_{ej}$, and $\rho_i$ is the fraction of the nuclear spins in the $i$th unshifted NMR branch among the total number of nuclei involved in the interaction.

All measurements were performed in a continuous-wave wide-band NMR spectrometer, described in detail in Ref. 11, with a re-entrant resonator and frequency modulation. The spectra were obtained on single-crystal samples by passing through resonance with respect to the magnetic field at $T = 1.3$ K.

The measured NMR spectra with $\phi \approx 0.5°$ and $\phi = 7°$ are presented in Figs. 1 and 2

(open circles). In fields less than 39 kOe, five branches are observed, which, when the DFS is taken into account, correspond to the well-known low-field magnetic structure for $CsMnI_3$. The dot-and-dash line shows the calculation from Ref. 10. The splitting of the NMR spectrum in zero magnetic field, due to the fact that $\langle S_A \rangle \neq \langle S_B \rangle$, is also explained there.

In high fields two regions of rearrangement of the NMR spectrum are observed at $H_{c1} \approx 39$ kOe and $H_{sf} = 52.5$ kOe. The position of the upper feature coincides with the transition, determined according to the maximum of $d\mathcal{M}/dH$, in the high-field phase[3,2] and manifests the characteristic features of a spin-flop transition — sharp restructuring into one branch, the presence of absorption of width $\sim 0.2$ kOe at $H_{sf}$ in a wide frequency range (the almost vertical branch in Fig. 1), and the existence of a feature only for small angles $\varphi \approx 0.5°$ (compare with Fig. 2). This means that for small angles $\varphi$ the rotation of the spin plane to a position perpendicular to the external field occurs abruptly, i.e., model I is realized.

A sharp restructuring of the NMR spectrum occurs near 39 kOe, indicating a change in the angles between the $Mn^{2+}$ spins and the external field. Above the transition the top three branches in Fig. 1 continue to diverge from one another, i.e., rotation of the spin plane does not occur. For this reason, it is natural to suppose that the feature observed at $H_{c1}$ is due to reorientation within the spin plane. The behavior of the lowest NMR branch, which as $H \to H_{c1}$ becomes softer more rapidly than follows from the calculation (the dot-and-dash curve in Fig. 1), serves as an additional argument in favor of this conjecture. This means that the AFMR mode associated with it has the behavior $\omega_{e3} \to 0$ as $H \to H_{c1}$. This is the mode that determines the oscillations in the spin plane.

In the presence of a triangular spin structure in the spin plane, there are only two possible configurations that are symmetric with respect to **H**: The spins in one of the three AF chains are either parallel to the $C_6$ axis (the phase 1 structure) or perpendicular to it (see Fig. 1). We assumed that the latter configuration is realized for $H > H_{c1}$, and we checked its compatibility with the observed NMR spectrum. In this case, the unshifted NMR spectrum should consist of three twofold degenerate branches, whose frequencies in an approximation linear in $H/H_n$ (the designations $C$ and $D$ correspond to the inset in Fig. 1) are given by

$$\frac{\omega_{n1,2}}{\gamma_n} = H_{nD}\left[1 \pm \frac{H}{H_{nD}} \sin(\alpha/2)\sin(\psi - \varphi)\right], \quad \frac{\omega_{n3}}{\gamma_n} = H_{nC}, \tag{4}$$

where $\alpha$ is the angle between the directions of the neighboring AF chains $D$. The interaction with low-lying AFMR modes $\omega_{e2}$ and $\omega_{e3}$ lifts the degeneracy present in the unshifted spectrum, and when the DFS is taken into account, the NMR frequencies are roots of the two independent equations

$$(\omega_{e2,3}^2 - \omega^2) = \frac{\omega_T^2}{3} \sum_{i=1}^{3} \frac{\omega^2}{\omega_{ni}^2 - \omega^2}, \tag{5}$$

Let us analyze first the NMR spectrum at $\varphi \approx 7°$. For this angle $\omega_{e2}^2 \gg \omega_T^2$ in fields greater than 40 kOe,[9] and the DFS is negligibly small for the NMR branches interacting with this mode. They can be easily indentified, since the interaction always decreases the NMR frequency by an amount less than the distance to the neighbors of the unshifted branch.

For this reason, branches *1*, *3*, and *5* (see Fig. 2) should be described quite accurately by formulas (4), while the rest of the branches can be found from the solutions of Eq. (5) with $\omega_{e3}$. The result of Ref. 9 can be used to estimate $\omega_{e3}$ for $H>H_{sf}$: $\omega_{e3}^2 \sim \omega_{e3}^2(0)\varphi^6 \ll \omega_T^2$. Under this condition one of the solutions of Eq. (5) is small, $\omega_6^2 \ll \omega_n^2$, and the equation for the two remaining nuclear modes assumes the form

$$\sum_{i=1}^{3} \frac{1}{\omega_{ni}^2 - \omega^2} \approx 0. \tag{6}$$

Knowing the field dependences of $\omega_{ni}$ from experiment (branches *1*, *3*, *5*), one can check whether this relation is satisfied for branches *2* and *4* without using any additional constants. The result of such a recalculation is shown by in Fig. 2 (filled dots). One can see that there is good agreement with the experimental data, which attests to the validity of the model we have chosen for the magnetic structure.[b)] Likewise, we can determine from our experimental data $H_{nC}=\omega_3/\gamma_n \approx 365$ kOe and $H_{nD}=(\omega_1+\omega_5)/2\gamma_n \approx 385$ kOe. The angle $\alpha$ can be estimated from the maximum absorption frequency at $H_{sf}$ from the formula $\omega_{\max,\min}=\gamma_n|H_n \pm H \sin \alpha/2|$. We obtain $\alpha \approx 120°$, i.e., the spin structure is close to an equilateral triangular structure. Knowing $\alpha$ and $\varphi$, we determined the field dependence of the rotation angle $\psi$ of the spin plane. It turned out that it is described well by formula (1), i.e., the character of the rotation of the spin plane for $\varphi \approx 7°$ corresponds to model I. From the values we determined for the hyperfine fields, and with the value of the hyperfine constant $A_0=(-1.49\pm 0.04)\times 10^{-18}$ ergs,[12]) known from data on the ESR of $Mn^{2+}$ in $CsMnI_3$, we obtain $\langle S_C \rangle = 1.63$ and $\langle S_D \rangle = 1.72$.

Let us now return to the NMR spectrum for $\phi \approx 0.5°$. The calculation of the spectrum taking into account the interaction with the AFMR mode $\omega_{e2}$, using the values which we obtained for $H_{nC}$, $H_{nD}$, and $\alpha$ and with $\psi(H)$ calculated according to Eq. (1), is presented in Fig. 1 (solid lines). One can see that it describes branches *1*, *3*, and *5* quite well. To calculate the rest of the branches it is necessary to know $\omega_{e3}$. Unfortunately, there are no low-frequency experimental data for this mode in $CsMnI_3$. However, it is evident from the behavior of $\omega_6$ that the frequency $\omega_{e3}$ is close to zero at both phase transition points. We took the very simple field dependence satisfying this condition,

$$\omega_{e3}^2 = \omega_{e3}^2(0)\left|\left(1-\frac{H^2}{H_{c1}^2}\right)\left(1-\frac{H^2}{H_{sf}^2}\right)\right|. \tag{7}$$

Using Eq. (7), we obtained qualitative agreement with the frequencies of the rest of the NMR branches without introducing new constants (dashed line in Fig. 1).

Thus, it follows from our results that in $CsMnI_3$ with $\mathbf{H} \| C_6$ there exists an intermediate magnetic structure between the two known low-temperature phases. In this phase the normal to the spin plane is perpendicular to the hexagonal axis, while the spins form a close to 120-degree triangular structure, so that one-third of the spins are directed perpendicular to $C_6$. This reorientational transition also exists when the vector $\mathbf{H}$ tilts substantially away from $C_6$ ($\varphi \approx 7°$). The transition from the new phase into the high-field phase 2 exhibits the characteristic features of a spin-flop transition.

The nature of the phase transition at $H_{c1}$ remains unclear (we do not rule out the possibility of a double transition). The phase which we have discovered does not correspond to the magnetic structures calculated in Refs. 6–8. We believe that in order to

explain it, it will be necessary to take into account the reduction of the $Mn^{2+}$ spins. There also arises the question of a possible increase in the order of the multicritical point in the $H-T$ phase diagram of $CsMnI_3$.

In closing, we sincerely thank N. M. Kreĭnes, M. I. Kurkin, V. I. Marchenko, L. A. Prozorova, A. I. Smirnov, I. A. Fomin, and V. G. Kaloshnikov for fruitful discussions. This work was supported in part by Russian Fund for Fundamental Research Grant 98-02-16572 and by Grant RP1-207 from the U.S. Civilian Research & Development Foundation for the Independent States of the Former Soviet Union (CRDF). A. M. Tikhonov is grateful to Forschungszentrum Jülich GmbH.

[a)]This will be referred to below as the unshifted frequency.
[b)]We were unable to describe the NMR spectrum under the condition that the low-field phase *1* is preserved in the region $H_{c1}<H<H_{sf}$.

[1] M. F. Collins and O. A. Petrenko, Can. J. Phys. **75**, 605 (1997).
[2] H. A. Katori, T. Goto, and Y. Ajiro, J. Phys. Soc. Jpn. **62**, 743 (1993).
[3] H. W. Zandbergen, J. Solid State Chem. **35**, 367 (1980).
[4] A. Harrison, M. F. Collins, J. Abu-Dayyeh, and C. V. Stager, Phys. Rev. B **43**, 679 (1991).
[5] J. A. Rayne, J. G. Collins, and G. K. White, J. Appl. Phys. **55**, 2404 (1984).
[6] M. L. Plumer, A. Caille, and K. Hood, Phys. Rev. B **39**, 4489 (1989).
[7] M. L. Plumer and A. Caille, J. Appl. Phys. **70**, 5961 (1991).
[8] M. E. Zhitomirskiĭ, O. A. Petrenko, S. V. Petrov *et al.*, Zh. Éksp. Teor. Fiz. **108**, 343 (1995) [JETP **81**, 185 (1995)].
[9] S. I. Abarzhi, M. E. Zhitomirskiĭ, O. A. Petrenko *et al.*, Zh. Éksp. Teor. Fiz. **104**, 3232 (1993) [JETP **77**, 521 (1993)].
[10] B. S. Dumesh, S. V. Petrov, and A. M. Tikhonov, JETP Lett. **67**, 692 (1998).
[11] A. S. Borovik-Romanov, B. S. Dumesh, S. V. Petrov, and A. M. Tikhonov, Zh. Éksp. Teor. Fiz. **113**, 352 (1998) [JETP **86**, 197 (1998)].
[12] G. L. McPherson, R. C. Koch, and G. D. Stucky, J. Chem. Phys. **60**, 1424 (1974).

Translated by M. E. Alferieff

# Incremental expansions for Hubbard–Peierls systems

J. Malek, K. Kladko, and S. Flach
*Max-Planck-Institute for Physics of Complex Systems, D-01187 Dresden, Germany*

(Submitted 19 May 1998)
Pis'ma Zh. Éksp. Teor. Fiz. **67**, No. 12, 994–999 (25 June 1998)

The ground state energies of infinite half-filled Hubbard–Peierls chains are investigated by combining an incremental expansion with exact diagonalization of finite chain segments. The ground-state energy of equidistant infinite Hubbard (Heisenberg) chains is calculated with a relative error of less than $3\times10^{-3}$ for all values of $U$ using diagonalizations of 12-site (20-site) chain segments. For dimerized chains the dimerization order parameter $d$ as a function of the on-site repulsion interaction $U$ has a maximum at nonzero values of $U$, if the electron–phonon coupling $g$ is lower than a critical value $g_c$. The critical value $g_c$ is found with high accuracy to be $g_c=0.69$. For smaller values of $g$ the position of the maximum of $d(U)$ is approximately $3t$, and rapidly tends to zero as $g$ approaches $g_c$ from below. We show how our method can be applied to calculate breathers for the problem of phonon dynamics in Hubbard–Peierls systems. © *1998 American Institute of Physics.* [S0021-3640(98)00812-3]

PACS numbers: 72.60.+g, 63.20.Kr

The effect of correlations on the Peierls transition has been one of challenging problems in the theory of quasi-one-dimensional compounds. One of the most important theoretical treatments of the Peierls transition goes back to the solution of the exactly solvable model of noninteracting fermions proposed by Su, Schrieffer, and Heeger (SSH).[1] Although being successful in explaining a number of properties of real quasi-one-dimensional systems, the SSH model is in a clear disagreement with such experimental results as the emergence of negative spin magnetization densities for neutral solitons.[2] One is faced with the necessity of treating the Coulomb interaction in the electron subsystem. This interaction should be accounted for by including a positive Hubbard on-site interaction term in the SSH model. We refer to this extended model as the Peierls–Hubbard (PH) model. Due to strong one-dimensional quantum fluctuations a mean field theory calculation of the PH model gives qualitatively wrong results, predicting a constant dimerization for small $U$ and the abrupt disappearance of a bond order wave state as $U$ increases above a certain threshold at half filling.[3] Including many-body effects it has been shown by many authors (see Ref. 4 and citations therein) that the dimerization $d$ first increases up to a maximum and then decreases with further increase of $U$.

It is very difficult to perform an accurate exact-diagonalization investigation of the Peierls transition in the correlated regime. In the framework of a standard exact-

 

diagonalization approach the required cluster sizes are found to be far outreaching the capabilities of modern computer systems. Calculations which have been performed using available cluster sizes are drastically dependent on the boundary conditions (see Ref. 5, for instance), and the final conclusions have had to be based on extrapolations. The basic questions about the value of $g_c$, the behavior of the system near the critical point, and the position and value of the dimerization maximum $U_{\max}$ as a function of the electron phonon coupling have remained unanswered. The lack of accurate numerical results has made it hard to identify the values of model parameters for real systems. We will show that by combining an incremental expansion technique (IET) with numerically exact diagonalizations, one can overcome the above-mentioned difficulties and perform a reliable numerical calculation of correlated one-dimensional Peierls systems in both the strong and weak correlation regimes.

The quantum chemical method of increments has recently found a wide range of application in condensed matter (see Ref. 6 and references therein). The IET starts with the splitting of a given Hamiltonian operator $H$ into an unperturbed part $H_0$ and a number of perturbations $H_1+H_2+\ldots$, so that $H=H_0+\Sigma H_i$. The hierarchy of increments is defined in the following way. The first order increment $I_k^{(1)}$ is found by taking the ground-state energy $\mathcal{E}_k$ of the Hamiltonian $H_0+H_k$ and subtracting from it the ground-state energy $\mathcal{E}_0$ of $H_0$, $I_k^{(1)}=\mathcal{E}_k-\mathcal{E}_0$. Phenomenologically this increment represents the action of the perturbation $H_k$ separately from all other perturbations $H_i$. The total change of the unperturbed ground-state energy in first incremental order is then given by $\Sigma_i I_i^{(1)}$. The second order increment $I_{k,l}^{(2)}$ is found by taking the ground-state energy $\mathcal{E}_{k,l}$ of the Hamiltonian $H_0+H_k+H_l$ and subtracting from it $\mathcal{E}_0$ and the first order increments $I_k^{(1)}$ and $I_l^{(1)}$, $I_{k,l}^{(2)}=\mathcal{E}_{k,l}-I_k^{(1)}-I_l^{(1)}-\mathcal{E}_0$. The increments $I_{k,l}^{(2)}$ represent the difference between the combined action of a pair $H_i$, $H_k$ and the sum of the uncorrelated actions of both perturbations. In a similar manner higher-order increments are found. The change of the unperturbed ground-state energy of the full system is given exactly by the sum over all increments (all orders!). Since the increments are usually calculated numerically, the incremental expansion can be performed up to some given order. This expansion is nonperturbative since the increments are not related to some small parameter of a perturbation theory. The idea of the incremental expansion is similar to Faddeev's treatment of the 3-body problem wherein the unknown 3-body scattering matrix is expressed in terms of the exactly known 2-body scattering matrices. The discussion of the interrelation of increments and Faddeev equations and also the derivation of the incremental expansion by a resummation of the perturbation theory is given in Ref. 7.

Now we apply the outlined ideas to the PH Hamiltonian. This Hamiltonian is given by a sum of electronic and lattice parts $H=H_{\rm el}+H_{\rm lat}$. The electronic part in fermionic second quantization form is given by

$$H_{\rm el}=\sum_{i,\sigma} t_i(c_{i,\sigma}^{\dagger}c_{i+1,\sigma}+\text{h.c.})+U\sum_i (n_{i,\uparrow}n_{i,\downarrow}). \tag{1}$$

Here $U$ is an on-site Hubbard repulsion matrix element and $t_i$ is the hopping matrix element between the $i$th and $(i+1)$th sites. We consider the case of one electron per site (half filling). In the harmonic approximation the lattice part is given as $H_{\rm lat}=1/2K\Sigma_i v_i^2$. Here $v_i$ is a bond-length change (see, e.g., Ref. 4) and $K$ is the spring constant. The electron–lattice interaction is assumed to be of the form $t_i=-(t-\gamma v_i)$.

The strength of the electron–phonon interaction is measured by the dimensionless coupling $g=\gamma/\sqrt{Kt}$. Solving the PH model amounts to finding a minimum of the total energy of the system considered as a functional of the bond length changes $v_i$. A remarkable proof of Lieb and Nachtergaele[8] tells us that the minimum configuration has to be a dimerized state with alternating bond lengths $v_i=(-1)^i v_0$. In the following we will use the dimensionless dimerization $d=v_0\sqrt{K/t}$ (see Refs. 5 and 4).

Let us now formulate the incremental expansion of the PH model. A dimerized state represents a sequence of alternating weak and strong bonds formed by a modulation of the transfer integral $t_i$. It is natural to cut all the weak bonds and to consider the remaining set of noninteracting 2-site dimers as an unperturbed Hamiltonian $H_0$. The weak bonds are considered as a perturbation. The unperturbed Hamiltonian $H_0$ is written as

$$H_0=\sum_{k=-\infty}^{\infty} t_{2k}(c^{+}_{2k,\sigma}c_{2k+1,\sigma}+\text{h. c.})+U\sum_{i=-\infty,\sigma}^{\infty} n_{i,\uparrow}n_{i,\downarrow}. \tag{2}$$

The ground state of the Hamiltonian operator $H_0$ is known exactly and is a nondegenerate spin-singlet state $S=0$ formed by a set of noninteracting dimers having two electrons per dimer. The PH Hamiltonian $H$ is a sum of $H_0$ and a number of perturbations, formed by the (weak) bonds linking neighboring dimers,

$$H=H_0+\sum_k V_k, \quad V_k=\sum_\sigma t_{2k-1}(c^{+}_{2k-1,\sigma}c_{2k,\sigma}+\text{h. c.}).$$

The incremental expansion is generated in the following way. The first order increment corresponds to a bond inserted between two neighboring dimers. By virtue of the general principles outlined above, it has the form $I^{(1)}=E_4-2E_2$, where $E_{2n}$, $n=1,2,\ldots$ denotes the ground-state energy of a $2n$-site segment cut out of the infinite chain. The second-order increment is defined for a triple of neighboring dimers and follows from inserting two bonds into $H_0$. To find it one needs to subtract from the energy of three linked dimers the increments corresponding to 2 pairs of dimers and 3 single dimers in it, and hence the expression reads $I^{(2)}=E_6-2I^{(1)}-3E_2=E_6-2E_4+E_2$. Note that in the incremental expansion only connected clusters of dimers yield nonzero increments, since the energy of a disconnected cluster is just the sum of the energies of its parts. The expressions for higher-order increments are found in similar fashion. Due to the choice of $H_0$ (see Eq. (2)) the increments do not depend on the site indices. One proves by induction that the expression for the $n$th order increment, $n>2$, is

$$I^{(n)}=E_{2n+2}-2E_{2n}+E_{2n-2}. \tag{3}$$

In order to find the ground-state energy of the infinite system one needs to count the number of increments of each order per dimer. In the infinite $1-d$ lattice which we are considering, there exists exactly one increment of each order per dimer (we makes a one-to-one correspondence between dimers and increments of each order, assigning each increment to its left-most dimer). Therefore, taking into account that there are two sites per each dimer, we write the value of the ground-state energy of the infinite lattice per site as $\mathcal{E}=1/2(E_2+\Sigma_{n=1}^{N}I^{(n)})$. Here $N$ is the number of increments taken into account.

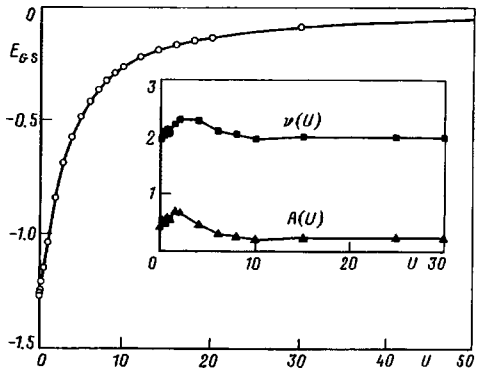


FIG. 1. Ground-state energy of the equidistant Hubbard model at half filling. Solid line — exact result,[10] open circles — IET result for $N=5$ (see text). Inset: $U$ dependence of prefactor $A$ and exponent $\nu$ of the obtained functional dependence of the relative error on $(2N+2)$ (see text).

The feature that the number of increments of any given order per site is constant is an exclusive property of one-dimensional lattices. In higher dimensions the number of increments of a given order per site grows rapidly with the order of the increment. This special property of one dimension leads to the following result:

$$\mathcal{E}(N)=\frac{1}{2}(E_{2N+2}-E_{2N}). \tag{4}$$

Formula (4) is quite remarkable, since the calculation of the ground-state properties amounts to the exact diagonalization of two open chains whose length differs by two. Note that expressions of the type (4) have previously been used intuitively in quantum chemical calculations (see, for instance, Ref. 9).

To check our method we first performed a calculation of the ground-state energy of an equidistant Hubbard infinite chain at half filling, where the solution is known exactly.[10] The equidistant case is the worst case for the method described above, since all the bonds have the same strength. The per site value of the ground-state energy $\mathcal{E}$ was calculated using formula (4) with the incremental order $N=1, 2, 3, 4, 5$. The calculation was performed using a Lanczos algorithm. The results for $N=5$ are shown in Fig. 1, where the exact $\mathcal{E}(U)$ dependence for $t=1$ (solid line) is plotted against the results of Eq. (4) (open circles). The relative error $R_E$ decays algebraically with increasing order of the increments $R_E=A(U)[2N+2]^{-\nu(U)}$. The exponent $\nu(U)$ and the prefactor $A(U)$ are plotted in the inset of Fig. 1. We find $\nu(U)\geqslant 2$ for all values of $U$. Note that $A(0)/A(\infty)\approx 2$, which implies that our results converge faster for large $U$. Note also that the errors are very small — typically below 0.1% for $N=6$. This has to be compared with a recent density matrix renormalization group (DMRG) calculation of the same system,[11] where system sizes up to 122 and extrapolations had to be used to achieve comparable precision.

Next we show the results of calculations of the dimensionless dimerization in the PH model as a function of $U$ and $g$ (Fig. 2). For $U=0$ the value of $d(g)$ is known exactly[1] (see the filled symbols for $U=0$ in Fig. 2). An analysis of the relative error $R_d$ of determining $d$ with the help of (4) yields exponential convergence $R_d\approx e^{-\lambda(g)(2N+2)}$. The

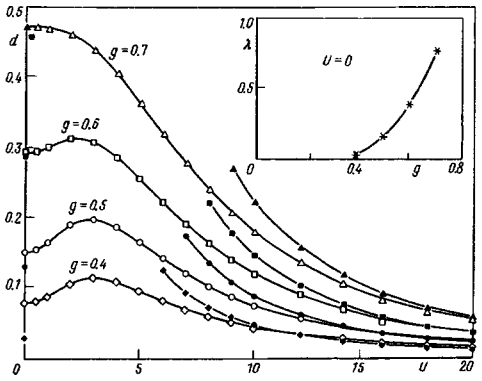


FIG. 2. Dimerization versus $U$ for different values of $g$. Open symbols — IET results for $N=5$, filled symbols for $U=0$ — exact results, filled symbols for $U>5$ — results for Heisenberg chains with IET and $N=8$. The solid lines are guides to the eye. Inset: $g$ dependence of the exponent $\lambda$ of the obtained functional dependence of the relative error on $(2N+2)$ for $U=0$ (see text).

dependence of $\lambda(g)$ is shown in the inset of Fig. 2. A crossover is detected around $g=0.4$, with $\lambda$ being suppressed to rather small values for $g\leqslant 0.4$. That implies that for small values of $U$ the IET method using exact diagonalizations is confined to values of the coupling constant $g>0.4$ if high precision is required. In Fig. 2 we present the dependence of $d(U)$ for $g=0.5$, 0.6, and 0.7 (open symbols). For $g=0.5$, 0.6 the dimerization $d$ first increases with $U$, and then decreases after reaching a maximum. For $g=0.7$ is a monotonically decreasing function of $U$. Therefore the system has a qualitatively different behavior for weak and strong couplings $g$, as predicted by the GA theory. On the other hand, our results agree well with the extrapolated values of $d$ obtained within the solitonic approach.[4]

We performed more calculations of $d(U)$ to obtain the dependence of the position of the maximum $U_{\max}$ on the coupling $g$ (see Fig. 3). In particular, we find $U_{\max}(g)$ to be a monotonically decreasing function with $U_{\max}=0$ at a critical coupling $g_c$. Since our method yields very small errors for $g\geqslant 0.6$ we can estimate the critical coupling $g$ where

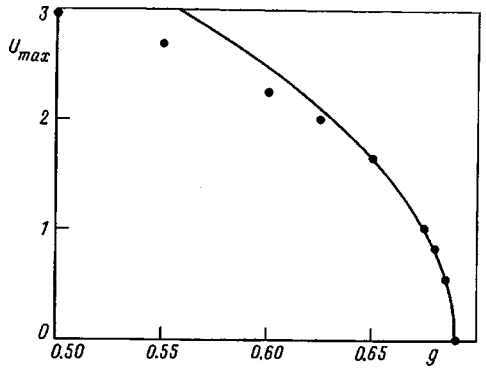


FIG. 3. Dependence of $U_{\max}$ on the coupling $g$ for the Hubbard–Peierls chains with IET and $N=5$. Circles — numerical results; line — best fit (see text).

$U_{\max}=0$ with high accuracy $R_d<10^{-3}$. It is found $g_c=0.69$. The GA prediction $g_c>0.74$ overestimates this result slightly. The GA gives the position of the dimerization maximum as $U_{\max}=4t$ for $g$ far below $g_c$. Our numerical calculation gives $U_{\max}\simeq 3t$. The small-$U$ behavior of $d$ is found to be $d\sim U^2$, which is consistent with the GA approach. Furthermore the GA approach predicts that $d$ is an analytic function of $U^2$. Then it follows that $U_{\max}(g)$ close to $g_c$ varies as $\kappa(g_c-g)^{1/2}$, which is what we find in Fig. 3 ($\kappa\approx 8.25$).

For large values of $U$ the system is equivalent to the Heisenberg spin-exchange model, with $J_i$ given by $J_i=4t_i^2/U$. We have calculated the spin-Peierls transition in this system separately, using the formula (4) and $N=8$. The results for the dimerization are plotted in Fig. 2 (filled symbols). Note that the dimerization $d(U)$ for the Hubbard and Heisenberg chains converge for large $U$, which supports the correctness of our calculations. For the spin-Peierls transition Inagaki and Fukuyama[12] found an asymptotic formula

$$\frac{32g^2}{\pi\sqrt{1+D}}\left(\frac{t}{U}\right)^{3/2}, \tag{5}$$

where $D$ is a constant which was assumed to be of the order of 1/2. Our results confirm this choice.

The above results show that the IET can be a key method for numerical study of the static properties of one-dimensional Peierls systems. Our recent calculations show that it can be equally well applied to spin-Peierls systems with frustration.[13] We believe also that this method could be applied to higher dimensional systems, namely to the Peierls transition in the two-dimensional Hubbard model. Since cancellation of the lower-order energies does not take place in the two-dimensional Hubbard model, the analog of formula (4) contains the energies of clusters of all sizes.

To further underline the applicability of the IET, we consider the *dynamical* properties of finite Hubbard—Peierls systems. The dynamics of classical degrees of freedom (phonons) $Q_i$ interacting on a lattice generically allows for time-periodic and spatially localized solutions, namely, discrete breathers, if the equations of motion include nonlinear terms (see Ref. 14 and citations therein). These discrete breather solutions can be localized on as few as three neighboring sites. If the electron–phonon coupling is taken into account and the Born–Oppenheimer approximation is used, the electronic subsystem generates an additional potential for the classical phonon degrees of freedom. To find once again the discrete breather solutions numerically, one needs the electronic energy $\mathcal{E}(\{Q_i\})$ as a function of the phonon degrees of freedom. For a lattice with $L$ sites this amounts to calculating the ground-state energy of the electronic system $L$ times on each time step in order to find the gradient of $H_{\rm el}$. Precalculating the function $H_{\rm el}$ on a grid is also impossible since it is a function of prohibitively many variables. In the static dimerization case, where it is known that the target state is a bond conjugate state, this problem is avoided, since there is only one variable $d$.

Again the IET helps to overcome this problem. Consider a finite chain with periodic boundary conditions. The first-order increment $I^{(1)}(x)$, which does not depend on the site index, is obtained by fixing all the $Q_i=0$ except one with $Q_l=x$, and calculating the change of the electronic energy as a function of $x$, $I^{(1)}(x)=\mathcal{E}(x)-\mathcal{E}(0)$. The second

order increment is obtained by fixing all phonon variables $Q_i=0$ except $Q_l=x$ and $Q_m=y$. Then the energy of the electronic system will depend on $k=l-m$, $x$ and $y$. The second order increment is $I_k^{(2)}(x,y)=\mathcal{E}(x,y)-I^{(1)}(x)-I^{(1)}(y)-\mathcal{E}(0)$. The higher-order increments are found in the same manner. Our calculations (see Ref. 15 for a detailed discussion) show that taking into account increments of first and second order is enough to calculate the ground-state energy of a 14-site Hubbard chain with periodic boundary conditions for an arbitrary configuration of $\{Q_i\}$. The relative error is less than $10^{-3}$. The increments are calculated on a two-dimensional grid to generate smooth functions. With the help of these functions the lattice dynamics can be calculated using ordinary molecular dynamics techniques.

In this paper we combined the IET with an exact-diagonalization method. It is known that the DMRG is especially accurate when applied to large but finite open chains, where one can achieve higher and higher accuracy by iteratively repeating the DMRG procedure.[16] Taking this into account, we think that the combination of the IET with the DMRG technique can significantly improve calculations.

We thank Prof. Peter Fulde for fruitful discussions and continuous support.

[1] W. P. Su, J. R. Schrieffer, and A. J. Heeger, Phys. Rev. Lett. **42**, 1698 (1979).
[2] H. Thomann, L. R. Dalton, Y. Tomkiewicz *et al.*, Phys. Rev. Lett. **50**, 553 (1983).
[3] R. A. Harris and L. M. Falicov, J. Chem. Phys. **51**, 5034 (1969).
[4] J. Malek, S. L. Drechsler, G. Paasch, and K. Hallberg, Phys. Rev. B **56** (1997), in press, http://xxx.lanl.gov/abs/cond-mat/9708234.
[5] V. Waas, H. Buettner, and J. Voit, Phys. Rev. B **41**, 9366, (1990).
[6] P. Fulde, *Electron Correlations in Molecules and Solids*, 3rd ed., Springer-Verlag, 1995.
[7] K. Kladko and P. Fulde, Int. J. Quant. Chem. in press, http://xxx.lanl.gov/abs/cond-mat/9709044.
[8] E. H. Lieb and B. Nachtergaele, Int. J. Quantum Chem. **58**, 699 (1996).
[9] Ming Yu, Simon Kalvoda, and Michael Dolg, Preprint MPIPKS, 1997.
[10] E. H. Lieb and F. Y. Wu, Phys. Rev. Lett. **20**, 1445 (1968).
[11] M.-B. Lepetit and G. M. Pastor, Phys. Rev. B **56**, 4447 (1997).
[12] S. Inagaki and H. Fukuyama, J. Phys. Soc. Jpn. **52**, 3620 (1983).
[13] S. Drechsler, J. Malek, S. Flach, and K. Kladko, in preparation.
[14] S. Flach and C. R. Willis, ''Discrete breathers,'' Phys. Rep. (1997), in press, http://xxx.lanl.gov/abs/patt-sol/9704004.
[15] S. Flach, K. Kladko, and J. Malek, in preparation.
[16] S. R. White, Phys. Rev. Lett. **69**, 2863 (1992).

Published in English in the original Russian journal. Edited by Steve Torstveit.

# Critical behavior of electron spin resonance in $La_{0.8}Sr_{0.2}MnO_3$ — a material with colossal magnetoresistance

K. V. Baginskiĭ, V. A. Aleshin, and V. A. Tulin[a)]
*Institute of Microelectronics Technology, Russian Academy of Sciences, 142432 Chernogolovka, Moscow Region, Russia*

A. A. Arsenov, D. A. Shulyatev, and Ya. M. Mukovskiĭ
*Moscow Institute of Steels and Alloys, 117936 Moscow, Russia*

(Submitted 21 May 1998)
Pis'ma Zh. Éksp. Teor. Fiz. **67**, No. 12, 1000–1004 (25 June 1998)

High-frequency absorption in the colossal magnetoresistance material $La_{0.8}Sr_{0.2}MnO_3$ is investigated near the critical temperature in a magnetic field. The temperature dependences of the width, position, and intensity of the ESR line are studied in the near-critical region.  [S0021-3640(98)00912-8]

PACS numbers: 75.70.Pa, 76.30.Kg, 76.50.+g, 75.40.Gb

In recent years there has been a great deal of interest in materials of the type $A_xB_{1-x}MnO_3$, which exhibit colossal magnetoresistance (CMR).[1–3] The CMR in these materials is due to the magnetization process in the magnetically ordered state.[4,5] To understand better the physics of the processes occurring in these materials it is important to study their magnetic properties. One of the most effective methods for studying such properties is to investigate the absorption of a high-frequency field in the sample. Electron spin resonance (ESR) is studied in the paramagnetic phase, ferro- or antiferromagnetic resonance is studied in the magnetically ordered phase, and the surface impedance is studied in the case of electrically conducting samples. This method makes it possible to study the dynamical properties of the electronic system without special preparation of the sample (in any case, in the paramagnetic phase). However, surprisingly, at present there are few works devoted to such investigations of these materials,[6–8] despite the very great interest in CMR materials and the many unclear aspects of both their magnetism and the behavior of the magnetoresistance.

In the present work we investigated the high-frequency (885 MHz) properties of $La_{0.8}Sr_{0.2}MnO_3$ in a magnetic field at temperatures near the critical temperature ($T_c \approx 300$ K) in an effort to determine the temperature dependence of the dynamic susceptibility (the area under the absorption curve in ESR) and of the width and position of the ESR line as fluctuation-sensitive quantities. ESR measurements in $La_{0.8}Sr_{0.2}MnO_3$ at 9 GHz were made in Ref. 9, but only one or two experimental points were reported in the temperature interval investigated in the present study. Here we shall show that fluctuation-induced variations of the quantities listed above are observed in a small temperature interval (10 degrees) above the Curie temperature.

 

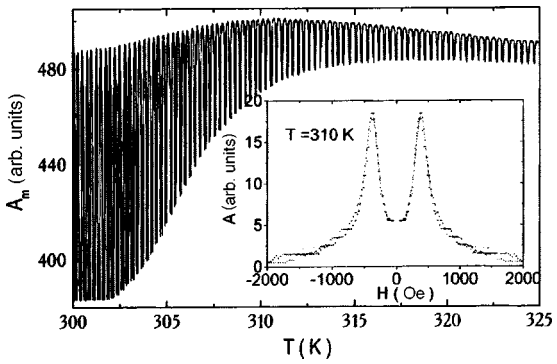


FIG. 1. Central fragment of the temperature dependence of the hf magnetoabsorption for a frequency of 885 MHz in an external magnetic field perpendicular to the plane of the sample. Inset: ESR absorption lines in $La_{0.8}Sr_{0.2}MnO_3$ at high temperatures.

A $La_{0.8}Sr_{0.2}MnO_3$ single crystal was grown by the floating-zone method with radiational heating.[10] Plates with dimensions $2\times1\times0.1$ mm were cut from the ingot. The plane of the sample was perpendicular to the external magnetic field. A high-frequency field was directed along the surface of the sample. The measurements were performed at 885 MHz. We employed a method described earlier,[11] observing the power passing through a helical resonator as the external magnetic field is varied. The helical resonator was constructed from a piece of copper wire with a diameter of 1 mm and a length $\lambda/2$, where $\lambda$ is the wavelength of the electromagnetic radiation employed. This wire was wound into a helix $\sim$1 cm in diameter and about 2 cm long. The change in the signal which passed through the resonator is proportional to the change in the absorption in the crystal as a function of the external conditions (temperature and magnetic field). The temperature was measured with a copper–Constantan thermocouple. The base contact was located in a thermally insulated vessel with a mixture of ice and water. The magnetic field was produced by an external electromagnet and measured with a Hall gauge. The temperature was varied slowly in the course of the measurements (approximately by 0.5 K over one period of variation of the magnetic field). This made it possible to obtain simultaneously the temperature and magnetic-field dependences of the absorption (magnetoabsorption). All three measured quantities — temperature, magnetic field, and amplitude of the hf signal passed through the resonator containing the sample — were entered into a personal computer through the data acquisition system. In such a variant the measurement cycle is about 10 h long. As a result, a nearly exhaustive data set is obtained and can then be systematically processed.

Figure 1 displays the central fragment of the temperature dependence of the hf magnetoabsorption for frequency 885 MHz and external magnetic field perpendicular to the plane of the sample. The ESR absorption line in $La_{0.8}Sr_{0.2}MnO_3$ at high temperatures is shown in the inset. In our measurements the magnetic field turned in only one direction. The absorption line was obtained from an individual fragment, corresponding to a single scan of the magnetic field, of the curve in Fig. 1. Using the symmetry of ESR with respect to the direction of the magnetic field, the data were mirror-reflected with respect to the $Y$ axis (preserving the data for the positive values of the magnetic field) and then relative to the $X$ axis (after which the change in the signal is proportional to the absorp-

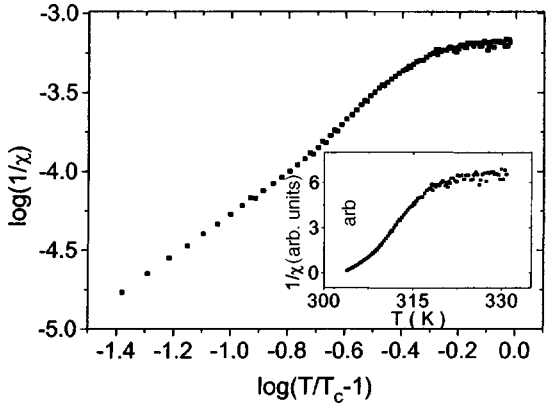


FIG. 2. Reciprocal of the hf susceptibility $(1/\chi_{\rm hf})$ versus $(T/T_c-1)$ in double-logarithmic coordinates, where $T_c=302.7$ K. Inset: Temperature dependence of $1/\chi$.

tion in the sample). Finally, a constant signal was subtracted out so that the signal level would be zero in high fields. As an approximation, a function corresponding to a Lorentzian ESR line with two values of the resonance field $+H_{\rm max}$ and $-H_{\rm max}$ was used on the section from $-1500$ Oe to $+1500$ Oe:

$$Y=a+b*\left(\frac{1}{(H-H_{\rm max})^2+d^2}+\frac{1}{(H+H_{\rm max})^2+d^2}\right). \tag{1}$$

Since the high-frequency susceptibility $\chi_{\rm hf}\sim b/d$ — the area under the absorption curve, we constructed the function $1/\chi_{\rm hf}(t)$ (see the inset in Fig. 2). To better determine the Curie temperature, we constructed the curve $\log(1/\chi_{\rm hf})$ versus $\log(T/T_c-1)$, where $T_c$ varied from 298 to 303 K (Fig. 2). Figure 2 shows a plot of such a function for the value $T_c=302.7$ K. This temperature was chosen so that the low-temperature part of the dependence would be linear in double-logarithmic coordinates. In this case, near the phase transition the behavior of the dynamic susceptibility is described by a power-law function $1/(T-T_c)^{\gamma}$ with exponent $\gamma=1.33$ and $T_c=302.7\pm0.5$ K.

Figure 3 shows the behavior of the ESR linewidth in $La_{0.8}Sr_{0.2}MnO_3$. The contribution of fluctuations is substantial near the transition. As a result of this, an appreciable broadening of the line is observed as the temperature of the transition to the ordered state is approached. Moreover, above 315 K the linewidth increases with temperature. In the temperature range from $T_c$ up to 315 K the behavior of the ESR linewidth can be described by a power-law function of the type $1/(T-T_c)^{\eta}$, where $\eta\approx0.72\pm0.05$ with $T_c=302.7$ K. For the high-temperature part of the temperature range which we studied, the linewidth varies according to a linear law. One circumstance (possibly accidental) in the behavior of the ESR linewidth should be noted. Its high-temperature part can be described on a temperature scale referenced to $T_c$, i.e., $\Delta H=8.9(T-T_c)$ Oe, with $T_c=302.7\pm5$ K. Qualitatively and quantitatively the high-temperature part of the results of our measurements of the linewidth closely follows the ESR data at 9 GHz.[9]

For us, the strong temperature dependence of the position of the ESR line in $La_{0.8}Sr_{0.2}MnO_3$ near $T_c$ was somewhat unexpected. Figure 4 shows the behavior of the

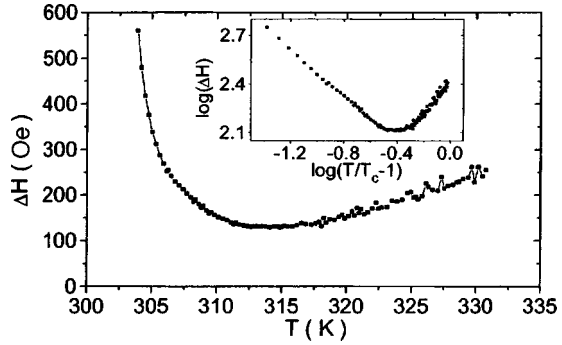


FIG. 3. Temperature dependence of the ESR linewidth. Inset: Same dependence in double-logarithmic coordinates with $T_c = 302.7$ K.

resonance absorption field in the paramagnetic region as a function of temperature. For magnetic resonance in the plate in a magnetic field perpendicular to the plane of the plate the frequency is given by the expression

$$\nu = g\mu_B(H - 4\pi M N_z), \tag{2}$$

where $g$ is the Landé factor, $\mu_B$ is the Bohr magneton, $H$ is the external magnetic field, $M$ is the magnetization of the material, and $N_z$ is a demagnetizing factor in a direction perpendicular to the plane of the plate ($N_z \approx 1$). The magnetization in the paramagnetic region can be expressed in terms of the static susceptibility

$$M = \int_0^{H_0} \chi(T,H)\,dH. \tag{3}$$

We attempted to describe the data in Fig. 4, using a linear approximation of the behavior of the magnetization as a function of the magnetic field, as is ordinarily done in investigations of the critical behavior near the Curie point for low values of the magnetic field, i.e., $\chi(T) \sim (T - T_c)^{-\beta}$. This attempt did not give reasonable results, possibly because of the nonlinear character of the behavior of the magnetization, i.e., $\chi(T,H)$, and because of

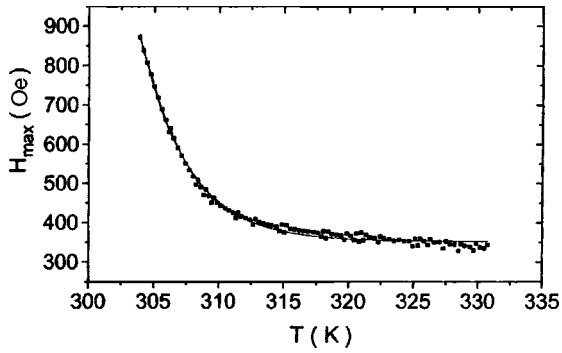


FIG. 4. Temperature dependence of the position of the ESR absorption line. The solid line shows the fit of the data by the function $H = H_0 + A^* e^{(T - T_c)/T_1}$.

the comparatively large values of the magnetic field (of the order of hundreds of oersteds). In this case it is better to talk about the magnetization rather than the susceptibility (possibly even about the ferromagnetic moment induced by the magnetic field).

The form of the results in Fig. 4 is closer to an exponential dependence. The approximation of the effective field by a decreasing exponential

$$H = H_0 + A^* e^{(T-T_c)/T_1} \tag{4}$$

with $T_c = 302.7$ K describes well the experimental results with the constants $H_0 = h\nu/g\mu_B = 352.4$ Oe, $A^* = 728.8$ Oe, and $T_1$ is a constant with the dimension of temperature, equal to 3.7°; $A^* = 4\pi M^* N_z$ is the demagnetizing field at $T_c$, and $M^*$ is the magnetization at $T_c$ in the corresponding magnetic field. From $A^*$ we obtain $M^* \approx 58$ cgs emu for $N_z \approx 1$, while the temperature behavior of the magnetization is determined by an expression of a type such as the second term in Eq. (4). From the value of $H_0$ we find the gyromagnetic ratio 2.51 GHz/kOe, whence we obtain the Landé factor $g \approx 1.8$.

In summary, in the present work we have studied the behavior of the ESR line in $La_{0.8}Sr_{0.2}MnO_3$ in the temperature range of the transition to the ferromagnetic state. we have determined the critical exponents for the temperature dependences of the intensity and width of the ESR line. We have estimated the specific magnetic moment of the material from the change in the position of the ESR line, and an exponential temperature dependence of the magnetization above the critical temperature in a magnetic field on the scale of 400 Oe was obtained.

This work was performed as part of Project Y-7 of the ''Statistical Physics'' area of the program ''Physics of Quantum and Wave Processes.''

[a)]e-mail: tulin@ipmt-hpm.ac.ru

[1] R. von Helmholt, J. Wecker, B. Holzapfel *et al.*, Phys. Rev. Lett. **71**, 2331 (1993).
[2] H. Y. Hwang, S. W. Cheong, P. G. Radaelli *et al.*, Phys. Rev. Lett. **75**, 914 (1995).
[3] C. Martin, A. Maignan, F. Damay, and B. Raveau, J. Solid State Chem. **134**, 198 (1997).
[4] É. L. Nagaev, Usp. Fiz. Nauk **166,** 833 (1996).
[5] P. G. de Gennes, Phys. Rev. **118**, 141 (1960).
[6] S. E. Lofland, P. H. Kim, P. Dahiroc *et al.*, J. Phys.: Condens. Matter **9**, 6697 (1997).
[7] S. E. Lofland, S. M. Bhagat, S. D. Tyagi *et al.*, J. Appl. Phys. **80**, 3592 (1996).
[8] S. B. Oseroff *et al.*, Phys. Rev. B **53**, 6521 (1996).
[9] S. E. Lofland, P. Kim, P. Dahiroc *et al.*, Phys. Lett. A **233**, 476 (1997).
[10] A. M. Balbashov, S. G. Karabashev, Ya. M. Mukovskiy, and S. A. Zverkov, J. Cryst. Growth **167**, 365 (1996).
[11] V. A. Alyoshin, V. A. Berezin, and V. A. Tulin, Phys. Rev. B **56**, 719 (1997).

Translated by M. E. Alferieff

# Measurements of core hole localization in x-ray Raman scattering

F. Gel'mukhanov

*Institute of Automation and Electrometry, Siberian Branch of the Russian Academy of Sciences, 630090 Novosibirsk, Russia; Institute of Physics and Measurement Technology, Linköping University, S-581 83, Linköping, Sweden*

H. Agren

*Institute of Physics and Measurement Technology, Linköping University, S-581 83, Linköping, Sweden*

(Submitted 21 May 1998)
Pis'ma Zh. Éksp. Teor. Fiz. **67**, No. 12, 1005–1008 (25 June 1998)

The problem of core hole localization in symmetrical systems is a fundamental problem of x-ray spectroscopy and concerns some basic aspects of quantum theory. Recent theoretical as well as experimental investigations of resonant x-ray Raman scattering indicate that the solution to this problem depends on the measurement. In the present work we propose an experimental scheme which allows a direct measurement of the atom to which the core hole is localized. The idea behind the proposal is based on the electron Doppler effect and the photoelectron–photoion coincidence technique. © *1998 American Institute of Physics.* [S0021-3640(98)01012-3]

PACS numbers: 32.30.Rj, 32.80.Hd

Despite the success of recent studies of the resonant x-ray Raman scattering (RXS) process,[1–3] one of its fundamental problems remains elusive when related to the world of our experience, namely the problem of the core hole localization (CHL) of x-ray excited symmetrical systems. Theory and recent synchrotron radiation experiments have demonstrated a close link between the CHL problem and the problem of quantum measurements. One can argue that a simple answer to the question of whether or not the core hole is localized does not exist by virtue of the fact that it depends strongly on the scheme of measurement. For example, RXS in the soft x-ray region demonstrates strict parity selection rules which has motivated a conclusion of delocalized core holes.[4–6] Due to the strong orientational dephasing these parity selection rules break down in the hard x-ray region.[4,7] A dephasing takes the quantum superposition into a statistical mixture of the localized core excited states, which is classically meaningful and interpretable. In this case a more adequate physical picture is based on the representation of localized core holes.[8,4] The results of these two experiments give an example, not uncommon in quantum physics, of a case where the measurements select the appropriate physical representation.[9]

The aim of this letter is to suggest alternative experiments that allow a direct mea-

 

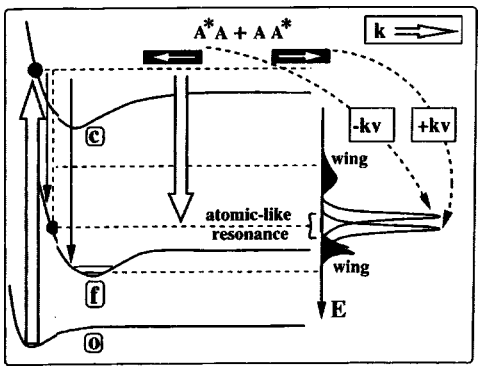


FIG. 1. Scheme of the formation of the RXS profile.

surement of localization of the core hole to one of the core excited state atoms in a diatomic molecule. The idea is based on the Doppler effect; while the ordinary photon Doppler effect in the x-ray region is negligibly small in comparison with the lifetime broadening $\Gamma$ of the core excited state, the Doppler shift of an Auger electron $\mathbf{k}\cdot\mathbf{v}$ is important if the molecule is core excited above the dissociation threshold.[10] Here $\mathbf{k}$ and $\mathbf{v}$ are the momentum of the Auger electron and speed of a core excited atom in the dissociative region of the molecular system of reference, respectively. This Doppler shift can exceed $\Gamma$ by several times when a molecule is core excited above the dissociation threshold.

It is, by now, well established[10–13] that when core excitation takes place above the dissociation threshold, the RXS spectral profile consists of a narrow atomic-like resonance and red and blue ''molecular'' wings (see Fig. 1). We consider the atomic-like resonance which is caused by the decay transitions in the dissociative region where the potentials of the core excited and final states ($U_c(R)$ and $U_f(R)$) are constant. The molecule is core excited by a soft x-ray photon from a *gerade* ground state to an *ungerade* core excited state. The wave function of the core excited state in the dissociative region is given by a superposition

$$\Psi_u = \frac{1}{\sqrt{2}}\left(\Psi(A^*A) - \mathcal{P}\Psi(AA^*)\right) \tag{1}$$

of the configurations $\Psi(A^*A)$ and $\Psi(AA^*)$ with the core hole on the left and right atoms, respectively. The sign of the factor $\mathcal{P}=\pm 1$ depends on the parities of the atomic orbitals involved in the photoabsorption transition. For more clarity we consider the realistic case when the electron Doppler shift is larger than $\Gamma$. In this case the interference of the scattering channels $A^*A$ and $AA^*$ is suppressed, and the cross section of an inelastic RXS event with emission of an Auger electron is simply the sum of the two contributions (Fig. 1)[10]

$$\sigma_{\mathbf{k}}(\omega,E) = \sigma^L_{\mathbf{k}}(\omega,E) + \sigma^R_{\mathbf{k}}(\omega,E), \quad \sigma^{L,R}_{\mathbf{k}}(\omega,E) \propto \frac{1}{(\Delta E \pm \mathbf{k}\cdot\mathbf{v})^2 + \Gamma^2}, \tag{2}$$

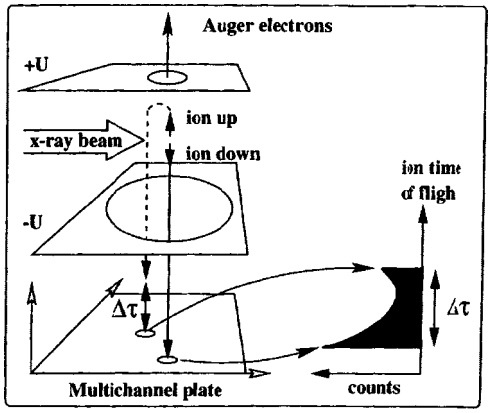


FIG. 2. Scheme of PEPICO experiment. The difference of the times of flight of up and down ions is denoted as $\Delta\tau$.

where $\Delta E = E - \omega_0$, $E$ is the energy of an Auger electron, $k = \sqrt{2E}$, $v \simeq ([U(R_0) - U_c(\infty)]/2m)^{1/2}$, $\omega_0 = U_c(\infty) - U_f(\infty)$ is the resonant frequency of the atomic-like resonance caused by decay transitions in the dissociative region. The partial cross sections $\sigma^L_{\mathbf{k}}(\omega,E)$ and $\sigma^R_{\mathbf{k}}(\omega,E)$ (2) correspond to the configurations $\Psi(A^*A)$ and $\Psi(AA^*)$, respectively (atomic units are used throughout the paper). Due to the Doppler shift $\mathbf{k}\cdot\mathbf{v}$ the directions of propagation of the Auger electron and the ions are strongly correlated when $kv \gg \Gamma$. This means that if the direction of the Auger electron propagation is fixed, the ions propagate in the vicinity of the dissociation cone, $\theta = \pm \arccos(\Delta E/kv)$, where $\theta$ is the angle between $\mathbf{k}$ and $\mathbf{v}$.

We can show how the scattering channel corresponding to the core excited state localized on a certain atom can be selected experimentally. This is possible by means of the PEPICO (photoelectron–photoion coincidence) technique, as used in a scheme[14] shown in Fig. 2. A permanent electric field is applied for electron extraction. The detection of an electron triggers an ion extraction pulse. The impact of an ion on a position-sensitive multichannel plate (MCP) starts a fast decoder system that reads the position. At the same time, the signal goes through a fast multiplexer enabling the detection of two ions in coincidence with an electron. The signals from up and down ions are measured separately due to the delay time of the up ions (Fig. 2).

The atom must be light to have a large Doppler shift, so low-$Z$ homonuclear diatomic molecules, like $N_2$, $O_2$, and $F_2$, which can be core excited above dissociation threshold are good candidates. Estimations show that one can expect Doppler shifts of $kv \lesssim 0.5$ eV while $\Gamma \sim 0.1$ eV for these molecules. Such Doppler shifts would be of the same order of magnitude as the the spectral resolution for current PEPICO measurements ($\sim 0.5$ eV).

The position of the Auger electron detector at one side of the region of ionization violates the symmetry of the composite system; measurement apparatus + molecule. Such an asymmetric measurement projects the quantum state (1) with an uncertain position of the core hole (Schrödinger-cat-like state: $\Psi_{CAT} = \Psi_{ALIVE} + \Psi_{DEAD}$) into a measurement eigenstate $\Psi(AA^*)$ (or $\Psi(A^*A)$) with a well-defined position of the core hole

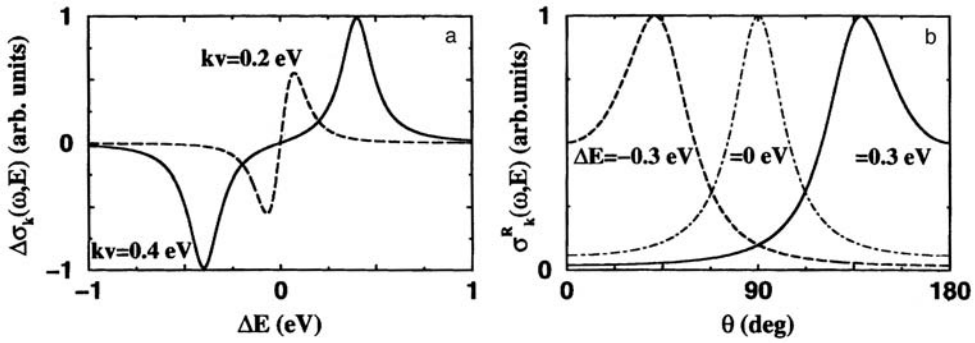


FIG. 3. a — The asymmetry of the ion yield (3). The propagation of the Auger electron along the photodissociation axis: $\theta=0°$. $\Gamma=0.1$ eV. b — The asymmetry of the Auger electron emission. $kv=0.4$ eV, $\Gamma=0.1$ eV.

due to the different Doppler labels for the two atoms. To see this directly it is convenient to use PEPICO to measure the difference of the partial cross sections (2)

$$\Delta\sigma_{\mathbf{k}}(\omega,E)=\sigma^R_{\mathbf{k}}(\omega,E)-\sigma^L_{\mathbf{k}}(\omega,E). \tag{3}$$

This function depends antisymmetrically on both the Auger electron energy $E$ and its momentum $\mathbf{k}$. Figures 1 and 3 show that core excited states with the core hole on the right atom ($AA^*$) give the main contribution to the signal (3) if the Auger electron energy is equal to $\Delta E=\mathbf{k}\cdot\mathbf{v}$ and vice versa if $\Delta E=-\mathbf{k}\cdot\mathbf{v}$. It is important to note that the averaging of $\Delta\sigma_{\mathbf{k}}(\omega,E)$ over $E$ or over directions of the Auger electron propagation leads to zero, $\overline{\Delta\sigma_{\mathbf{k}}(\omega,E)}=0$. The difference (3) is equal to zero also when the velocity selectivity is absent (small Doppler effect), $kv\ll\Gamma$. This means that only the PEPICO measurements in the systems with the large electron Doppler shift, $kv\gtrsim\Gamma$, allow one to select contributions to the RXS cross section from the core excited state with the core hole localized at a certain atom.

Thus one can conclude that asymmetric PEPICO measurements with the photoelectron detector at a certain side relative to the ionization region violate the symmetry of the $A^*A+AA^*$ system and select only one configuration, $A^*A$ or $AA^*$, depending on the Auger electron energy and the direction of $\mathbf{k}$. Such an appearance of classicality and of a change from the entangled (1) to disentangled states is caused by the asymmetrical macroscopic measuring apparatus and the electron Doppler effect, which thus destroys the quantum correlation between the localized states $A^*A$ and $AA^*$.

Equation (2) and Fig. 3b show that the Auger electron preferentially is emitted in the same ($\theta<90^o$) or opposite ($\theta>90^o$) directions as the $A^+$ ion if $\Delta E>0$ or $\Delta E<0$, respectively. This asymmetry is another evidence of the core hole localization on a particular atom.

This work was supported by the Swedish National Research council (NFR) and by the Russian Fund for Fundamental Research (Grant 96-02-19826). We greatly benefited from discussions of the experimental aspects with Drs. O. Björneholm, M. Simon, and Prof. S. Svensson.

[1] W. Eberhardt, in *Applications of Synchrotron Radiation*, edited by W. Eberhardt, Springer Series in Surface Sciences, Vol. 35, Springer-Verlag, Berlin, Heidelberg, 1995, p. 203.
[2] J. Nordgren. J. Phys. (Paris) **7**, C2–9 (1997).
[3] N. Mårtensson, M. Weinelt, O. Karis *et al.*, Appl. Phys. **A65**, 159 (1997).
[4] F. Gel'mukhanov and H. Ågren, Phys. Rev. A **49**, 4378 (1994).
[5] P. Glans, K. Gunnelin, P. Skytt *et al.*, Phys. Rev. Lett. **76**, 2448 (1996).
[6] P. Glans, P. Skytt, K. Gunnelin *et al.*, J. Electron Spectrosc. Relat. Phenom. **82**, 193 (1996).
[7] J. D. Mills, J. A. Sheehy, T. A. Ferrett *et al.*, Phys. Rev. Lett. **79**, 383 (1997).
[8] F. Gel'mukhanov, L. N. Mazalov, and N. A. Shklyaeva, Zh. Éksp. Teor. Fiz. **69**, 1971 (1975) [Sov. Phys. JETP **42**, 1001 (1976)].
[9] R. P. Feynman, R. B. Leighton, and M. L. Sands, *The Feynman Lectures on Physics, Vol. III: Quantum Mechanics*, Addison-Wesley, California, 1989.
[10] F. Gel'mukhanov, H. Ågren, and P. Sałek, Phys. Rev. A **57**, 2511 (1998).
[11] F. Gel'mukhanov and H. Ågren, Phys. Rev. A **54**, 379 (1996).
[12] O. Björneholm, S. Sundin, S. Svensson *et al.*, Phys. Rev. Lett. **79**, 3150 (1997).
[13] S. Tanaka, Y. Kayanuma, and K. Ueda, Phys. Rev. A **57**, 3437 (1998).
[14] A. V. Golovin, F. Heiser, C. J. K. Quayle *et al.*, Phys. Rev. Lett. **79**, 4554 (1997).

Published in English in the original Russian journal. Edited by Steve Torstveit.

# Transition between non-Fermi-liquid and Fermi-liquid states as a result of tunneling

L. A. Manakova
*Kurchatov Institute Russian Science Center, 123182 Moscow, Russia*

(Submitted 9 April 1998; resubmitted 21 May 1998)
Pis'ma Zh. Éksp. Teor. Fiz. **67**, No. 12, 1009–1014 (25 June 1998)

It is shown that additional scattering due to tunneling induces a transition of the system from a non-Fermi-liquid into a Fermi-liquid state as the distance between the Fermi level in the walls and the 2D-band edge is varied in a double-barrier quantum well, doped with transition-metal impurities and having an intrinsic two-dimensional continuum.
 [S0021-3640(98)01112-8]

PACS numbers: 71.10.Hf, 71.27.+a, 73.20.Dx

**1**. The multichannel spin Kondo model with a non-Fermi-liquid (NFL) elementary excitation spectrum at the Fermi level was proposed almost two decades ago in Ref. 1. Great interest in NFL states arose after physical realizations of the two-channel orbital Kondo model in heavy-fermion systems and high-temperature superconductors appeared.[2] However, the mechanisms of tunneling in quantum structures with a NFL-continuum in the walls are at present poorly understood. In Ref. 3 the temperature dependence of the conductance was estimated in a model of resonance tunneling through a quasilocalized state. These calculations were carried out in order to explain the experimental results obtained in Ref. 4, where, apparently, crossover was observed between NFL and Fermi-liquid (FL) states in an external magnetic field. Tunneling mechanisms in which a two-dimensional continuum in a double-barrier quantum well (DBQW) plays a fundamental role were studied in Ref. 5 for the case of orbitally nondegenerate impurity states. In the present letter new physical realizations of a two-channel orbital Kondo model in a quantum well are proposed, and the mechanism of a tunneling-induced transition between NFL and FL states is described.

**2**. A transition-metal impurity engenders a deep level $E_d$ in the band gap of the inner layer of the DBQW. This layer also possesses a two-dimensional continuum with a dispersion law $\epsilon_{\mathbf{k}_\perp}$. In the present problem we shall be interested in the case where the Fermi level in the walls lies near the conduction-band bottom of the inner layer. Since in the crystalline field a fivefold degenerate $d$ level splits into a twofold degenerate $e_g$ level and a threefold degenerate $t_{2g}$ level, the eigenfunctions and quantum numbers of an electron in a $d$ level are, respectively, the cubic $d$ functions and the number $\mu$ of the row of the irreducible representation of the point group: $\mu_{e_g}=\pm 1$, $\mu_{t_{2g}}=0,\pm 1$, and $E_d=E_{e_g,t_{2g}}$. As was shown in Ref. 6, because the symmetry of the states of the conduction band in the well is lowered (as compared with a bulk semiconductor), both the $t_{2g}$ and $e_g$ levels can hybridize with them. The Hamiltonian of the tunneling system with an $E_d$ level

 

in a quantum well has the form $H=H_{00}+H_t+H_{\rm int}$, where $H_{00}=H_{00}^{\nu}+H_{00}^{d}+H_{00}^{c}$ is the Hamiltonian of the independent walls and the well, and $H_t$ is the tunneling Hamiltonian

$$H_t=H_{td}+H_{tc}=\sum_{\mathbf{k}\nu\sigma\mu}(T_{\mathbf{k}d}^{\nu\mu}a_{\mathbf{k}\nu\sigma}^{+}d_{\sigma\mu}+\text{h.c.})+\sum_{\mathbf{k}\nu\sigma}\sum_{\mathbf{k}_\perp'}(T_{\mathbf{k}\mathbf{k}_\perp'}^{\nu}a_{\mathbf{k}\nu\sigma}^{+}c_{\mathbf{k}_\perp'\sigma}+\text{h.c.}). \tag{1}$$

The operators $a_{\mathbf{k}\nu\sigma}$ describe electronic states in the left-hand (L) and right-hand (R) walls of the tunneling contact. The operators $d_{\sigma\mu}$ and $c_{\mathbf{k}_\perp}$ in the well correspond to the wave functions of the hybridized localized $\psi_{d\mu}(\mathbf{r})$ and itinerant $\Psi(\mathbf{k}_\perp,\mathbf{r})$ states. The tunneling matrix elements in Eq. (1) equal[5]

$$T_{\mathbf{k}d}^{\nu\mu}=B^{\mu}(\mathbf{k}_\perp)T_d^{\nu}(k_l),\quad T_{\mathbf{k},\mathbf{k}_\perp'}^{\nu}=\left(T_0^{\nu}(k_l)\delta_{\mathbf{k}_\perp\mathbf{k}_\perp'}+\sum_{\mu\mu'}T_c^{\nu}(k_l)B_{\mu}(\mathbf{k}_\perp)B_{\mu'}(\mathbf{k}_\perp')\right). \tag{2}$$

Here $B_{\mu}(\mathbf{k}_\perp)=V_{\mathbf{k}_\perp d}^{\mu}/(E_{d\mu}-\varepsilon_{\mathbf{k}_\perp})$ and $V_{\mathbf{k}_\perp d}^{\mu}$ is the matrix element of hybridization in the well

$$V_{\mathbf{k}_\perp d}^{\mu}=\int d\mathbf{r}\varphi_{d\mu}(\mathbf{r})U(\mathbf{r})\Psi(\mathbf{k}_\perp,\mathbf{r})=\int d\mathbf{r}\varphi_{d\mu}(\mathbf{r})U(\mathbf{r})\psi(\mathbf{k}_\perp,\rho)\varphi(z). \tag{3}$$

In Eq. (2) $\mathbf{k}=\mathbf{k}_\perp$, $k_l$ and it was assumed that the longitudinal and transverse motion of electrons in the walls are separate. In Ref. 5 it was shown that the restructuring of the band spectrum in the well on account of tunneling between the walls and the well, corresponding to the term with $T_0^{\nu}(k_l)$ in $T_{\mathbf{k},\mathbf{k}_\perp'}^{\nu}$, can be described by means of a transformed density of states near the 2D-band edge: $\rho_c(\varepsilon)=(\rho_{0c}/\pi)(\tan^{-1}[(\varepsilon-\varepsilon_c)/\gamma_0]-\tan^{-1}[(\varepsilon-W_c)/\gamma_0])$. Here $\rho_{0c}$ is the threshold density of states of the undisturbed 2D band, $\varepsilon_c, W_c\sim\rho_{0c}^{-1}$ are, respectively, the edge and width of the 2D band, $\gamma_0\sim\Sigma_\nu|T_0^{\nu}(\varepsilon_c)|^2\rho_{0\nu}$, $\rho_{0\nu}\sim W_a^{-1}$ is the corresponding tunneling width, and $W_a$ is the width of the conduction band in the walls.

In an interacting system it is convenient to transform the tunneling Hamiltonian $H_t$ to a ''one-band'' form by means of a linear transformation: $a_{\mathbf{k}\sigma}=u_{\mathbf{k}}a_{\mathbf{k}L\sigma}+v_{\mathbf{k}}a_{\mathbf{k}R\sigma}$, $b_{\mathbf{k}\sigma}=u_{\mathbf{k}}a_{\mathbf{k}R\sigma}-v_{\mathbf{k}}a_{\mathbf{k}L\sigma}$, and $u_{\mathbf{k}}=T_{\mathbf{k}d}^{L\mu}/[(T_{\mathbf{k}d}^{L\mu})^2+(T_{\mathbf{k}d}^{R\mu})^2]^{1/2}$, where $u_{\mathbf{k}}^2+v_{\mathbf{k}}^2=1$. It can be verified directly that in the new representation only one kind of quasiparticles, with the operators $a_{\mathbf{k}\boldsymbol{\sigma}}$, hybridize with both the localized state and the two-dimensional continuum. The Hamiltonian $H_t^{(a)}$ can be obtained from $H_t$ in Eq. (1) by means of the substitutions $a_{\mathbf{k}\nu\sigma}^{+}\to a_{\mathbf{k}\sigma}$, $T_{\mathbf{k}d}^{\nu\mu}\to T_{\mathbf{k}d}^{a\mu}=[(T_{\mathbf{k}d}^{L\mu})^2+(T_{\mathbf{k}d}^{R\mu})^2]^{1/2}$, and $T_{\mathbf{k}\mathbf{k}_\perp'}^{\nu}\to T_{\mathbf{k}\mathbf{k}_\perp'}^{a}=T_{\mathbf{k}\mathbf{k}_\perp'}^{L}u_{\mathbf{k}}+T_{\mathbf{k}\mathbf{k}_\perp'}^{R}v_{\mathbf{k}}$. The term $H_{tc}^{a}$ in the tunneling Hamiltonian gives rise to new resonance states near the 2D-band edge.[5] Another source of features in this region are the interactions in $H_{\rm int}$. Since only the states $a_{\mathbf{k}\sigma}$ appear in the tunneling Hamiltonian, the interaction Hamiltonian $H_{\rm int}$ is also determined for them.

**3**. The interactions between the metallic electrons in the walls and an orbitally degenerate impurity state in the well are due to the Hubbard repulsion between electrons at a deep level: $H_U=\Sigma_{\mu,\mu';\sigma,\sigma'}U_{\mu\mu'}n_{d\mu\sigma}n_{d\mu'\sigma'}(1-\delta_{\mu\mu'}\delta_{\sigma\sigma'})$. Applying the Schrieffer–Wolff transformation to the generalized Anderson Hamiltonian $H_A=H_{00}^{a}+H_{td}^{a}+H_{00}^{d}+H_U$, $H_{00}^{d}=\Sigma_{\mu\sigma}E_d d_{\mu\sigma}^{+}d_{\mu\sigma}$, and retaining the interaction which is an exchange interaction with respect to the orbital indices but a ''non-Kondo'' interaction with respect to the spin variables, we obtain

$$H_{\rm int}=\sum_{\mathbf{k}\mathbf{k}'}\sum_{\mu\mu'\sigma}V^{\mu\mu'}_{\mathbf{k}\mathbf{k}'}a^{+}_{\mathbf{k}\sigma}a_{\mathbf{k}'\sigma}d^{\dagger}_{\mu}d_{\mu'},$$

$$V^{\mu\mu'}_{\mathbf{k}\mathbf{k}'}=-T^{a\mu}_{d\mathbf{k}}T^{a\mu'}_{\mathbf{k}'d}\left(\frac{1}{E_d-\varepsilon_{\mathbf{k}a}}-\frac{1}{E_d+U_{\mu\mu'}-\varepsilon_{\mathbf{k}'a}}\right). \tag{4}$$

This interaction is the main interaction when the spin degeneracy of a level is completely lifted or when both spin-degenerate levels lie below the Fermi level. Both situations can be realized in a quantum well for ''light'' transition-metal impurities (of the type $V^{2+}$).[6] The interaction matrix elements with $\mu\neq\mu'$ exist on account of the breaking of the axial symmetry of the spatially quantized states in the well. Indeed, taking account of the dependence of the wave functions of the two-dimensional continuum on the transverse spatial coordinates in expression (3) for the matrix elements $V^{\mu}_{\mathbf{k}_\perp d}$ results in the fact that they have nonzero values for all $d$-state components with $\mu_{e_g}=\pm1$, $\mu_{t_{2g}}=0,\pm1$. Correspondingly, the matrix elements $T^{a\mu}_{\mathbf{k}d}$ for all $\mu$ are also different from zero. As follows from the definition (2), a direct consequence of the breaking of axial symmetry is spatial nonlocality of the tunneling matrix elements $T^{a\mu}_{\mathbf{k}d}$. The Hamiltonian in Eq. (4) reduces to the Hamiltonian of the multichannel orbital Kondo model if the operators $a_{\mathbf{k}\sigma}$ and matrix elements $V^{\mu\mu'}_{\mathbf{k}\mathbf{k}'}$ in Eq. (4) are expanded in cubic harmonics $K_{\Gamma\gamma}(\Omega_{\mathbf{k}})$, $\Gamma=e_g,t_{2g}$, and $\gamma$ is the number of the row of the irreducible representation of the point group, and use is made of the fact that the interaction matrix elements $V^{\mu\mu'}_{\gamma\gamma'}(kk')$ with $\gamma,\gamma'$ are different from zero on account of the dependence of the tunneling matrix elements on the direction of the momentum $\mathbf{k}$. In the simplest case, where the 2D-continuum states can be described by plane waves, one has $\gamma=\mu$ and $\gamma'=\mu'$. We shall employ the fact that the $e_g$ and $t_{2g}$ states are separated by a quite large energy interval (compared with the energy scales of interest to us in this problem), so that their mixing in the interaction matrix elements can be neglected. Let us assume, bearing in mind the results of Ref. 6, that the deep level closest to the 2D-band edge is an $e_g$ doublet. On this basis we obtain from Eq. (4) the two-channel orbital exchange scattering:

$$H^{(\mu)}_{ex}=\sum_{kk'\sigma}\sum_{i=x,y,z}\sum_{\gamma,\gamma'=\pm1}V^{i}_{\gamma\gamma'}(kk')a^{+}_{k\gamma\sigma}a_{k'\gamma'\sigma}\hat{\tau}^{i}_{d},\quad \hat{\tau}^{i}_{d}=\sum_{\mu\mu'=\pm1}d^{\dagger}_{\mu}\tau^{i}_{\mu\mu'}d_{\mu'}, \tag{5}$$

$$\sum_{\mu=\pm1}d^{\dagger}_{\mu}d_{\mu}=1.$$

It is convenient to describe the twofold degenerate $e_g$ level with one electron (or hole) by a pseudospin variable $\hat{\tau}_d$, whose projection on the $z$ axis has two values: $\hat{\tau}^{z}_{d}=(1/12)[3L^2_z-L(L+1)]=\pm(1/2)$, corresponding to occupied $d_{z^2}$ ($L_z=2$) and $d_{x^2-y^2}$ ($|L_z|=0$) orbitals, $\hat{L}$ is the angular momentum operator. The operator $\hat{\tau}^{x}_{d}\sim L^2_x-L^2_y$ flips the pseudospin. The operators $\hat{\tau}^{z}_{d}$ and $\hat{\tau}^{x}_{d}$ are components of the quadrupole moment tensor. Therefore the two values of the quantum number $\mu=\pm1$ correspond to two projections of the quadrupole moment on the $z$ axis, i.e., the interaction (5) represents quadrupole exchange scattering. The model (5) with quadrupole exchange differs from the models proposed in Ref. 2 with a physical mechanism for the appearance of exchange.

It is convenient to solve first the problem of the interaction of the electrons in the walls with a localized state in the well by one of the methods developed for the two-channel Kondo scattering problem[7,8] and then to use this solution as a basis for the tunneling problem. In other words, the solution of the problem with the Hamiltonian $H_0=H_{00}+H_{ex}^{(\mu)}$ will give NFL states at the Fermi level in the walls and the corresponding state at an impurity level. Then taking account of the tunneling term $H_{tc}^a$ gives additional scattering of the 2D electrons of the defective layer by states of the walls and the impurity level, which were obtained with the interaction taken into account.

**4**. In the case of a level which is twofold degenerate with respect to the orbital or spin variables of the level, so that the main effect of the interaction reduces to the existence of a multiparticle resonance at the Fermi level, the approximate expressions for the Green's functions of the conduction electrons can be obtained by the equations-of-motion method[7]

$$G_{0\beta}^a(\mathbf{k}\mathbf{k}';z)=\delta_{\mathbf{k}\mathbf{k}'}G_{00\beta}^a(\mathbf{k};z)+G_{00\beta}^a(\mathbf{k};z)T_{\mathbf{k}d}^{a\beta *}G_{d\beta}(z)T_{\mathbf{k}'d}^{a\beta}G_{00\beta}^a(\mathbf{k}';z). \quad (6)$$

Here $\beta=[\sigma,\mu]$ for spin or orbital exchange scattering, respectively; $G_{00\beta}^a(\mathbf{k};z)$ is the Green's function of noninteracting electrons. To determine the form of $G_{d\gamma}(z)$ in the case of a two-channel exchange interaction, we shall employ a resonance-level model which was obtained in Ref. 8 for the Hamiltonian (5) by the bosonization method. The collective variables which are described by the Fourier components of the Bose fields correspond to charge, spin (color), pseudospin, and mixed (pseudospin–color) density operators. In these variables the Hamiltonian $H_0=H_{00}^a+H_{ex}^{(\mu)}$ can be represented as a sum of four terms corresponding to four spinless fermion collective channels. Two of these channels (charge and color) are not coupled with the impurity pseudospin. A remarkable property of the model of Ref. 8 is that the hybridization and interaction between the electronic variables and the impurity pseudospin $\hat{\tau}$ are ''spread'' over different channels. Hybridization occurs in the mixed channel. Correspondingly, the NFL peak at the Fermi level is formed by the pseudospin–color mode. The interaction in the pseudospin channel is of a screening character and leads to effective broadening of the resonance level (see Eq. (7)). In Refs. 8 and 9 a solution was obtained neglecting the interaction in the pseudospin channel: $\lambda_z\equiv V_z-\pi v_F=0$ or for $\lambda_z\ll 1$, in which case the interaction is taken into account in second-order perturbation theory. However, for the tunneling problem under study here the form of $G_d(z)$ with a finite interaction $\lambda_z$ is important. As will be shown below, there exists a critical value of the interaction constant for which the character of the scattering of electrons from the vicinity of the 2D-band edge by excitations from the Fermi level changes qualitatively. For $\lambda_z\neq 0$ the Hamiltonian can be diagonalized by a method which in its time was applied in the famous problem of x-ray absorption in metals.[10] The expression obtained at long times $\varepsilon_F t\gg 1$ for the Green's function of the resonance level in the energy representation has the form

$$\hat{G}_d(z)=A\left[\frac{\hat{\tau}_0-\hat{\tau}_x}{z-E_{2K}}\left(\frac{z-E_{2K}}{\varepsilon_F}\right)^{\alpha_d}+\frac{\hat{\tau}_0+\hat{\tau}_x}{z}\left(\frac{z}{\varepsilon_F}\right)^{\alpha_d}\right],\quad A=e^{i\pi(1/2-\alpha_d)}\Gamma(1-\alpha_d), \quad (7)$$

$\alpha_d=(\delta/\pi)^2$, $\delta$ is the phase shift, $E_{2K}=\varepsilon_F+i\Gamma_K$, $\Gamma_K\sim V_x^2/\varepsilon_F$ is the width of the resonance level, and $\Gamma(x)$ is the gamma function. Using expressions (7) and (6), the density of states can be calculated in the standard manner:

$$\rho_a(\varepsilon)=\rho_{0a}+A_\rho(\gamma_d\rho_{0a})\sum_{i=1,2}\frac{\sin[(1-\alpha_d)\tan^{-1}(\Gamma_i/\varepsilon)]}{\varepsilon_F^{\alpha_d}(\varepsilon^2+\Gamma_i^2)^{(1-\alpha_d)/2}},\quad \gamma_d\sim\gamma_0|B|^2,\quad \varepsilon>0. \tag{8}$$

The widths $\Gamma_1\equiv\delta\to 0$ and $\Gamma_2\equiv\Gamma_K$ correspond to two terms in the Green's function $\hat{G}_d(z)$, $A_\rho\sim 1$.

**5**. We shall now take into account the additional scattering of quasi-two-dimensional electrons inside the well by excitations from the Fermi level of the walls as a result of the tunneling term $H_{tc}^a$. The states of the electrons at the Fermi level and at the impurity level are described by the Green's functions (6) and (7), respectively. The scattering matrix $\mathcal{T}_\sigma^{cc}(\mathbf{k}_\perp,\mathbf{k}'_\perp;z)$ for an electron inside the well is determined from the Green's function $G_\sigma^{cc}(\mathbf{k}_\perp,\mathbf{k}'_\perp;z)=\langle c_{\mathbf{k}_\perp}|\hat{I}(z-\hat{H})^{-1}|c_{\mathbf{k}'_\perp}\rangle=\delta_{\mathbf{k}_\perp,\mathbf{k}'_\perp}G_{0\mathbf{k}_\perp}(z)+G_{0\mathbf{k}_\perp}(z)\times\mathcal{T}_\sigma^{cc}(\mathbf{k}_\perp,\mathbf{k}'_\perp;z)G_{0\mathbf{k}'_\perp}(z)$, $G_{0\mathbf{k}_\perp}(z)=[z-\tilde{\varepsilon}_{\mathbf{k}_\perp}]^{-1}$,

$$\mathcal{T}_\sigma^{cc}(\mathbf{k}_\perp,\mathbf{k}'_\perp;z)=\frac{T_0(z)B(\mathbf{k}_\perp)B^*(\mathbf{k}'_\perp)}{1-T_0(z)J_c(z)};\quad T_0(z)=|\Sigma_{dc}(z)|^2G_{d\sigma}(z)+\Sigma_{cc}(z). \tag{9}$$

For a deep level $B(\mathbf{k}_\perp)\approx B(\varepsilon_c)\equiv\Sigma_\mu B_\mu(\varepsilon_c)$.

In the important energy range it is convenient to write $\Sigma_{cc}(z)$ and $\Sigma_{dc}(z)$ in the form of a spectral representation of the Green's function $G_{0\mathbf{k}}^a(z)=\langle a_{\mathbf{k}\sigma}|\hat{I}(z-\hat{H}_0)^{-1}|a_{\mathbf{k}\sigma}\rangle=[z-\varepsilon_{\mathbf{k}a}]^{-1}$ of the interacting electrons:

$$\Sigma_{cc}(z)=\sum_{k\gamma\sigma}\frac{|T_{kc\gamma}^a|^2f(\varepsilon_{ka})}{(z-\varepsilon_c)-(\varepsilon_{ka}-\varepsilon_c)}=\sum_\gamma|T_{k_Fc\gamma}^a|^2\int_{-\infty}^0 d\varepsilon\frac{\rho_a(\varepsilon)}{(z-\varepsilon_c)-\varepsilon}. \tag{10}$$

The expression for $\Sigma_{dc}(z)$ is similar to Eq. (10) with the substitution $|T_{kc\mu}^a|^2\to T_{kc\mu}^{a*}T_{kd\mu}^a$, $f(\varepsilon)$ is the Fermi function, and $\rho_a(\varepsilon)$ is determined by expression (8). The energies are measured from $\varepsilon_F\to\varepsilon_c$. The single-particle and multiparticle resonances strongly influence one another in this region. The self-energy functions $\Sigma_{cc}(z)$ and $\Sigma_{dc}(z)$ have singularities at the Fermi level which correspond to NFL peaks in the density of states $\rho_a(\varepsilon)$ (8). Substituting expression (8) into Eq. (10), we obtain the contribution of the resonance level $E_{2K}$ to the self-energy functions $\Sigma_{cc,dc}(z)$:

$$\Sigma_{cc,dc}(z)=A_{1,2}\gamma_d^2\frac{(z+i\Gamma_K)^{1-\alpha_d}-(z-i\Gamma_K)^{1-\alpha_d}}{\varepsilon_F^{\alpha_d}(z^2+\Gamma_K^2)^{(1-\alpha_d)}},\quad |A_{1,2}|\sim 1. \tag{11}$$

The integral $J_c(z)$ is the Hilbert transform of the quasi-two-dimensional single-particle density of states $\rho_c(\varepsilon)$. For $|z-\varepsilon_c|/\gamma_0\ll 1$ this integral has a logarithmic singularity

$$J_c(z)=\int d\varepsilon\frac{\rho_c(\varepsilon)|B(\varepsilon)|^2}{z-\varepsilon}=-\frac{1}{2}\tilde{\rho}_{0c}\ \mathrm{Ln}\left(\frac{z-\varepsilon_c}{\gamma_0}\right);\quad \tilde{\rho}_{0c}=\rho_{0c}(\varepsilon_c)|B(\varepsilon_c)|^2. \tag{12}$$

The logarithmic behavior of the self-energy part $J_c(z)$ signifies that it engenders single-particle resonances in the same energy region where a multiparticle resonance exists. Since the multiparticle resonance at the Fermi level determines the singularities of $T_0(z)$, the low-energy poles of the scattering matrix are determined by the self-consistent equation

$$1-T_0(z)J_c(z)=0. \tag{13}$$

Using expressions (11) and (12) it is easily verified that Eq. (13) possesses a solution of the edge-resonance type with energy $z_r=\varepsilon_c+i\gamma_r$. The resonance component of $T_0(z)$ makes the main contribution to the formation of the edge resonance. The width $\gamma_r$ of the resonance is determined by the expressions

$$\gamma_r=A_{r1}\varepsilon_F|B|^{2/(1-\alpha_d)}\left(\frac{\rho_{0c}}{\rho_{0a}}\right)^{1/(1-\alpha_d)}\left(\frac{\gamma_d}{\varepsilon_F}\right)^{4/(1-\alpha_d)}, \quad |\gamma_r|\ll\Gamma_K; \tag{14}$$

$$\gamma_r\approx\Gamma_K-A_{r2}\varepsilon_F|B|^{2/3(1-\alpha_d)}\left(\frac{\rho_{0c}}{\rho_{0a}}\right)^{1/3(1-\alpha_d)}\left(\frac{\gamma_d}{\varepsilon_F}\right)^{4/3(1-\alpha_d)}, \quad |\Gamma_K-\gamma_r|\ll\Gamma_K, \tag{15}$$

$A_{r1}$, $A_{r2}\sim 1$.

The edge resonance exists for $|B|^{2(6\alpha_d-1)}<(W_c/W_a)(\gamma_0/\varepsilon_F)^{2(1-3\alpha_d)}$, $\alpha_d>1/6$, i.e., only for finite values of the interaction constant $\lambda_z$ and a sufficiently deep $d$ level. For all other values of the parameters, including the point $\lambda_z=0$, the scattering matrix has no poles.

We can see that the additional scattering of electrons from the region near the 2D-band edge by NFL excitations from the Fermi level on account of the tunneling $H_t^a$ engenders a Fermi-liquid resonance at the edge of the 2D band in the well, since it corresponds to a simple pole in the Green's function. If scattering processes due to tunneling are neglected, the power-law singularity in the Green's function $G_{0\mathbf{k}}^a(z)$ and accordingly in the density of states $\rho_a(\varepsilon)$ corresponds to a NFL state of the electrons in the walls (see, specifically, Ref. 10 as well as the solution obtained in the present letter).

In summary, as the Fermi level of the walls approaches the 2D-band edge, a transition between NFL and FL tunneling regimes can occur. The conditions for the transition are identical to the conditions for the existence of solutions of Eq. (13).

**6**. Using for the elastic tunneling probability the formula $W(\mathbf{k},\varepsilon_{\mathbf{k}}^L;\mathbf{k}',\varepsilon_{\mathbf{k}'}^R)=2\pi|\mathcal{T}(\mathbf{k},\varepsilon_{\mathbf{k}}^L;\mathbf{k}',\varepsilon_{\mathbf{k}'}^R)|^2\delta(\varepsilon_{\mathbf{k}}^L-\varepsilon_{\mathbf{k}'}^R)$ with tunneling-transition amplitude $\mathcal{T}(\mathbf{k},\varepsilon_{\mathbf{k}}^L;\mathbf{k}',\varepsilon_{\mathbf{k}'}^R)=\Sigma_{\mathbf{pp}'\sigma}\langle a_{\mathbf{k}L\sigma}|H_t|c_{\mathbf{p}\sigma}\rangle\langle c_{\mathbf{p}\sigma}|G|c_{\mathbf{p}'\sigma}\rangle\langle c_{\mathbf{p}'\sigma}|H_t|a_{\mathbf{k}'R\sigma}\rangle=u_{\mathbf{k}}v_{\mathbf{k}'}\Sigma_{\mathbf{pp}'\sigma}\langle a_{\mathbf{k}\sigma}|H_t|c_{\mathbf{p}\sigma}\rangle\langle c_{\mathbf{p}\sigma}|G|c_{\mathbf{p}'\sigma}\rangle\langle c_{\mathbf{p}'\sigma}|H_t|a_{\mathbf{k}'\sigma}\rangle$, we find that the maximum contribution of the edge resonance (14) to the transmission equals

$$\sigma_r^{\max}(\varepsilon_F)=\frac{e^2}{4\pi}S(\varepsilon_F); \quad S(\varepsilon_F)\sim\left(\frac{\gamma_0}{\gamma_r}\right)^2\left(\frac{\varepsilon_F}{\gamma_0}\right)^{2(1-2\alpha_d)}|B|^{4(1+2\alpha_d)}\gg 1.$$

Edge resonances make the main contribution to the transmission and dictate a FL tunneling regime so long as the distance between the Fermi level and the 2D-band edge is less than the width of the bare NFL resonance at the Fermi level: $|\varepsilon_F-\varepsilon_c|<\Gamma_K$. If the Fermi level lies at a distance from the 2D-band edge greater than the width of the bare NFL resonance at the Fermi level, then the latter makes the main contribution to the tunneling transmission and thereby dictates a NFL tunneling regime. For a fixed position of the Fermi level $|\varepsilon_F-\varepsilon_c|>\Gamma_K$, a transition between FL and NFL states occurs either with the impurity level becoming ''shallower'' or with a decrease of the interaction $\lambda_z$.

I thank L. A. Maksimov for critical remarks. This work is supported by the Russian Fund for Fundamental Research.

[1] P. Nozieres and A. Blandin, J. Phys. (Paris) **41**, 193 (1980).
[2] D. J. Cox, Phys. Rev. Lett. **59**, 1240 (1987); D. J. Cox *et al.*, Phys. Rev. Lett. **62**, 2188 (1989).
[3] M. H. Hettler, J. Kroha and S. Hershfield, Phys. Rev. Lett. **73**, 1967 (1994).
[4] D. C. Ralph and B. A. Buhrman Phys. Rev. Lett. **72**, 3401 (1994).
[5] K. A. Kikoin and L. A. Manakova, Phys. Rev. B **57**, 4863 (1997); K. A. Kikoin and L. A. Manakova, JETP Lett. **65**, 484 (1997).
[6] K. A. Kikoin and L. A. Manakova, Fiz. Tekh. Poluprovodn. **29**, 291 (1995) [Semiconductors **29**, 145 (1995)].
[7] A. C. Hewson, *The Kondo Problem to Heavy Fermions*, Cambridge University Press, 1993.
[8] V. J. Emery and S. Kivelson, Phys. Rev. B **46**, 10812 (1992).
[9] A. M. Sengupta and A. Georges, Phys. Rev. B **49**, 1020 (1994).
[10] K. D. Schotte and U. Schotte, Phys. Rev. **182**, 479 (1969); P. Nozieres and C. T. de Dominicis, Phys. Rev. **178**, 1097 (1969).

Translated by M. E. Alferieff

# Hamiltonian dynamics of vortex lines in hydrodynamic-type systems

E. A. Kuznetsov and V. P. Ruban

*L. D. Landau Institute of Theoretical Physics, Russian Academy of Sciences, 117334 Moscow, Russia*

(Submitted 25 March 1998; resubmitted 30 April 1998)
Pis'ma Zh. Éksp. Teor. Fiz. **67**, No. 12, 1015–1020 (25 June 1998)

It is shown that the degeneracy of the noncanonical Poisson bracket operating on the space of solenoidal vector fields that arises due to the freezing-in of the curl of the velocity [E. A. Kuznetsov and A. V. Mikhailov, Phys. Lett. A **77**, 37 (1980)] is lifted when the vorticity $\mathbf{\Omega}$ is represented in terms of vortex lines. This representation makes it possible to integrate the equation of motion of the vorticity for a system with the Hamiltonian $\mathcal{H}=\int|\mathbf{\Omega}|d\mathbf{r}$. © *1998 American Institute of Physics.* [S0021-3640(98)01212-2]

PACS numbers: 47.32.−y

**1**. There are a large number of works on the Hamiltonian description of ideal hydrodynamics (see, for example, the review in Ref. 1 and the references cited therein). This question was first studied by Clebsch (a citation can be found in Ref. 2), who introduced the pair of variables $\lambda$ and $\mu$ (later called Clebsch variables) to describe nonpotential flows of an incompressible liquid. In these variables the dynamics of the liquid is such that the vortex lines consist of the intersection of the surfaces $\lambda=$ const and $\mu=$ const, while the variables themselves, being canonically conjugate quantities, are transported together with the liquid. However, as is well known (see, for example, Ref. 3), these variables describe only flows of a special type. If $\lambda$ and $\mu$ are single-valued functions of the coordinates, then the degree of linkage of the vortex lines, which is characterized by the Hopf invariant,[4] is identically equal to zero. The Hamiltonian formulation of the equations of incompressible ideal hydrodynamics for arbitrary flows was given by Arnol'd.[5] The Euler equation for the curl of the velocity $\mathbf{\Omega}=\mathrm{curl}\ \mathbf{v}$

$$\partial\mathbf{\Omega}/\partial t=\mathrm{curl}\,[\mathbf{v}\times\mathbf{\Omega}]\equiv-(\mathbf{v}\cdot\nabla)\mathbf{\Omega}+(\mathbf{\Omega}\cdot\nabla)\mathbf{v},\quad \nabla\cdot\mathbf{v}=0 \tag{1}$$

can be written in the Hamiltonian form

$$\partial\mathbf{\Omega}/\partial t=\{\mathbf{\Omega},\mathcal{H}\} \tag{2}$$

by means of the noncanonical Poisson bracket[3]

$$\{F,G\}=\int(\mathbf{\Omega}[\mathrm{curl}(\delta F/\delta\mathbf{\Omega})\times\mathrm{curl}(\delta G\,\delta\mathbf{\Omega})])d\mathbf{r} \tag{3}$$

and the Hamiltonian $\mathcal{H}_h=(1/2)\int\mathbf{\Omega}\cdot\Delta^{-1}\mathbf{\Omega}d^3\mathbf{r}$, which equals the energy of the liquid.

Despite the fact that the bracket (3) makes it possible to describe flows with arbitrary topology, its main drawback is degeneracy. As a result of this, it is impossible to formu-

 

late a variational principle over the entire space $\mathcal{S}$ of solenoidal vector fields.

The reason for the degeneracy — the presence of Casimirs, which make the bracket vanish — is related to the existence of a special symmetry which forms an entire group — the group of transformations of Lagrangian labels (see Refs. 7 and 1 for a detailed discussion of this). This symmetry engenders all known vorticity conservation laws. The main one is the law of freezing-in of vortex lines in a liquid. A local Lagrangian invariant — the Cauchy invariant — is responsible for this. The present letter examines a method for lifting the degeneracy of noncanonical Poisson brackets by introducing new variables — Lagrangian labels which enumerate each vortex line. This approach is based on an integral representation of the condition of freezing-in of the curl of the velocity, making it possible to switch to new objects — vortex lines. This approach, which employs a mixed Lagrangian–Eulerian description, makes it possible to write down a variational principle and study quite simply the limit of thin vortex filaments. The Hamiltonian structure introduced makes it possible to integrate the three-dimensional Euler equation (2) with Hamiltonian $\mathcal{H}=\int|\mathbf{\Omega}|d\mathbf{r}$. In terms of vortex lines this Hamiltonian decomposes into a set of Hamiltonians of noninteracting vortex lines. The dynamics of each line is described by an equation of vortex induction, which can be reduced by a Hasimoto transformation[7] to an integrable one-dimensional nonlinear Schrödinger equation.

**2**. Let us consider the Hamiltonian dynamics of a solenoidal vector field $\mathbf{\Omega}(\mathbf{r},t)$ given by the Poisson bracket (3) with Hamiltonian $\mathcal{H}$:

$$\partial\mathbf{\Omega}/\partial t=\mathrm{curl}\,[\mathrm{curl}\,(\delta\mathcal{H}/\delta\mathbf{\Omega})\times\mathbf{\Omega}]. \tag{4}$$

As we have said, the bracket (3) is degenerate, as a result of which it is impossible to formulate a variational principle on the entire space $\mathcal{S}$ of solenoidal vector fields. It is known[1] that Casimirs $f$, which make the bracket vanish, distinguish in $\mathcal{S}$ invariant manifolds $\mathcal{M}_f$ (simplectic sheets) on each of which it is possible to introduce the standard Hamiltonian mechanics and accordingly to write down a variational principle. We shall show that for Eqs. (4) all linkages due to Casimirs can be resolved with the aid of the freezing-in property of the field $\mathbf{\Omega}(\mathbf{r},t)$.

To each Hamiltonian $\mathcal{H}$ — a functional of $\mathbf{\Omega}(\mathbf{r},t)$ — we associate the generalized velocity

$$\mathbf{v}(\mathbf{r})=\mathrm{curl}(\delta\mathcal{H}/\delta\mathbf{\Omega}). \tag{5}$$

A comparison of Eq. (1) with the equation for the tangent vector $\mathbf{R}_{s_0}$ to a vortex line,

$$[\partial/\partial t+(\mathbf{v}\cdot\nabla)]\mathbf{R}_{s_0}=(\mathbf{R}_{s_0}\cdot\nabla)\mathbf{v}, \tag{6}$$

where $s_0$ is a Lagrangian variable labeling a particle along a vortex line, shows that the field lines of the field $\mathbf{\Omega}$ are frozen into a substance whose transport velocity is $\mathbf{v}(\mathbf{r})$. However, the generalized velocity $\mathbf{v}(\mathbf{r})$ itself is determined to within a component which is longitudinal with respect to $\mathbf{\Omega}$: In Eq. (4) the substitution

$$\mathrm{curl}(\delta\mathcal{H}/\delta\mathbf{\Omega})\to\mathrm{curl}(\delta\mathcal{H}/\delta\mathbf{\Omega})+\alpha\mathbf{\Omega},$$

can be made without changing the equation in any way. Under the condition $(\mathbf{\Omega}\cdot\nabla\alpha)=0$ the new generalized velocity will possess zero divergence, while the freezing-in equation (4) and Eq. (6) can now be rewritten for the new velocity $\mathbf{v}(\mathbf{r})$. It is obvious that the previous parameter $s_0$ will no longer label a particle along a line — a new variable $s$

is required. Adding a Casimir to the Hamiltonian $\mathcal{H}\to\mathcal{H}+f$; $\{f,.\}=0$, corresponds to changing the gauge of the generalized velocity. On this basis it becomes obvious that the transformation $\mathbf{r}=\mathbf{R}(\mathbf{a},t)$ of the initial arrangement of the ''liquid'' particles $\mathbf{R}(\mathbf{a},0)=\mathbf{a}$ by the generalized velocity field $\mathbf{v}(\mathbf{r})$ is not determined uniquely because Eq. (5) does not determine $\mathbf{v}(\mathbf{r})$ uniquely.

This assertion agrees with the possibility of gauge transformations in the following general expression for $\mathbf{\Omega}(\mathbf{r})$, fixing all topological properties of the system that are determined by the initial field $\mathbf{\Omega}_0(\mathbf{a})$:

$$\mathbf{\Omega}(\mathbf{r},t)=\int \delta(\mathbf{r}-\mathbf{R}(\mathbf{a},t))(\mathbf{\Omega}_0(\mathbf{a})\cdot\nabla_{\mathbf{a}})\mathbf{R}(\mathbf{a},t)d^3\mathbf{a}. \tag{7}$$

As can be easily checked, it follows from the condition $\nabla_{\mathbf{a}}\cdot\mathbf{\Omega}_0(\mathbf{a})=0$ that the divergence of expression (7) vanishes identically; the Jacobian $J=\det\|\partial\mathbf{R}/\partial\mathbf{a}\|$ of the transformation is not assumed to equal 1.

The gauge transformation $\mathbf{R}(\mathbf{a})\to\mathbf{R}(\tilde{\mathbf{a}}_{\Omega_0}(\mathbf{a}))$ leaves this integral unchanged if $\tilde{\mathbf{a}}_{\Omega_0}$ is obtained from $\mathbf{a}$ by an arbitrary nonuniform displacement along the field lines of the field $\mathbf{\Omega}_0(\mathbf{a})$. Therefore the invariant manifold $\mathcal{M}_{\Omega_0}$ of the space $\mathcal{S}$, on which the variational principle holds, is obtained from the space $\mathcal{R}$:$\mathbf{a}\to\mathbf{R}$ of arbitrary continuous one-to-one three-dimensional mappings by identifying in $\mathcal{R}$ elements that are obtained from one another by means of a gauge transformation with a fixed solenoidal field $\mathbf{\Omega}_0(\mathbf{a})$.

The integral representation for $\mathbf{\Omega}$ (7) is a different formulation of the freezing-in condition — from the integral relation (7) over the area $\sigma$ transverse to the lines of $\mathbf{\Omega}$ follows that the flux of this vector remains constant in time: $\int_{\sigma(t)}\mathbf{\Omega}\cdot d\mathbf{S}_{\mathbf{r}}=\int_{\sigma(0)}\mathbf{\Omega}_0\cdot d\mathbf{S}_{\mathbf{a}}$.

It is also important that $\mathbf{\Omega}_0(\mathbf{a})$ can be expressed explicitly in terms of the instantaneous value of the vorticity and the inverse mapping $\mathbf{a}=\mathbf{a}(\mathbf{r},t)$. By integrating over the variables $\mathbf{a}$ in the relation (7) (compare with Ref. 1),

$$\mathbf{\Omega}(\mathbf{R})=J^{-1}(\mathbf{\Omega}_0(\mathbf{a})\cdot\nabla_a)\mathbf{R}(\mathbf{a}), \tag{8}$$

$\mathbf{\Omega}_0(\mathbf{a})$ can be represented in the form $\mathbf{\Omega}_0(\mathbf{a})=J(\mathbf{\Omega}(\mathbf{r})\cdot\nabla)\mathbf{a}$. This formula is an expression for the Cauchy Lagrangian invariant (see, for example, Ref. 2). We note that according to Eq. (8) the vector $\mathbf{b}=(\mathbf{\Omega}_0(\mathbf{a})\cdot\nabla_{\mathbf{a}})\mathbf{R}(\mathbf{a})$ is tangent to $\mathbf{\Omega}(\mathbf{R})$. It is natural to introduce a parameter $s$ as an element of arc of the initial vortex line $\mathbf{\Omega}_0(\mathbf{a})$ so that $\mathbf{b}=\Omega_0(\nu)\partial\mathbf{R}/\partial s$. In this expression $\Omega_0$ depends on the transverse parameter $\nu$ labeling each vortex line. Accordingly, the representation (7) can be written in the form

$$\mathbf{\Omega}(\mathbf{r},t)=\int \Omega_0(\nu)d^2\nu\int \delta(\mathbf{r}-\mathbf{R}(s,\nu,t))\partial\mathbf{R}/\partial\mathbf{s}ds, \tag{9}$$

whence the meaning of the new variables becomes clearer: To each vortex line $\nu$ there is associated a closed line $\mathbf{r}=\mathbf{R}(s,\nu,t)$, and the integral (9) itself is a sum over vortex lines. We note that the parametrization by introduction of $s$ and $\nu$ is local. Therefore, just like the global representation, the representation (9) is suited only for distributions with closed vortex lines.

To obtain the equation of motion for $\mathbf{R}(\nu,s,t)$ the representation (9) (in the general case (7)) must be substituted into the Euler equation (1) and a Fourier transform with respect to the coordinates performed. A simple integration gives

$$\left[\mathbf{k}\times\int\Omega_0(\nu)d^2\nu\int ds e^{-i\mathbf{k}\cdot\mathbf{R}}[\mathbf{R_s}\times\{\mathbf{R_t}(\nu,s,t)-\mathbf{v}(\mathbf{R},t)\}]\right]=0.$$

This equation can be solved by assuming that the integrand is identically equal to zero:

$$[\mathbf{R_s}\times\mathbf{R_t}(\nu,s,t)]=[\mathbf{R_s}\times\mathbf{v}(\mathbf{R},t)]. \tag{10}$$

With this choice there remains freedom in changing the parameter $s$ and relabeling $\nu$ of the transverse coordinates. In the general case of arbitrary topology of the field $\mathbf{\Omega}_0(\mathbf{a})$ the vector $\mathbf{R_s}$ in Eq. (10) must be replaced by the vector $\mathbf{b}=(\mathbf{\Omega}_0(\mathbf{a})\cdot\nabla_\mathbf{a})\mathbf{R}(\mathbf{a},t)$.

The description of vortex lines by means of Eqs. (9) and (10) is a mixed Lagrangian–Eulerian description: The parameter $\nu$ has a transparent Lagrangian origin, while the coordinate $s$ remains Eulerian.

**3**. The key observation for formulating a variational principle is that the following general equality is holds for functionals that depend only on $\mathbf{\Omega}$:

$$[\mathbf{b}\times\mathrm{curl}(\delta F/\delta\mathbf{\Omega}(\mathbf{R}))]=\delta F/\delta\mathbf{R}(\mathbf{a})\big|_{\mathbf{\Omega}_0}. \tag{11}$$

For this reason, the right-hand side of Eq. (10) equals the variational derivative $\delta\mathcal{H}/\delta\mathbf{R}$:

$$[(\mathbf{\Omega}_0(\mathbf{a})\cdot\nabla_\mathbf{a})\mathbf{R}(\mathbf{a})\times\mathbf{R}_t(\mathbf{a})]=\delta\mathcal{H}\{\mathbf{\Omega}\{\mathbf{R}\}\}/\delta\mathbf{R}(\mathbf{a})\big|_{\mathbf{\Omega}_0}. \tag{12}$$

It is easy to verify that the equation obtained is equivalent to the requirement that the action with the Lagrangian

$$\mathcal{L}=(1/3)\int d^3\mathbf{a}([\mathbf{R}_t(\mathbf{a})\times\mathbf{R}(\mathbf{a})]\cdot(\mathbf{\Omega}_0(\mathbf{a})\cdot\nabla_\mathbf{a})\mathbf{R}(\mathbf{a}))-\mathcal{H}(\{\mathbf{\Omega}\{\mathbf{R}\}\}), \tag{13}$$

assumes an extremal value ($\delta S=0$).

Therefore we have introduced a variational principle for the Hamiltonian dynamics of a solenoidal vector field topologically equivalent to $\mathbf{\Omega}_0(\mathbf{a})$.

Let us discuss some properties of the equation of motion (12) which are associated with the excess parametrization of elements of $\mathcal{M}_{\Omega_0}$ by objects from $\mathcal{R}$. From Eq. (11) follows the property that the vector $\mathbf{b}$ and $\delta F/\delta\mathbf{R}(\mathbf{a})$ are orthogonal for all functionals defined on $\mathcal{M}_{\Omega_0}$. In other words the variational derivative of the gauge-invariant functionals should be understood (specifically, in Eq. (11)) as $\hat{P}(\delta F/\delta\mathbf{R}(\mathbf{a}))$, where $\hat{P}_{ij}=\delta_{ij}-\tau_i\tau_j$ is a projector, and $\tau=\mathbf{b}/|\mathbf{b}|$ is a unit vector tangent to a vortex line. Using this property as well as the transformation formula (11), it is possible to obtain by a direct calculation of the bracket (3) a Poisson bracket (between two gauge-invariant functionals) expressed in terms of vortex lines:

$$\{F,G\}=\int\frac{d^3\mathbf{a}}{|\mathbf{b}|^2}\left(\mathbf{b}\cdot\left[\hat{P}\frac{\delta F}{\delta\mathbf{R}(\mathbf{a})}\times\hat{P}\frac{\delta G}{\delta\mathbf{R}(\mathbf{a})}\right]\right). \tag{14}$$

The new bracket (14) does not contain variational derivatives with respect to $\mathbf{\Omega}_0(\mathbf{a})$. Therefore, with respect to the initial bracket the Cauchy invariant $\mathbf{\Omega}_0(\mathbf{a})$ is a Casimir, fixing the invariant manifolds $\mathcal{M}_{\Omega_0}$ on which it is possible to introduce the variational principle (13).

In the case of the hydrodynamics of a superfluid liquid a Lagrangian of the form (13) was apparently first used by Rasetti and Regge[8] to derive an equation of motion, identical to Eq. (10), for a separate vortex filament. Later, on the basis of the results of Ref. 8, Volovik and Dotsenko Jr.[9] obtained the Poisson bracket between the coordinates of the vortices and the components of the velocity for a continuous distribution of vorticities. The expressions for these brackets can be extracted without difficulty from the general form for the Poisson brackets (14). However, the noncanonical Poisson brackets obtained in Refs. 8 and 9 must be used with care. Their direct application gives for the equation of motion of the coordinate of a vortex filament an answer that is not gauge-invariant. For a general variation of the ''longitudinal'' parameter, which depends on time, additional terms describing transport along a vortex line appear in the equation of motion. For this reason, the dynamics of curves (including vortex lines) is in principle ''transverse'' with respect to the curve itself.

We note that for two-dimensional flows (in the $x-y$ plane) the variational principle for the action with the Lagrangian (13) leads to the well-known fact that the coordinates $X(\nu,t)$ and $Y(\nu,t)$ of each vortex are canonically conjugate quantities (see Ref. 2).

**4**. We shall now give an example of hydrodynamic-type equations whose integrability (4) can be established by switching to the vortex-line representation.

Let us consider the Hamiltonian

$$\mathcal{H}\{\mathbf{\Omega}(\mathbf{r})\}=\int |\mathbf{\Omega}|d\mathbf{r} \tag{15}$$

and the freezing-in equation (4), following from it, with the generalized velocity $\mathbf{v}=\mathrm{curl}\,(\mathbf{\Omega}/\Omega)$. Let us assume that the vortex lines are closed, and let us use the representation (9). Then, by virtue of Eq. (8), the Hamiltonian in terms of vortex lines decomposes into a sum of the Hamiltonians of the vortex lines:

$$\mathcal{H}\{\mathbf{R}\}=\int |\Omega_0(\nu)|d^2\nu\int |\partial\mathbf{R}/\partial\mathbf{s}|ds. \tag{16}$$

The integral over $s$ appearing here is the length of a vortex filament with index $\nu$. According to Eq. (12), the equation of motion for the vector $\mathbf{R}(\nu,s)$ is local with respect to these variables (it does not contain an interaction with other vortices)

$$\eta[\mathbf{R_s}\times\mathbf{R_t}(\nu,s,t)]=[\tau\times[\tau\times\tau_s]]. \tag{17}$$

Here $\eta=$ sign $(\Omega_0)$ and $\tau=\mathbf{R_s}/|\mathbf{R_s}|$ is a unit vector tangent to a vortex line.

This equation is invariant under the substitution $s\to\tilde{s}(s,t)$. Therefore Eq. (17) can be solved for $\mathbf{R}_t$ to within a displacement along the vortex filament — a transformation leaving the vorticity $\mathbf{\Omega}$ unchanged. This means that to find $\mathbf{\Omega}$ it is sufficient to find any solution of the equation $\eta|\mathbf{R_s}|\mathbf{R}_t=[\tau\times\tau_\mathbf{s}]+\beta\mathbf{R}_s$, which follows from Eq. (17), for some value of $\beta$. The equation arising hence for $\tau$ as a function of the filament length $l$ ($dl=|\mathbf{R}_s|ds$) and time $t$ (with the choice of the new value $\beta=0$) reduces to an integrable one-dimensional Landau–Lifshitz equation for a Heisenberg ferromagnet:

$$\eta\frac{\partial\tau}{\partial t}=\left[\tau\times\frac{\partial^2\tau}{\partial l^2}\right].$$

This equation is gauge equivalent to the nonlinear Schrödinger equation (NSE)[10] and, for example, it can be reduced to it by a Hasimoto transformation:[7] $\psi(l,t)=\kappa(l,t)\cdot\exp(i\int^l\chi(l,t)dl)$, where $\kappa(l,t)$ is the curvature and $\chi(l,t)$ the torsion of a line.

The system under study with Hamiltonian (15) has a direct relation to hydrodynamics. As is well known (see Ref. 7 and the references cited therein), the local approximation for a thin vortex filament (with a small ratio of the filament thickness to a characteristic longitudinal length) leads to a Hamiltonian of the form (16) for only one filament. Accordingly, the equations (4) with the Hamiltonian (15) can be used to describe the motion of several vortex filaments whose thicknesses are small compared with the distance between them. The (nonlinear) dynamics of each filament is independent of what happens with its neighbors. In this model the appearance of singularities (crossing of vortices) is of an inertial character, very similar to breaking of waves in gasdynamics. Of course, this approximation does not work over distances comparable to the distance between filaments. It is important that for the present approximation the Hamiltonian of a vortex filament is proportional to the length of the filament, whence follows its conservation. This, however, in no way corresponds to the behavior of vortex lines in turbulent flows, where intense stretching of the lines occurs. Therefore it is desirable to have a more refined model that is free of this drawback, which would necessarily take nonlocality effects into account.

We wish to add to what we have said above that Eq. (15) does not exhaust the list of equations (4) that can be integrated by means of the representation (9). Thus, a system with Hamiltonian $\mathcal{H}=\int|\Omega|\chi d\mathbf{r}$ likewise reduces to an integrable system in terms of vortex lines. It turns out to be gauge-equivalent to a modified KdV equation $\psi_t+\psi_{lll}+(3/2)|\psi|^2\psi_l=0$ — the second equation, after the NSE, in the hierarchy engendered by the Zakharov–Shabat operator. In contrast to Eq. (15), a physical application of this model has not yet been found.

**5**. We thank A. B. Shabat for helpful discussions of the relation between the NSE and Eqs. (4). We also thank the referee for calling our attention to Refs. 8 and 9. This work was supported by the Russian Fund for Fundamental Research under Grant 97-01-00093. E. K. was supported in part by INTAS Grant 96-0413 and V. R. was supported by a Landau Scholarship grant.

[1] V. E. Zakharov and E. A. Kuznetsov, Usp. Fiz. Nauk **167**, 1137 (1997).
[2] H. Lamb, *Hydrodynamics*, Cambridge Univ. Press, 1932 [Russian translation, Gostekhizdat, Moscow, 1947].
[3] E. A. Kuznetsov and A. V. Mikhailov, Phys. Lett. A **77**, 37 (1980).
[4] J. J. Moreau, C. R. Acad. Sc. Paris **252**, 2810 (1961); H. K. Moffatt, J. Fluid Mech. **35**, 117 (1969).
[5] V. I. Arnol'd, Dokl. Akad. Nauk SSSR **162**, 773 (1965); Usp. Mat. Nauk **24**(3), 225 (1969).
[6] R. Salmon, Annu. Rev. Fluid Mech. **20**, 225 (1988).
[7] R. Hasimoto, J. Fluid Mech. **51**, 477 (1972).
[8] M. Rasetti and T. Regge, Physica A **80**, 217 (1975).
[9] G. E. Volovik and V. S. Dotsenko Jr., JETP Lett. **29**, 576 (1979).
[10] V. E. Zakharov and L. A. Takhtadzhyan, Teor. Mat. Fiz. **38**, 26 (1979).

Translated by M. E. Alferieff

# $U(N)$ monopoles on Kerr black holes

Yu. P. Goncharov
*Experimental Physics Department, State Technical University, 195251 St. Petersburg, Russia*

(Submitted 5 May 1998)
Pis'ma Zh. Éksp. Teor. Fiz. **67**, No. 12, 1021–1026 (25 June 1998)

We describe $U(N)$ monopoles ($N>1$) on Kerr black holes by the parameters of the moduli space of holomorphic vector $U(N)$ bundles over $S^2$ with the help of the Grothendieck splitting theorem. For $N=2, 3$ we estimate the corresponding monopole masses.
 [S0021-3640(98)01312-7]

PACS numbers: 04.70.Dy

**1.** The present paper is a natural continuation of our previous work.[1] One of the motivations for writing that paper[1] was to implement in the Kerr black hole case the program performed in Refs. 2 and 3 for the Schwarzschild and Reissner–Nordström black holes, namely, to try to find the additional quantum numbers (nonclassical hair) characterizing Kerr black holes that might help in building a statistical ensemble necessary to generate the Kerr black hole entropy.

A description of $U(1)$ (Dirac) monopoles on Kerr black holes was obtained in Ref. 1. The present paper is devoted to the extension of the constructions of Ref. 1 to $U(N)$ monopoles ($N>1$) on Kerr black holes. In the present paper, however, we shall use a gauge somewhat different from the gauge employed in Ref. 1 to avoid unnecessary complications.

In the Kerr black hole case we use the ordinary set of the local Boyer–Lindquist coordinates $t$, $r$, $\vartheta$, $\varphi$ covering the standard topology $R^2\times S^2$ of the 4D black hole space–times except for a set of the zero measure. At this the surface $t=$ const, $r=$ const is an oblate ellipsoid with topology $S^2$ and focal distance $a$, while $0\leqslant\vartheta<\pi$, $0\leqslant\varphi<2\pi$. Under the circumstances, we write down the Kerr metric in the form

$$ds^2=g_{\mu\nu}dx^\mu\otimes dx^\nu\equiv(1-2Mr/\Sigma)dt^2-\frac{\Sigma}{\Delta}dr^2-\Sigma d\vartheta^2-[(r^2+a^2)^2-\Delta a^2\sin^2\vartheta]\frac{\sin^2\vartheta}{\Sigma}d\varphi^2+\frac{4Mra\sin^2\vartheta}{\Sigma}dtd\varphi, \tag{1}$$

with $\Sigma=r^2+a^2\cos^2\vartheta$, $\Delta=r^2-2Mr+a^2$, $a=J/M$, where $J,M$ are, respectively, the black hole mass and angular momentum. The components of metric $g^{\mu\nu}$ in the cotangent bundle of the manifold $R^2\times S^2$ with the metric (1) (in the tangent bundle) needed in the calculations below can be found in Ref. 1. In addition, we have $\delta=|\det(g_{\mu\nu})|=(\Sigma\sin\vartheta)^2$, $r_\pm=M\pm\sqrt{M^2-a^2}$, and so $r_+\leqslant r<\infty$, $0\leqslant\vartheta<\pi$, $0\leqslant\varphi<2\pi$.

 

Throughout the paper we employ the system of units with $\hbar = c = G = 1$, unless explicitly stated. Finally, we shall denote by $L_2(F)$ the set of the modulo square integrable complex functions on any manifold $F$ furnished with an integration measure.

**2.** In order to obtain the infinite families of $U(N)$ monopoles for $N>1$, we should use the Grothendieck splitting theorem,[4,5] which asserts that any complex vector bundle over $S^2$ (and, as a consequence, over $R^2\times S^2$) of rank $N>1$ is a direct sum of $N$ suitable complex line bundles over $S^2$. It is known[6] that there exists a countable number of nontrivial complex vector bundles of any rank $N>1$ over $R^2\times S^2$. The sections of such bundles can be qualified as topologically inequivalent configurations (TICs) of an $N$-dimensional (massless) complex scalar field. The standard classification associates some $n\in Z$ with each $U(N)$ bundle over $R^2\times S^2$ topology. In what follows we shall call it the Chern number of the corresponding bundle. The TIC with $n=0$ can be called *untwisted*, while the rest of the TICs with $n\neq 0$ should be referred to as *twisted*.

So far we have tacitly assumed that the $U(N)$ bundles are differentiable. In reality they admit holomorphic structures, and since each differentiable complex line bundle over $S^2$ admits only one holomorphic structure, the Grothendieck splitting theorem in fact gives a description of the moduli space $M_N$ of $N$-dimensional holomorphic complex vector bundles over $S^2$. Namely, each $N$-dimensional holomorphic complex vector bundle over $S^2$ is specified by only an $N$-plet of integers $(k_1,k_2,\ldots,k_N)\in Z^N$, $k_1\geqslant k_2 \geqslant \ldots \geqslant k_N$. Two of such $N$-plets $(k_i)$ and $(k_i')$ specify the same differentiable $N$-dimensional bundle if and only if $\Sigma_i k_i = \Sigma_i k_i'$.

As was shown in Ref. 1 each complex line bundle (with the Chern number $k_i$, $i=1,2,\ldots,N$) over $R^2\times S^2$ with the metric (1) has a complete set of sections in $L_2(R^2\times S^2)$, so that by using the fact that all the $U(N)$ bundles over $R^2\times S^2$ can be trivialized over the bundle chart of local coordinates $(t,r,\vartheta,\varphi)$ covering almost the whole manifold $R^2\times S^2$, the aforementioned set can be written on the given chart in the form

$$f^{a\omega_i}_{k_i l_i m_i} = \frac{1}{\sqrt{r^2+a^2}} e^{i\omega_i t} R^{a\omega_i}_{k_i l_i m_i}(r) Y_{k_i l_i m_i}(a\omega_i,\vartheta,\varphi), \quad l_i = |k_i|,|k_i|+1,\ldots,|m_i| \leqslant l_i, \tag{2}$$

where some properties of both the *monopole oblate spheroidal harmonics* $Y_{k_i l_i m_i}(a\omega_i,\vartheta,\varphi)$ and the conforming eigenvalues $\lambda_i = \lambda_{k_i l_i m_i}(a\omega_i)$ can be found in Ref. 1, but we shall not need them further. As to the functions $R^{a\omega_i}_{k_i l_i m_i}(r) = R$ then, in the gauge under discussion, they obey the equation

$$\frac{d}{dr}\Delta\frac{d}{dr}\left(\frac{R}{\sqrt{r^2+a^2}}\right) + \frac{(r^2+a^2)^2\omega_i^2 - 4Mm_i r a\omega_i + m_i^2 a^2}{\Delta}\frac{R}{\sqrt{r^2+a^2}}$$

$$= -(\lambda_i + k_i^2)\frac{R}{\sqrt{r^2+a^2}}, \quad \text{with } l_i = |k_i|,|k_i|+1,\ldots,|m_i| \leqslant l_i. \tag{3}$$

Now, in accordance with the Grothendieck splitting theorem, any section of $N$-dimensional complex bundle $\xi_n$ over $R^2\times S^2$ with the Chern number $n\in Z$ can be represented by an $N$-plet $(\phi_1,\ldots,\phi_N)$ of complex scalar fields $\phi_i$, where each $\phi_i$ is a

section of a complex line bundle over $R^2\times S^2$. According to the above, we can consider $\phi_i$ the section of complex line bundle with the Chern number $k_i\in Z$, where the numbers $k_i$ are subject to the conditions

$$k_1\geqslant k_2\geqslant \ldots \geqslant k_N, \quad k_1+k_2+\cdots+k_N=n. \tag{4}$$

As a consequence, we can require the $N$-plets $(f^{a\omega_1}_{k_1 l_1 m_1}, \ldots, f^{a\omega_N}_{k_N l_N m_N})$ to form a basis in $[L_2(R^2\times S^2)]^N$ for the sections of $\xi_n$, $l_i=|k_i|,|k_i|+1,\ldots,|m_i|\leqslant l_i$, and this will define the wave equation for a section $\phi=(\phi_1,\ldots,\phi_N)$ of $\xi_n$ with respect to the metric (1):

$$\left[ I_N\Box - \frac{1}{\Sigma^2\sin^2\vartheta}\begin{pmatrix} 2ik_1\cos\vartheta(a\sin^2\vartheta\partial_t+\partial_\varphi)-k_1^2\cos^2\vartheta & 0 & \ldots \\ 0 & 2ik_2\cos\vartheta(a\sin^2\vartheta\partial_t+\partial_\varphi)-k_2^2\cos^2\vartheta & \ldots \\ \ldots & \ldots & \ldots \\ 0 & 0 & \ldots \\ \ldots & 0 & \\ \ldots & 0 & \\ \ldots & \ldots & \\ \ldots & 2ik_N\cos\vartheta(a\sin^2\vartheta\partial_t+\partial_\varphi)-k_N^2\cos^2\vartheta & \end{pmatrix}\right]\begin{pmatrix}\phi_1\\ \phi_2\\ \vdots\\ \phi_N\end{pmatrix}=0, \tag{5}$$

where $I_N$ is the $N\times N$ unit matrix, and $\Box=(\delta)^{-1/2}\partial_\mu(g^{\mu\nu}(\delta)^{1/2}\partial_\nu)$ is the conventional wave operator conforming to metric (1).

Equation (5) will, in turn, correspond to the Lagrangian

$$\mathcal{L}=\delta^{1/2}g^{\mu\nu}\overline{\mathcal{D}_\mu\phi}\mathcal{D}_\nu\phi, \tag{6}$$

with $\phi=(\phi_i)$ and a covariant derivative $\mathcal{D}_\mu=\partial_\mu-igA^a_\mu T_a$ on sections of the bundle $\xi_n$, while the overbar in (6) signifies Hermitian conjugation, and the matrices $T_a$ will form a basis of the Lie algebra of $U(N)$ in $N$-dimensional space (as is accepted in physics, we consider the matrices $T^a$ to be Hermitian), $a=1,\ldots,N^2$, $g$ is a gauge coupling constant, i.e., we come to a theory describing the interaction of an $N$-dimensional twisted complex scalar field with the gravitational field described by metric (1). The coefficients $A^a_\mu$ will represent a connection in the given bundle $\xi_n$ and will describe some non-Abelian $U(N)$ monopole.

As can be seen, Eq. (5) has the form $\mathcal{D}^\mu\mathcal{D}_\mu\phi=0$, where $\mathcal{D}^\mu$ is a formal adjoint to $\mathcal{D}_\mu$ with regards to the scalar product induced by metric (1) in $[L_2(R^2\times S^2)]^N$. That is, the operator $\mathcal{D}^\mu$ acts on the differential forms $a_\mu dx^\mu$ with coefficients in the bundle $\xi_n$ in accordance with the rule

$$\mathcal{D}^\mu(a_\nu dx^\nu)=-\frac{1}{\sqrt{\delta}}\partial_\mu(g^{\mu\nu}\sqrt{\delta}a_\nu)+ig\overline{A_\mu}g^{\mu\nu}a_\nu, \tag{7}$$

with $A_\mu=A^a_\mu T_a$.

As a result, the equation $\mathcal{D}^\mu\mathcal{D}_\mu\phi=0$ takes the form

$$I_N\Box\phi-\frac{ig}{\sqrt{\delta}}\partial_\mu(g^{\mu\nu}\sqrt{\delta}A_\nu\phi)-(ig\overline{A_\mu}g^{\mu\nu}\partial_\nu+g^2g^{\mu\nu}\overline{A_\mu}A_\nu)\phi=0. \tag{8}$$

Comparing (5) with (8) gives

$$A_r^aT_a=A_\vartheta^aT_a=0\,, \tag{9}$$

$$A_t^aT_a=\frac{a\cos\vartheta}{g\Sigma}\begin{pmatrix} k_1 & 0 & \dots & 0\\ 0 & k_2 & \dots & 0\\ \dots & \dots & \dots & \dots\\ 0 & 0 & \dots & k_N\end{pmatrix}, \tag{10}$$

$$A_\varphi^aT_a=-\frac{(r^2+a^2)\cos\vartheta}{g\Sigma}\begin{pmatrix} k_1 & 0 & \dots & 0\\ 0 & k_2 & \dots & 0\\ \dots & \dots & \dots & \dots\\ 0 & 0 & \dots & k_N\end{pmatrix}. \tag{11}$$

Under the circumstances the connection in the bundle $\xi_n$ is $A=A_\mu^aT_adx^\mu=A_t^a(r,\vartheta)T_adt+A_\varphi^a(r,\vartheta)T_ad\varphi$ which yields the curvature matrix $F=dA+A\wedge A$ for $\xi_n$ bundle in the form

$$F=F_{\mu\nu}^aT_adx^\mu\wedge dx^\nu=-\partial_r(A_t^aT_a)dt\wedge dr-\partial_\vartheta(A_t^aT_a)dt\wedge d\vartheta$$
$$+\partial_r(A_\varphi^aT_a)dr\wedge d\varphi+\partial_\vartheta(A_\varphi^aT_a)d\vartheta\wedge d\varphi, \tag{12}$$

because the exterior differential $d=\partial_tdt+\partial_rdr+\partial_\vartheta d\vartheta+\partial_\varphi d\varphi$ in the coordinates $t,r,\vartheta,\varphi$. From here it follows that the first Chern class $c_1(\xi_n)$ of the bundle $\xi_n$ can be chosen in the form

$$c_1(\xi_n)=\frac{g}{4\pi}\,\mathrm{Tr}(F), \tag{13}$$

so that, when integrating $c_1(\xi_n)$ over any surface $t=\mathrm{const}$, $r=\mathrm{const}$, we shall have, using (4) and (11):

$$\int_{S^2}c_1(\xi_n)=\frac{g}{4\pi}\int_{S^2}\mathrm{Tr}\,[\partial_\vartheta(A_\varphi^aT_a)]d\vartheta\wedge d\varphi$$
$$=-\frac{n}{4\pi}\int_{S^2}\frac{(r^2+a^2)(a^2\cos^2\vartheta-r^2)}{\Sigma^2}\sin\vartheta d\vartheta\wedge d\varphi=n, \tag{14}$$

which is equivalent to the conventional Dirac charge quantization condition

$$qg=4\pi n, \tag{15}$$

with (non-Abelian) magnetic charge

$$q=\int_{S^2}\mathrm{Tr}(F). \tag{16}$$

Introducing the Hodge star operator $*$ conforming metric (1) on 2-forms $F=F^a_{\mu\nu}T_a dx^\mu\wedge dx^\nu$ with the values in the Lie algebra of $U(N)$ by the relation (see, e. g., Refs. 7)

$$(F^a_{\mu\nu}dx^\mu\wedge dx^\nu)\wedge(*F^a_{\alpha\beta}dx^\alpha\wedge dx^\beta)=(g^{\mu\alpha}g^{\nu\beta}-g^{\mu\beta}g^{\nu\alpha})F^a_{\mu\nu}F^a_{\alpha\beta}\sqrt{\delta}\;dx^0\wedge\cdots\wedge dx^3, \tag{17}$$

written in local coordinates $x^\mu$ [there is no summation over $a$ in (17)], in coordinates $t,r,\vartheta,\varphi$ we have for $F$ of (12)

$$\begin{aligned}*F=*F^a_{\mu\nu}T_a dx^\mu\wedge dx^\nu=&\left(g^{t\varphi}g^{\vartheta\vartheta}\frac{\partial A_t}{\partial\vartheta}+g^{\vartheta\vartheta}g^{\varphi\varphi}\frac{\partial A_\varphi}{\partial\vartheta}\right)\sqrt{|g|}dt\wedge dr-\left(g^{\varphi t}g^{rr}\frac{\partial A_t}{\partial r}\right.\\&\left.+g^{rr}g^{\varphi\varphi}\frac{\partial A_\varphi}{\partial r}\right)\sqrt{|g|}dt\wedge d\vartheta+\left(g^{tt}g^{\vartheta\vartheta}\frac{\partial A_t}{\partial\vartheta}+g^{\vartheta\vartheta}g^{t\varphi}\frac{\partial A_\varphi}{\partial\vartheta}\right)\sqrt{|g|}dr\wedge d\varphi\\&-\left(g^{tt}g^{rr}\frac{\partial A_t}{\partial r}+g^{rr}g^{t\varphi}\frac{\partial A_\varphi}{\partial r}\right)\sqrt{|g|}d\vartheta\wedge d\varphi,\end{aligned} \tag{18}$$

with $A_t=A^a_t T_a$ and $A_\varphi=A^a_\varphi T_a$ of (10)–(11). We can now consider the Yang–Mills equations

$$dF=F\wedge A-A\wedge F, \tag{19}$$

$$d*F=*F\wedge A-A\wedge *F. \tag{20}$$

It is clear that (19) is identically satisfied by the above $A$, $F$ — this is just the Bianchi identity holding true for any connection.[7]

As to Eq. (20), then, it is easy to check with the help of (10), (11), and (18) that $*F\wedge A=A\wedge *F$. In this situation, it follows from (18) that the condition $d*F=0$ is equivalent to the equations

$$\frac{\partial}{\partial r}\left[\sqrt{|g|}\left(g^{rr}g^{\varphi t}\frac{\partial A_t}{\partial r}+g^{rr}g^{\varphi\varphi}\frac{\partial A_\varphi}{\partial r}\right)\right]+\frac{\partial}{\partial\vartheta}\left[\sqrt{|g|}\left(g^{t\varphi}g^{\vartheta\vartheta}\frac{\partial A_t}{\partial\vartheta}+g^{\vartheta\vartheta}g^{\varphi\varphi}\frac{\partial A_\varphi}{\partial\vartheta}\right)\right]=0, \tag{21}$$

$$\frac{\partial}{\partial r}\left[\sqrt{|g|}\left(g^{tt}g^{rr}\frac{\partial A_t}{\partial r}+g^{rr}g^{t\varphi}\frac{\partial A_\varphi}{\partial r}\right)\right]+\frac{\partial}{\partial\vartheta}\left[\sqrt{|g|}\left(g^{tt}g^{\vartheta\vartheta}\frac{\partial A_t}{\partial\vartheta}+g^{\vartheta\vartheta}g^{t\varphi}\frac{\partial A_\varphi}{\partial\vartheta}\right)\right]=0. \tag{22}$$

The direct evaluation with the aid of (10), (11) shows that (21), (22) are satisfied. As a consequence, Eq. (20) is fulfilled.

One can notice, moreover, that

$$\begin{aligned}Q_e=\int_{S^2}\mathrm{Tr}(*F)=&-\int_{S^2}g^{rr}\;\mathrm{Tr}\left(g^{tt}\frac{\partial A_t}{\partial r}+g^{t\varphi}\frac{\partial A_\varphi}{\partial r}\right)\sqrt{|g|}d\vartheta\wedge d\varphi\\=&-\frac{4\pi anr}{e}\int_{-1}^{1}\frac{x\,dx}{\Sigma^2}=0,\end{aligned} \tag{23}$$

where $x=\cos\vartheta$. As a result, an external observer does not see any (internal) non-Abelian electric charge $Q_e$ of the Kerr black hole for any given $N$. Besides, it should be empha-

sized that the total (internal) non-Abelian magnetic charge $Q_m$ of a black hole, which should be considered as the one summed up over all the $U(N)$ monopoles for any given $N$, remains equal to zero because

$$Q_m=\frac{4\pi}{g}\sum_{n\in\mathbb{Z}} n=0, \tag{24}$$

so the external observer does not see any non-Abelian magnetic charge of the Kerr black hole either, even though $U(N)$ monopoles are present on the black hole in the sense described above.

To estimate the monopole masses we should use the $T_{00}$ component of the energy–momentum tensor

$$T_{\mu\nu}=\frac{1}{4\pi}\left(-F^a_{\mu\alpha}F^a_{\nu\beta}g^{\alpha\beta}+\frac{1}{4}F^a_{\beta\gamma}F^a_{\alpha\delta}g^{\alpha\beta}g^{\gamma\delta}g_{\mu\nu}\right). \tag{25}$$

Since we are in an asymptotically flat space–time, we can calculate the masses sought according to

$$m_{\mathrm{mon}}(k_1,\ldots,k_N)=\int_{t=\mathrm{const}} T_{00}\sqrt{\gamma}\; dr\wedge d\vartheta\wedge d\varphi, \tag{26}$$

where

$$\sqrt{\gamma}=\sqrt{\det(\gamma_{ij})}=\sqrt{\Sigma/\Delta}\;\sin\vartheta\sqrt{(r^2+a^2)^2-\Delta a^2\sin^2\vartheta} \tag{27}$$

for the metric $d\sigma^2=\gamma_{ij}dx^i\otimes dx^j$ on the hypersurface $t=$ const, while $T_{00}$ is computed at the given $U(N)$ monopole. Under the circumstances it is not complicated to check that the leading term in asymptotic of $T_{00}\sqrt{\gamma}$ at $r\to\infty$ will be defined by the addend $g^{\vartheta\vartheta}g^{\varphi\varphi}(F^a_{\vartheta\varphi})^2$ of (25), so one should solve the equation

$$F^a_{\vartheta\varphi}T_a=\partial_\vartheta(A^a_\varphi T_a)\rangle, \tag{28}$$

with $A^a_\varphi T_a$ of (11). Let us concretize it for $N=2,3$.

**3**. At $N=2$ we can take $T_1=I_2$, $T_a=\sigma_{a-1}$ at $a=2,3,4$, where $\sigma_{a-1}$ are the ordinary Pauli matrices. Then the Eq. (28) gives $F^2_{\vartheta\varphi}=F^3_{\vartheta\varphi}=0$, while

$$F^1_{\vartheta\varphi}=\frac{1}{2}(k_1+k_2)f(r,\vartheta),\quad F^4_{\vartheta\varphi}=\frac{1}{2}(k_1-k_2)f(r,\vartheta) \tag{29}$$

with

$$f(r,\vartheta)=-\partial_\vartheta\left[\frac{(r^2+a^2)\cos\vartheta}{g\Sigma}\right]. \tag{30}$$

This yields at $r\to\infty$

$$T_{00}\sqrt{\gamma}\sim\frac{\sin\vartheta}{64\pi g^2 r^2}[(k_1+k_2)^2+(k_1-k_2)^2]. \tag{31}$$

As a result, we can estimate (in usual units) according to (26)

$$m_{\mathrm{mon}}(k_1,k_2)\sim\left(\frac{\hbar^2c^2}{G}\right)\frac{(k_1+k_2)^2+(k_1-k_2)^2}{16g^2}\int_{r_+}^{\infty}\frac{dr}{r^2}$$

$$=\frac{(k_1+k_2)^2+(k_1-k_2)^2}{16g^2r_+}\left(\frac{\hbar^2c^2}{G}\right). \tag{32}$$

At $N=3$ we can take $T_1=I_3$, $T_a=\lambda_{a-1}$ at $a=2,\ldots,9$, where $\lambda_{a-1}$ are the Gell-Mann matrices. From (28) this yields $F^2_{\vartheta\varphi}=F^3_{\vartheta\varphi}=F^5_{\vartheta\varphi}=F^6_{\vartheta\varphi}=F^7_{\vartheta\varphi}=F^8_{\vartheta\varphi}=0$, while

$$F^1_{\vartheta\varphi}=\frac{1}{3}(k_1+k_2+k_3)f(r,\vartheta),\quad F^4_{\vartheta\varphi}=\frac{1}{2}(k_1-k_2)f(r,\vartheta),$$

$$F^9_{\vartheta\varphi}=\frac{\sqrt{3}}{6}(k_1+k_2-2k_3)f(r,\vartheta) \tag{33}$$

with $f(r,\vartheta)$ of (30). This gives

$$m_{\mathrm{mon}}(k_1,k_2,k_3)\sim\left[(k_1+k_2+k_3)^2+\frac{9}{4}(k_1-k_2)^2+\frac{3}{4}(k_1+k_2\right.$$

$$\left.-2k_3)^2\right]\frac{1}{36g^2r_+}\left(\frac{\hbar^2c^2}{G}\right). \tag{34}$$

It is clear that the case of arbitrary $N$ can be treated analogously, but we shall not dwell upon this here. We only note that the important case is the one of $U(4)$ monopoles, because 4-dimensional complex vector bundles could describe TICs of both spinors and vector charged fields, i.e., these TICs physically could arise due to interaction with $U(4)$ monopoles. But this task requires a separate consideration.

Under the circumstances, evaluating the corresponding Compton wavelength $\lambda_{\mathrm{mon}}(k_i)=\hbar/m_{\mathrm{mon}}(k_i)c$, we can see that at any $n\neq 0$, $N\geqslant 1$, $\lambda_{\mathrm{mon}}(k_i)\ll r_g$, where $r_g=r_+G/c^2$ is a gravitational radius of Kerr black hole, if $g^2/\hbar c\ll 1$. As a consequence, we come to the conclusion that under certain conditions $U(N)$ monopoles might reside in Kerr black holes as quantum objects and, e.g., to markedly modify the Hawking radiation[8,9] or to generate the black hole entropy.[3]

Thus we can see that the masses of $U(N)$ monopoles really depend on the parameters of the moduli space $M_N$ of holomorphic vector bundles over $S^2$.

**4.** The results of both the present paper and Refs. 1–3, 8, 9 show that the 4D black hole physics can have a rich fine structure connected with the topology $R^2\times S^2$ underlying the 4D black hole space–time manifolds. It seems to be quite probable that this fine structure is tied with the moduli spaces $M_N$ of $N$-dimensional holomorphic vector bundles over $S^2$ and could manifest itself in solving a number of problems within the 4D black hole physics, so it seems that one should study thoroughly the possibilities that arise, and, in particular, the Kerr–Newman metric case, as a natural charged generalization of Kerr metric. We hope to pursue this study elsewhere.

The work was supported in part by the Russian Fund for Fundamental Research (Grant 98-02-18380-a) and also by GRASENAS (Grant 6-18-1997).

[1] Yu. P. Goncharov, Phys. Lett. B **398**, 32 (1997).
[2] Yu. P. Goncharov, Nucl. Phys. B **460**, 167 (1996).
[3] Yu. P. Goncharov, Int. J. Mod. Phys. A **12**, 3347 (1997).
[4] M. F. Atiyah, *Geometry of Yang-Mills Fields* (Fermi Lectures), Scuola Normale Superiore, Pisa, 1979; C. Okonek, M. Schneider, and H. Spindler, *Vector Bundles on Complex Projective Spaces*, Birkhäuser, Boston, 1980.
[5] A. Grothendieck, Am. J. Math. **79**, 121 (1956).
[6] D. Husemoller, *Fibre Bundles*, McGraw-Hill, New-York, 1966.
[7] *Géométrie Riemannian en Dimension 4*, Seminaire Arthur Besse, Cedic/Fernand Nathan, Paris, 1981; M. M. Postnikov, *Differential Geometry*, Nauka, Moscow, 1988.
[8] Yu. P. Goncharov and J. V. Yarevskaya, Mod. Phys. Lett. A **10**, 1813 (1995).
[9] Yu. P. Goncharov and N. E. Firsova, Int. J. Mod. Phys. D **5**, 419 (1996); Nucl. Phys. B **486**, 371 (1997).

Published in English in the original Russian journal. Edited by Steve Torstveit.